The environmental drivers of white spruce growth and regeneration at Arctic treeline in a changing climate

Johanna Elizabeth Jensen

Submitted in partial fulfillment of the
requirements for the degree of
Doctor of Philosophy
under the Executive Committee
of the Graduate School of Arts and Sciences

COLUMBIA UNIVERSITY

2023

© 2023

Johanna Elizabeth Jensen

All Rights Reserved

Abstract

The environmental drivers of white spruce growth and regeneration at Arctic treeline in a changing climate

Johanna Elizabeth Jensen

As a temperature-delineated boundary, Arctic treeline is predicted to shift poleward and tree growth is expected to increase in response to rapid warming. The massive scale of the Arctic treeline magnifies these changes to impact energy balance, carbon balance, and climate-related feedbacks at local, regional, and global scales. Yet, not all sections of the Arctic treeline are reporting growth, suggesting factors other than temperature may be becoming more limiting as the climate continues to change. This dissertation investigates how water availability and tree size may modify the response to climate change of a dominant conifer species (white spruce, Picea glauca) growing at an Arctic treeline site in the Brooks Range, Alaska, USA. The first chapter examines the influence of temperature and water availability on population regeneration and individual tree growth during the 20th century. A climatic shift towards a warmer and drier climate after 1975 caused divergent responses of sapling regeneration and mature tree growth, suggesting that, while individuals have grown, this section of treeline has remained relatively stationary. The second chapter explores the present-day relationships between tree size,

temperature, moisture availability, and tree growth by examining the response of intra-annual radial stem growth rate to changing environmental conditions at the Arctic treeline. Tree size and water availability play important roles in moderating the growth response to climate change. Finally, in the third chapter, the environmental cues which trigger the onset of radial stem growth in spring are identified. The results suggest a combination of winter chilling and subsequent spring heat accumulation initiates onset, like trees growing at lower latitudes. However, the chilling and heating thresholds at this Arctic treeline site were far colder than those identified at lower latitudes, suggesting local adaptation to harsh Arctic winters and springs. Through these new findings, this dissertation advances our understanding of Arctic treeline dynamics and will help to predict the future of the Arctic treeline more accurately in a rapidly changing climate.

Table of Contents

List of Tables and Figures

Acknowledgments

This dissertation would not have been possible with the support and guidance of colleagues, friends, and family. To my stalwart advisors, Kevin Griffin and Natalie Boelman: thank you for teaching me how to remain positive and dedicated despite freezing temperatures, perfectionism, and snowshoe hares destroying the dendrometers. Kevin, your joy of learning and teaching about forest ecology, ecophysiology, and the scientific process is infectious and made learning from you the past several years so wonderful. Thank you also for teaching me the importance of making science accessible to all those hoping to learn. Natalie, your determination, breadth of knowledge, and ability to build a team is truly admirable. Thank you for your playfulness and willingness to laugh; it buoyed me throughout this process and taught me to roll with the punches. I especially cherish the moments spent in magnificent forests with the both of you – from New York to Alaska – running through botanical gardens, burying dendrometer cables under chicken wire, using a cherry picker to measure canopy branches on my birthday, and tundra napping.

I am extremely grateful to my committee members: Duncan, Shahid Naeem, and Jan Eitel. Duncan, thank you for teaching me to start small before building complexity, to look at the bigger picture, to remain curious and open to new ideas, and for helping me in all things math and statistics. Your friendship, mentorship, and belief in me as a scientist over the last several years has meant so much. Shahid, thank you for the many wonderful conversations about science

and life. Your unique perspective on ecology is invigorating and your enthusiasm to cross scientific disciplines, inspiring. Jan, thank you for being the fearless leader of Team Krumholtz! Your insightful comments have substantially strengthened and clarified my work and it's been a pleasure to spend time with you in Idaho, Canada, and Alaska.

And to the members of Team Krumholtz – Jan, Kevin, Natalie, Lee Vierling, Andy Maguire, Jyoti Jennewein, William Weygint, and Kathryn Baker, thank you for your hard work and dedication in the field and on the other side of zoom. We haven't always been in the same place, but we've always been on the same team! I couldn't have been asked for a more fun-loving and collaborative crew. Thank you for your humor, feedback, and adventurous spirits.

To my wonderful department (E3B) and cohort, you made NYC home. Thanks for all the wild fun (winter games!), laughter, and friendship through the highs and lows of graduate school. To my cohort, I could not have been blessed with a finer group of people to learn and grow alongside. It's been a privilege. To the Griffin-Boelman lab group: Sarah Bruner, Stephanie Schmiege, Elizabeth Min, Angelica Patterson, Mukund Rao, and Rose Oelkers, your feedback and collaboration has truly made me a better scientist. And to the Menge Lab group for the same.

Finally, I thank my family and friends. I would not be where I am without your encouragement. To Emma, your love, support, and faith in me have made this journey the success that it is. And to Gabriel, ditto bro. To my mom, Judy, and dad, Bo, for your unwavering support and love. Thank you for encouraging me to follow my passion and for fostering my love of the natural world. To my brother, JJ, thank you for always supporting me but not letting me take myself too seriously. To 'The Peaches' – somehow our odd group of art historians, ecologists, and dogs became family; what a gift. Thank you for celebrating successes, weathering

storms, and silently puzzling with me. And to all those who touched my life during graduate school, thank you for making this experience so meaningful.

Dedication

For my given and chosen families.

Introduction

Biomes represent broad biological communities formed in response to several ecological filters (Smith et al. 1997). Most often, terrestrial biomes can be defined by just two filters: temperature and precipitation regimes (Whittaker 1970). For example, the seminal Whittaker biome graph (1970) categorizes Earth's terrestrial ecosystems into nine biomes with long-term temperature and precipitation as the defining features. However, as climate change continues to substantially alter temperature and precipitation regimes worldwide, plants and animals must either adapt or move to occupy spaces with suitable climate. The best place to study how biomes are reacting to climate change is at their ecotones, or the transition zones between biomes, which are already existing at the physiological extreme. Therefore, changes occur here first and hold key clues to understanding the future.

The Arctic treeline (a.k.a. the forest-tundra ecotone) represents the transition from the coniferous boreal forest to the south and treeless Arctic tundra to the north (Callaghan et al. 2002a, Körner 2012). Arctic treeline spans the circumpolar region crossing 13,400 km through the United States (Alaska), Canada, Iceland, Norway, Finland, and Russia (Callaghan et al. 2002b). When observed from air or space, Arctic treeline may look like a continuous line. However, on the ground, this interface between ecosystems is complex and varies in space and time due to numerous local and regional conditions. Decades of research conclude that the position of treeline is delineated by an air temperature isotherm of 6.4 °C (Paulsen and Körner 2014) and that growth of individuals here was limited by temperature (Körner 2012).

However, as the Arctic warms at more than four times the global average (Rantanen et al. 2022), the temperature-limitation on the current treeline should be alleviated and the treeline should advance to keep pace with the northward/poleward shifting isotherm (ACIA 2005, Callaghan et al. 2005, Pearson et al. 2013, Zhang et al. 2013). Trees should grow more, therefore increasing the above-ground C sink and helping to mitigate climate change (ACIA 2005, Callaghan et al. 2005, Pearson et al. 2013, Zhang et al. 2013).. Such change would significantly influence global energy balance (Harding et al. 2002), biodiversity (Skre et al. 2002), ecosystems services (Callaghan et al. 2002a), biogeochemical cycling (Zhang et al. 2013), carbon balance, and climate-related feedbacks (Wilmking et al. 2006, Pearson et al. 2013).

However, evidence of treeline advance and increased tree growth is not ubiquitous (Harsch et al. 2009, Rees et al. 2020), despite relatively uniform increases in temperature (Overland et al. 2019), highlighting that temperature is not the only limiting factor at treeline position and tree growth (Rees et al. 2020). Instead, increasing evidence points toward the interaction between temperature and water regimes in explaining this unexpected result (e.g., see Wilmking et al. 2004, 2005, Driscoll et al. 2005, Wilmking and Juday 2005, Lange et al. 2020, Rees et al. 2020, Camarero et al. 2021). While temperature has increased across the Arctic, precipitation varies locally, based on factors such as topography, and regional weather patterns. Over the last several decades, both treeline advance and individual tree growth have increased in wetter sections of treeline, such as those in the Western Brooks Range, AK, USA, whereas drier sections have remained stationary and individual tree growth has decreased (Wilmking and Juday 2005, Rees et al. 2020). Of course, many other factors can affect the position and growth of treeline (e.g., see Lloyd 2005, Kambo and Danby 2018a, 2018b, Gustafson et al. 2021, Maher et al. 2021), but the strong association between limited/decreased water availability (including

drought) (Rees et al. 2020), decreased growth, and no change in treeline position suggest a strong mechanistic link at play.

Water availability can influence treeline behavior (i.e., advance, stationary, or retreat; Rees et al. 2020) and individual tree growth in many ways. Snowfall in winters protects seedlings and young saplings from harsh winter conditions by creating a protective boundary layer under the snow (Körner 2012, 2016). Therefore, less snowpack can decrease the depth of the boundary layer and expose young trees earlier than experienced by trees established in previous decades. Additionally, less snowpack can decrease the amount of water available in spring, which is particularly important during the rehydration of the stem an onset of growth in spring (Vaganov et al. 1999). Warmer temperature in spring and fall can lengthen the growing season and increase growth, provided that water is available to supply the necessary turgor pressure when growing new cells. Summertime growth has been particularly linked with water availability (e.g., low VPD, high RH, high precipitation). Survival of seedlings through the summer also relies on water availability as young trees have smaller root systems, preventing them from reaching deeper water reserves available to larger, mature trees. The dynamics between water availability and temperature are complex and require an in-depth examination to help us understand treeline behavior and help predict how treeline will respond to future climate change.

In this dissertation, I present three studies that investigate why Arctic treeline has exhibited such diverse responses in treeline behavior and growth. All three chapters focus on white spruce (*Picea glauca*) growing at Arctic treeline in the Brooks Range, AK, USA and are linked by a common pair of questions: How do temperature and water availability influence growth of white spruce at Arctic treeline; and how do these relationships change between

saplings and trees? In the first chapter, I identify how trees at our study site responded to climate change in the past (i.e., during the 20th century). In the second and third chapters, I narrow my focus to the present-day relationships between weather and growth at an intra-annual timescale using highly resolved point dendrometers. Ultimately, the two hypotheses I assess, in different ways in each chapter, are that (1) water availability is a secondary control on growth so that when temperature limitation is alleviated, water availability dictates the growth response at Arctic treeline and (2) the secondary control of water availability is more intense for saplings than trees.

In Chapter 1, I use historical records of temperature and precipitation, present-day age structure, and tree ring records to investigate the relationships between climate change, treeline behavior, and tree growth during the 20th century. I found that a warmer but significantly drier climate beginning circa 1975 was strongly associated with decreased regeneration of saplings, suggesting treeline remained stationary despite climate warming. This finding supports our hypothesis that once temperature limitation is alleviated, water availability acts as a secondary control on growth at Arctic treeline in saplings. However, our data also showed a significant increase in growth of mature trees after 1975. These opposite responses of saplings and mature trees support our hypothesis that the secondary control of water availability is more severe for saplings than mature trees. Further, the tree ring records revealed temperature divergence after circa 1990, suggesting additional drying in the future will begin to negatively impact growth of mature trees.

In Chapter 2, I explore the present-day relationships between tree life stage, temperature, moisture availability, and radial stem growth by examining the response of intra-annual radial stem growth rate to changing environmental conditions at Arctic treeline. To do so, I used a

generalized linear mixed effects model to predict radial stem growth rate using air temperature, vapor pressure deficit (VPD), volumetric water content, and their interactions as drivers. Diameter at breast height (DBH) is added to the model as a proxy for tree life stage. Our results sugest that VPD and VWC are influence growth rate more than air temperature. In addition, while low VPD increased growth in both saplings and mature trees, the effect was greater in mature trees. These results support our hypothesis that trees at our Arctic treeline site are increasingly water-stress with rapid warming, and that tree size plays an important role in determining the growth response. The result of this study suggests that we may be currently witnessing that the transition towards water-limitation predicted from Chapter 1.

In Chapter 3, I explore how the onset of intra-annual radial stem growth will change in response to climate change. Using a Bayesian analysis, I compare the process of onset of radial stem growth and the type of environmental triggers (air temperature, soil temperature, or both). In this chapter, I used soil temperature as a proxy for water availability in spring, as discontinuous permafrost will not allow liquid water to be available for plant uptake until soil temperatures exceed freezing. Our results suggest that air temperature was a better predictor of the onset of radial growth in spring than either soil temperature or a combination of both. I also found that a combination of extreme cold followed by heat accumulation triggers radial growth. These results suggest that air temperature is more important than water availability in dictating the start of the growing season.

Chapter 1: Growth increases but regeneration declines in response to warming and drying at Arctic treeline in white spruce (*Picea glauca*)

Johanna Jensen, Natalie Boelman, Jan Eitel, Lee Vierling, Andrew Maguire, Rose Oelkers, Carlos Silva, Laia Andreu-Hayes, Rosanne D'Arrigo, Kevin L. Griffin

1.1 Abstract

As a temperature-delineated boundary, the Arctic treeline is predicted to shift northward in response to warming. However, the evidence for northward movement is mixed, with some sections of the treeline advancing while others remain stationary or even retreat. To identify the drivers of this variation, we need a landscape-level understanding of the interactions occurring between climate, tree growth (i.e., radial stem growth), and regeneration. In this study, we assess population regeneration alongside annual tree growth and climate during the 20th century. To do so, we use an age-height model combined with tree height estimates from aerial lidar to predict age structure of 38,652 white spruce trees (*Picea glauca*) at a section of Arctic treeline in the central Brooks Range, Alaska, USA. We then use age structure analysis to interpret the trends in regeneration and tree-ring analysis to interpret changes in annual radial stem growth. Results show that the climate became significantly warmer and drier circa 1975, coinciding with divergent responses of regeneration and radial tree growth. Circa 1975, regeneration of saplings (trees ≤ 2 m tall) decreased compared to previous decades whereas annual growth in mature trees (trees > 2 m tall) increased by 54% after 1975 ($p < 0.0001$, Wilcoxon test). Tree ring width was positively correlated with May - August temperature ($p < 0.01$, Pearson coefficient) during the 20th century. However, the presence of temperature divergence and strong positive correlation

with July precipitation ($p < 0.01$, Pearson coefficient), suggests that continued drying may limit future growth at this section of Arctic treeline. We conclude that while warmer temperatures appear to benefit annual radial stem growth in mature trees, the warmer and drier environmental conditions in spring and summer inhibit regeneration and therefore may be inhibiting the northward advance at this Arctic treeline site. Researchers should consider the interactions between temperature, water availability, and tree age when examining the future of treeline in a changing climate.

1.2 Introduction

Biomes and the ecotones, or transitions, between them are expected to shift as individual species respond to climate change (Körner 2012). The Earth's largest ecotone, the Arctic treeline, extends more than 13,400 km around the circumarctic region (Callaghan et al. 2002a, Ranson et al. 2011), and is believed to be delineated by an isotherm beyond which constraints on physiological processes prohibit the growth and establishment of trees (Sveinbjörnsson et al. 2002, Körner 2012, Paulsen and Körner 2014, Körner et al. 2016). As the Arctic is warming at nearly four times the rate of the global average (Rantanen et al. 2022), the treeline-delineating Arctic isotherm is expected to shift poleward (Körner 2012). If treeline species can keep pace with the shifting isotherm, models suggest that individual trees will increase in size (Körner 2012) and treeline may advance 7 – 20 km poleward per year and displace 11% to 50% of Arctic tundra with woody growth (trees and shrubs) by 2050-2080 (ACIA 2005, Callaghan et al. 2005, Pearson et al. 2013, Zhang et al. 2013). The combination of individual growth and population regeneration of treeline at this scale would have profound local, regional, and global impacts on energy balance (Harding et al. 2002), biodiversity (Skre et al. 2002), ecosystem services

(Callaghan et al. 2002a), biogeochemical cycling (Zhang et al. 2013), carbon balance, and climate-related feedbacks (Wilmking et al. 2006, Pearson et al. 2013).

However, the evidence for such rapid northward advance of Arctic treeline is mixed (Harsch et al. 2009, Van Bogaert et al. 2011, Mamet and Kershaw 2012, Rees et al. 2020, Maher et al. 2021), suggesting a potential delayed response (Körner 2021) and suggesting that temperature alone does not accurately describe treeline position and behavior (i.e., advance, stationary, retreat) (Rees et al. 2020, Maher et al. 2021). For example, in a recent circumarctic meta-analysis of 151 altitudinal and latitudinal treelines, Rees et al. (2020) found that 52.3% of the sites studied showed advancing, whereas 45.6% exhibited no change, and 2.1% showed retreating treeline behavior. Further, they found that variation in treeline behavior was mainly associated with precipitation rather than temperature, during both the growing and non-growing seasons (Rees et al. 2020). Evidence of increased individual tree growth (i.e., radial stem growth) due to warming is also mixed; some treeline sites have shown increased growth while others have mixed or no response, a difference largely attributed to changes in water regimes (Briffa et al. 1998, Barber et al. 2000, Wilmking and Juday 2005, D'Arrigo et al. 2008). Therefore, when attempting to understand what drives the response of Arctic treeline to climate change, researchers must increasingly consider the influence of temperature alongside variables related to water availability (Rees et al. 2020), such as precipitation, snow and vapor pressure deficit (VPD).

Temperature and water availability impact treeline behavior both at the individual level through tree growth and at the population level through regeneration. The influences of temperature and water availability on tree growth at treeline can vary with tree size due to several physiological constraints in saplings, including higher respiration rates (Griffin et al. 2021) and limited root

structures (Smith et al. 2003) compared to mature trees. Here, we consider early life stages as trees < 2 m tall, hereafter referred to as 'saplings'; conversely, mature trees are ≥ 2m tall (Tranquillini 1979). Mature tree growth at treeline generally increases with increasing temperature (Kozlowski et al. 2008, Körner 2012). However, the correlation between temperature and radial stem growth (i.e., the growth of annual tree rings) is fading in areas of the Arctic treeline across the globe (Camarero et al. 2021), particularly in the boreal forest (Briffa et al. 1998, D'Arrigo et al. 2008, Andreu-Hayles et al. 2011), while the correlation between radial stem growth and precipitation typically strengthens. This phenomenon, known as 'temperature divergence,' may suggest that radial stem growth at treeline is switching from temperature- to water-limited (Hofgaard et al. 2019). The causes of this phenomenon, called 'temperature divergence,' are still under debate but some proposals include recent warming, global dimming (i.e., decrease in solar radiation in recent decades), and temperature-induced drought stress which may indicate a shift from temperature-limited growth to water-limited growth (D'Arrigo et al., 2008). Therefore, dissecting the nuances of how temperature and water availability influence growth is necessary to understand the future of this ecotone.

In addition to growth, we must investigate how climate change has influenced population regeneration, as treeline advance cannot occur without population growth. Population regeneration is defined here as the cumulative effect of recruitment and mortality of new trees during early life stages (i.e., several years), hereafter, simply "regeneration." Regeneration is influenced by temperature and water availability (Holtmeier 2009, Brodersen et al. 2019, Holtmeier and Broll 2019). However, investigating treeline regeneration in response to changing temperature and water availability poses several practical challenges that call for the development of novel approaches. Current *in situ* methods which measure forest recruitment,

survival, and individual tree growth via plot-level monitoring or age-structure reconstructions are the gold standard. However, these methods are labor-intensive, restricted to relatively accessible portions of the Arctic treeline, and—in the case of plot-level monitoring—require decades of historical data to capture the current effects of climate change on demographic rates. Further, while Rees et al. (2020) provide the most comprehensive plot-level dataset of circumarctic treeline behavior to date, large portions of Arctic treeline have not been studied as they are difficult to access. Products from satellite remote sensing, such as those derived from Landsat, e.g., Global Forest Cover (Ranson et al. 2011, Hansen et al. 2013), offer access to remote sections of treeline but cannot distinguish between tall shrubs and trees and so greatly overestimate treeline advance (Timoney and Mamet 2020). A more accurate estimate can be obtained via high spatial resolution satellite imagery, but such data do not extend far enough back in time to evaluate the status of treeline advance (Rees et al. 2020). Lastly, the methods to observe treeline must be more easily repeatable to actively monitor changes in treeline behavior in response to climate change.

In this study, we present a novel approach that is uniquely adapted to improve understanding of the impacts of climate change on treeline behavior. Our methodology requires minimal *in situ* labor, approximates historical demographic trends with one year of forest structure data (aerial lidar-derived tree height), and estimates forest regeneration on a scale that better reflects the scale of the Arctic treeline (hundreds of hectares and 10^4 to 10^5 trees) than plot-level studies (typically tens of hectares and 10^2 of trees). We implement this method at an Alaskan Arctic treeline site with the following exploratory goals: (1) to reveal qualitative trends in regeneration of a dominant treeline species (white spruce, *Picea glauca*) during the 20th century and evaluate the trends alongside historical climate; (2) to use tree-ring analyses to

observe if and how growth of both saplings and mature trees at our study site responded to climate change. We hypothesize that warmer but drier conditions in recent decades have caused trees growing at Arctic treeline become more water limited. Therefore, we predict that a study of climate, growth, and regeneration over the 20th century will show that growth and regeneration would decrease if conditions became drier; however, if conditions stayed the same or became wetter, growth and regeneration would increase.

1.3 Methods

1.3.1 Study Area

Field data were collected south of the Brooks Range in Alaska (AK), USA. We established a short (5.5 km) north-south transect at the Arctic treeline along the Dalton Highway (67°59′ 40.92'' N, 149°45′ 15.84''W, 727 m a.s.l.) (Figure 1.1). Along this transect, pockets of boreal forest transition into treeless tundra along the floodplain of the Dietrich River and gently sloping lower elevations before tundra vegetation dominates at only slightly higher elevations.

We obtained monthly measurements from 1900-2015 of temperature, vapor pressure deficit (VPD), and precipitation at the study area from the Integrated Ecosystem Model for Alaska and Northwest Canada (McGuire et al. 2016). The average annual temperature from 2000-2015 was -8.25 ± 0.65°C and the average growing season temperature (May – July) was 7.15 ± 0.91°C (mean ± SD). The area is a semi-arid environment (Simpson et al. 2002), receiving 304 ± 77.1 mm of precipitation per year, 45% of which is snow.

Continuous permafrost underlies the Arctic treeline where tree cover predominantly consists of white spruce (*Picea glauca* (Moench) Voss) with occasional black spruce (*Picea mariana* (Mill.) BSP). The understory is dominated by tundra vegetation such as sedges (e.g.,

Eriophorum spp.), moss and lichen (e.g., *Cladonia rangiferina*), short evergreen shrubs (e.g., *Arctostaphylos uva-ursi*), and low (< 1.5 m) deciduous shrubs (e.g., *Salix* spp., *Betula nana* L., *Alnus* spp.). White spruce, our study species, are monoecious and produce cones every year that shed seeds from late August to September (Walker et al. 2012). To the best of our knowledge, there have been no stand clearing disturbances (e.g., fires, insect outbreaks, stand clearing floods) within the study area in the last 200 years, minimizing transient dynamics associated with stand development and succession that otherwise could confound the effects of climate on demographic history (e.g., self-thinning, succession). We found no evidence of bark beetle outbreaks in the field or in tree cores sampled from the area. There are very few standing dead trees (*personal observation*), likely due to the harsh winter winds and thawing permafrost which can topple dead trees.

1.3.2 Summarizing climate conditions during the 20th century

Using the historical climate data, we calculated the monthly precipitation received as snow (SNO) from the monthly temperature and precipitation means; if the mean monthly temperature was ≤ 0°C, the mean monthly precipitation was considered SNO. The annual amount of SNO received was calculated by summing the SNO during the growth year (Aug – Jul). To better understand the overall growing conditions during the 20th century, we used a modified version of the climate index developed by Barber et al. (2000). The climate index differentiates between cool and moist years (positive values) and warm and dry years (negative values) by subtracting the normalized growing season temperature from normalized growth year precipitation. We modified the months included in the growing season to Jun-Aug and growth year to Sep-Aug based on the observed start and end dates of radial stem growth at our sites (Eitel et al. 2020).

1.3.3 Assessing qualitative regeneration at Arctic treeline

We assessed the qualitative regeneration at treeline by first creating a model fitted with *in situ* data that predicts tree age from tree height (Section *'Age Height Model'*). We then obtained individual tree heights in a 278-ha forest stand using aerial lidar scanning and an individual tree detection algorithm (Section *'Aerial lidar observations of tree height across forest stands'*). The lidar-derived tree height was then used within the age-height model to predict the age of each tree identified by the tree detection algorithm. Static age structure was constructed by binning the number of individuals in each age class into one-year bins (Section '*Constructing static age structure'*). We then interpreted the shape of the static age structure to assess the forest regeneration (Section '*Deducing regeneration from age structure*').

Development of the age-height model from ground observations

Field sampling of tree age and height occurred at six study plots in June 2016 and 2017. All sampled trees were selected within a 20 m radius of a previously established plot center (Eitel et al. 2019). To obtain tree age, a tree core or stem disk was collected from white spruce trees in a random stratified sampling format with five height classes: 0-0.49 m, 0.5-0.99 m, 1-1.49 m, 1.5 – 1.99 m, ≥ 2 m. At each site, one tree from each of the four smallest height classes and three or more trees in the tallest class (≥ 2 m) were selected (n = 70). Additionally, 33 seedlings (≤ 0.3 m) growing in 48 one-meter square quadrants were included (eight quadrants per site, located 10 m from plot center in the cardinal directions; total n = 103).

Tree Age

Seedling age was measured by counting the number of whorls (i.e., annual terminal bud scars) on the main stem while in the field (n = 33). To determine the age of mature trees, cores

were extracted using increment borers (5.15 mm diameter) and stem disks were collected by felling trees. For trees < 5 cm basal diameter, we collected stem disks at basal height (0 cm) (n = 28). In trees ≥ 5 cm basal diameter, cores were extracted at ~ 25 cm height to accommodate the 12" increment borer handle (n = 34). Cores and disks were transported to the Lamont Doherty Earth Observatory's Tree Ring Lab (LDEO-TRL) for tree-ring measurements. Cores and stem disks were stored in cool, dry conditions before being mounted, sanded with progressively finer sandpaper, and scanned using a high-resolution flatbed scanner (3200 dpi resolution). Tree-ring boundaries were marked digitally on the scanned images to the micrometer resolution (0.001mm) and widths were measured and cross-dated using the computer software programs CooRecorder and CDendro 8.1 (Larsson 2016, Stockton Maxwell and Larsson 2021). The age of a tree was calculated as the number of rings between the innermost ring, or pith, and the ring corresponding to 2016, when height was measured. In cases where the cores did not contain a pith (23% of samples), the number of years to the pith was estimated by using CooRecorder's digital pith estimator. In these cases, the estimated number of rings to the pith ranged from 1-7 rings. Ring widths were cross-dated against an existing white spruce tree-ring chronology site near Dalton Highway in Alaska (68.5N, -141.63W) (Jacoby and Davi 2000). Cores that could not be cross-dated, either due to very low correlation with the Dalton tree-ring chronology or rot near the pith, were excluded from the study. The final dataset for the age-height model included 94 trees.

We defined 'tree age' as a tree's age in 2016, when height was measured. The 'year of establishment' is the year a tree germinated. Because cored trees were sampled at ~25 cm rather than at basal height, the true age of cored trees would have been slightly older than the age at the core's pith. To compensate for the time it took a cored tree to grow to 25 cm tall, we added 14

years, the equivalent to the mean age of a 25 cm tall tree in an age-height model of only trees sampled at basal height (trees aged via whorls or stem disks; n = 63).

Tree Height

Tree height was measured in the field (for trees < 1.5 m tall) or by high-resolution terrestrial lidar scans (TLS) of the study plots taken in June 2016 with a Leica Scan Station C10 (Leica Geosystems Inc., Heerbrugg, Switzerland, see Maguire et al., 2019). The laser instrument has a beam divergence of 0.14 mrad, a scan rate of up to 50,000 points s^{-1}, a maximum sample density of < 1 mm, and a maximum range of 134 m at 18% albedo. The nominal distance accuracy is 4 mm and the nominal positional accuracy is 6 mm. Each study plot was scanned from four to six positions to minimize occlusion by vegetation canopies. Three common reflectance targets surrounding each plot were geolocated with a global positioning system (GPS - Trimble R7, Trimble, Dayton, Ohio) and an external Zephyr Geodetic antenna. Both the vertical and horizontal accuracy of the GPS are ± 5 mm (Trimble, Dayton, Ohio). For each plot, scans were georegistered using these common reflectance targets using Cyclone 9.1 software (Leica Geosystems Inc., Heerbrugg, Switzerland). UTM coordinates for each tree were manually extracted from the georegistered TLS point cloud for the top of each tree crown. Crown height for each tree was derived from the georegistered TLS point cloud by manually identifying the top of crown and base of bole laser returns, respectively, using Cyclone 9.1 and calculating the difference of the z-values of UTM coordinates (1 cm resolution).

Age-Height Model

Age and height were log-transformed to achieve normality and homoscedasticity prior to fitting a simple linear model. In linear space, the linear model becomes a power function with the form

$$y = b * x^m \quad \textbf{Eq. 1.1}$$

where y is tree age, x is tree height, and b and m are model coefficients describing the y-intercept and rate of increase, respectively. To obtain posterior distributions of coefficients b and m, we fit the linear model to a random subset (75%) of the log-transformed data for 100,000 iterations in R statistical software (R Core Team 2021). Model iterations which were identified as heteroscedastic using a Breusch-Pagan test were excluded from the study (0.4%), resulting in 99,638 final iterations. Model fitting parameters (i.e., r^2 and root mean squared error, RMSE) were calculated for each model iteration.

Aerial lidar observations of tree height across forest stands

An individual tree detection (ITD) algorithm (Silva et al. 2016) identified the location and height of each tree within five ALS tiles containing the six study plots taken by the Alaska Department of Transportation (Hubbard et al. 2011) in May and July 2011 (Figure 1.1b) covering 278 ha of Arctic treeline. ALS data were collected by a Leica ALS60 sensor mounted on a Cessna Caravan 208Bs aircraft (Hubbard et al. 2011). ALS data were processed using LAStools (Isenburg 2017) in three steps using the lidar point cloud data to ultimately obtain the canopy height model. First, ground returns were classified using progressive triangulated irregular network densification algorithm (Axelsson 2000), to create a one-meter resolution digital terrain model. Second, height above ground was normalized by subtracting the elevation of the digital terrain model. Lastly, a 0.5-m resolution canopy height model was created. ALS-

derived 0.5 m canopy height models were smoothed by a 3 × 3 mean filter to remove spurious local maxima caused by tree branches, and individual trees were detected using fixed treetop window size of 3x3 (Silva et al. 2016). In addition, we limited the study to trees ≥ 30 cm tall as is typical in lidar studies elsewhere in at the Arctic treeline (Streutker and Glenn 2006, Naesset and Nelson 2007).

To ensure the trees included in the study were white spruce, as opposed to tall *Salix spp.*, the tiles were visually classified into six land cover types using high resolution (1.8 x 1.8 m) World-View 2 (WV-2) imagery in QGIS (QGIS Development Team 2022): white-spruce-dominated canopy, tundra, rivers, ravines, roads, and pipeline. Only trees within the spruce-dominated canopy were considered in this analysis. To reduce the influence of an anthropologically created edge and/or hydrology on growth rate, trees were excluded from the study if growing within a 20 m buffer of roads (Dalton highway and pull outs) and the Dietrich River (flood plains) as well as those within 15 m of ravines and the Dalton Highway pipeline. Such supervised classification based on collocated imagery of shrubs is commonly done with great success (Timoney and Mamet 2020).

Constructing static age structure

To obtain the static age structure of our study area, we used the age-height model (Section '*Age-Height Model'*) to predict the age of each tree detected in the ALS tiles (Section '*Aerial lidar observations of tree height across forest stands'*). To ensure that the error of the age-height model would not alter our conclusions of regeneration, we propagated the model error into the age structure in the following manner. First, we randomly sampled the posterior distributions of the parameters once (posterior distributions were obtained by fitting the model 100,000 times) and predicted the age of each tree detected in the ALS tile. Then, we constructed

age structure by binning the number of trees in each one-year age class. We repeated this process 1,000 times starting with another random sample (with replacement) from the posterior distributions each time to create 1,000 possible versions of age structure at our study area. Then, we averaged the number of individuals in each one-year bin across the 1,000 age structures to obtain a mean and 95% confidence interval of the number of individuals in each age class. Lastly, because aerial tree detection of trees was limited to trees ≥ 30 cm tall (Section '*Aerial lidar observations of tree height across forest stands'*), the age structure was truncated to the corresponding age (i.e., 16 years according to the age-height model).

Deducing regeneration from age structure

We deduced regeneration by observing the shape of static age structure, or the number of trees in each age class at a given time. The age structure in mature, undisturbed forests has many saplings and exponentially fewer old trees (e.g., negative exponential shape). This shape, called a Type III survival curve, is representative of a forest that is continuously regenerating and therefore maintaining or growing the population (Vlam et al. 2017). However, if a regeneration has recently failed to recruit new individuals into the population, the static age structure is unimodal: the drop in older trees is due to accumulated mortality, while the drop in younger trees is due to decreased regeneration relative to previous rates. In this way, the shape of a forests' static age structure is indicative of the relative rates of regeneration influenced by favorable or unfavorable conditions (Vlam et al. 2017).

1.3.4 Radial stem growth during the 20th century

Growth of saplings and mature trees before and after 1975

Circa 1975, climate factors, tree ring chronologies, and tree age structures all underwent notable changes (see Results). Therefore, we further analyzed changes in growth in two periods: before and after the year 1975. To evaluate the degree to which the growth rate of saplings and mature trees varied with tree age before and after 1975, we repurposed the tree cores and disks that were collected and measured for tree age (see Section '*Tree Age'*). Growth rate was calculated from the raw ring width as the basal area increment per year, or BAI ($cm^2\ yr^{-1}$). BAI was derived by first calculating basal area over the tree's lifetime via the area of a circle where the radius is the cumulative sum of ring widths from the pith to the respective year. BAeis then the difference in basal area between the current and previous year. We then developed two generalized linear models with the form

$$y_{before} = B_0 + B_1 a + \epsilon \qquad \textbf{Eq. 1.2}$$

$$y_{after} = B_2 + B_3 a + \epsilon \qquad \textbf{Eq. 1.3}$$

where y is growth rate and the subscript indicates *before* or *after* 1975; a is tree age; B_0 and B2 are the y-intercepts; and B_1 and B_3 are coefficients.

We assembled separate datasets for saplings and mature trees, and applied both models to each. Both datasets included cores with complete ring records from pith to 2016. Missing rings, which frequently occur in conifers during particularly stressful years (e.g., defoliation or dry growing conditions; see Wilmking et al. 2012a, Leland et al. 2016, Novak et al. 2016), were identified via cross-dating and interpreted as zero growth. We considered a sapling to be < 2 m tall, which is generally equivalent to < 50 years old (see Results, Figure 1.4a). However, because the oldest trees established after 1975 were 40 years (i.e., oldest in 2016), we limited our analysis of saplings to those ≤ 40 years old. Additionally, we restricted our data set for saplings to basal

area grown during the period in which the tree was established to avoid any unintended bias (i.e., we excluded cases where trees established before 1975 grew after 1975). Outliers beyond the 5th and 95th percentiles were removed to reduce noise in evaluating relationships. The final data set for saplings included 59 trees with 1,483 observations of growth rate. For the analysis of mature trees, we selected trees ≥ 50 years old (≥ 2 m tall; see Results) which grew both before and after 1975, resulting in 14 trees with 910 observations of growth rate (age range: 68 to 153 years).

Because growth rate was non-normally distributed, we employed generalized linear models fit by maximum likelihood estimation (Laplace Approximation) using the 'lme4' package in R (Bates et al. 2015). We selected the best distribution and link function by comparing the Akaike Information Criterion (AIC) (Akaike 1973) of models with two types of distributions (i.e., Gamma and Poisson) and three types of link functions (i.e., 'log', 'inverse' and 'identity' link functions). For both saplings and mature trees, we selected the gamma distribution with 'identity' link function because it had the lowest AIC, and therefore best fit. We added tree ID as a random effect to address the repeated sampling structure of our data (Supplementary Material Table 1.1). However, since this made the sapling models singular, the random effect was retained only in the mature tree model. We then compared the model equations (Eq. 1.2 and and Eq. 1.3) within each group (saplings and mature trees). For the sapling models, we used a t-test while the random intercept of the mature tree models required a z-test (Bates et al. 2015). A significant difference between the two models would indicate that the relationship between age and growth rate changed after 1975.

Relationships between radial stem growth and 20th century climate

We compared the tree-ring width record with meteorological data to elucidate the effects of temperature, precipitation, VPD, and SNO on radial stem growth during the 20th century. To

ensure that the trees selected for tree-ring analysis exhibited little-to-no age-related growth trends, we limited our sample to trees whose cores spanned at least 100 years from 1900-2015 (sampled in 2016). The radial-growth sample includes 22 cores from our six study plots, 17 of which cover the entire study period and the remainder covering at least 103 years (mean age 141 years; range: 103 to 232 years). Therefore, this tree-ring analysis is representative of only mature white spruce trees at the Arctic treeline study site.

Raw tree ring widths were used to build ring width chronologies and then compared to monthly climate during the 20th century. Following standard dendrochronology practices (Cook and Kairiukstis 1990), the ring widths were detrended using two methods: (1) a modified negative exponential (MNE) which removes age-related changes in ring width and (2) a two-thirds spline which ensures a minimum loss of low-frequency variance (Cook 1985, Cook et al. 1995). Using the resulting detrended data, we built two mean tree-ring chronologies (TRC) which provide annual tree-ring width. The detrended data were whitened prior to averaging using an autoregressive time series model. The chronologies were truncated to the year in which the sample depth (number of cores in the chronology) was substantial enough to create a minimum subsample signal strength of 0.85 (Cook and Kairiukstis 1990).

Pearson correlations coefficients, *r*, were calculated from the TRC and monthly climatic data from previous January to current September. Stationary bootstrapping was used to calculate the significance and confidence intervals of each correlation according to Politis and White (2004). Correlations were considered significant at $\alpha = 0.01$. To elucidate how the climate variables which were significantly correlated with TRC changed over the 20th century, we compared the mean monthly climate before and after 1975 using a t-test.

We used the two chronologies to satisfy different purposes: First, we interpreted the MNE chronology as analogous to that of annual production or growth since the effect of detrending with the MNE method is generally modest in mature trees (Cook and Kairiukstis 1990). This was corroborated by the fact that there was no major difference between the correlations of the MNE chronology and climate and those of raw ring width and climate. Therefore, correlations between climate and the MNE chronology can be interpreted as the correlations between climate and annual growth. We also evaluated the stability between TRC, radial stem growth, and climate during the 20th century by computing 31-year rolling correlations between the standard TRC and the mean monthly temperature and precipitation to assess divergence. Tree-ring analyses were facilitated using the R package 'dplR' (Bunn et al. 2010) for detrending and building chronologies, and the R package 'treeclim' (Zang and Biondi 2015) for conducting climate analyses.

1.4. Results

1.4.1 Climate during the 20th century: Before and after 1975

We found that the climate index decreased after 1975, revealing a significantly warmer and drier climate compared to previous decades ($p < 0.001$; Table 1.1, Figure 1.2). For example, from 1900 to 1975, only 37% of the years were classified as warm and dry while the remainder were typically cool and wet. However, from 1975 - 2015, the number of years classified as warm and dry was much higher at 74%. This shift to a warmer and drier climate is reflected in the annual temperature, precipitation, and SNO during the 20th century (Figure 1.3). After 1975, annual temperature increased by 1°C (t-test, $p < 0.001$) (Table 1.1; Figure 1.3a). However, growing year (August-July) precipitation remained relatively stable throughout the 20th century ($p > 0.05$) (Table 1.1, Figure 1.3c). The growing year SNO decreased significantly by an average

of 25.7 mm after 1975 ($p < 0.01$) (Table 1.1, Figure 1.3d). The drying trend was not reflected in annual VPD ($p > 0.05$) (Table 1.1, Figure 1.3b); however, summer months were significantly drier after 1975 relative to before (Table 1.1, Figure 1.3*f*).

For coherency and conciseness, we present only trends in monthly climate variables which were significantly correlated with TRC (see Section 3.4.1). Trends in monthly climate variables are generally similar to annual trends, with the exception of VPD. Mean temperatures during spring and summer (i.e., May, June, July, and August) increased by 0.9 – 1.4°C after 1975 ($p < 0.0001$) (Table 1.1, Figure 1.3e). Additionally, there was no significant difference in July precipitation between the periods prior to and after 1975 ($p > 0.05$) (Table 1.1, Figure 1.3g). SNO in March and May decreased by 38% and 50% after 1975, respectively ($p < 0.01$), while September SNO remained stable throughout the study period ($p > 0.05$) (Table 1.1, Figure 1.3h). VPD increased in May and June by 12% and 5%, respectively ($p <0.001$), and decreased by 33% in February ($p < 0.01$) (Table 1.1, Figure 1.3f).

1.4.2 Assessing regeneration: tree age-height relationship and stand-level height and age structure

Figure 1.4a shows the relationship between age and height in log and linear space. The value of the y-intercept, *b*, and the exponential rate of increase, *m*, were 32.44 ± 0.71 and 0.58 ± 0.01, respectively (mean ± SD). The average r^2 value of the model was $0.8932 \pm 9.90 \times 10^{-8}$ (mean ± SEM) and ranged from 0.8453 to 0.9293. The RMSE was 23.8 years.

The individual tree detection algorithm identified 38,652 white spruce trees at our study area. The average observed height was 2.46 ± 1.47 m (mean ± SD) and the maximum height was 15.28 m. The stem density at the study plots was 427.07 ± 46.04 stems ha^{-1} and ranged between

358.1 – 501.34 stems ha^{-1}. At the landscape level (i.e., across the ALS tiles), the average stem density was 513.12 ± 252.86 stems ha^{-1} and ranged between 100 – 1400 stems ha^{-1}. The height structure at the study area revealed an exponential relationship in stems 1.4 m – 15.28 m tall (Figure 1.4b). However, the number of stems in each 0.1 m bin between 0.3 m (lowest detectable height) and 1.4 m tall were approximately equal.

The age structure at our study area was unimodal with a peak in the number of trees which were 36 years old in 2011 (year of aerial lidar scanning; see Section 2.3.2) (Figure 1.4c), which corresponds to a tree established circa 1975 (Figure 1.4a). The predictions of individual tree age ranged from 16 – 182 years old. The average and median age of trees was 48.4 and 47 years old, respectively. Data could not be derived for trees less than 16 years old as these trees were < 0.3 m tall and therefore undetectable by the individual tree detection algorithm (see Section 2.3.2). According to age structure analyses (see e.g., Vlam et al. 2017), unimodal age structure such as that observed in Figure 1.4c is indicative of a population which has recently failed to recruit new individuals, so regeneration has decreased.

1.4.3 Growth rate of saplings and mature trees

The models of growth rate in saplings and mature trees were both statistically different from the null model (ANOVA, chi-squared $p << 0.0001$), confirming that growth rate did vary with age. In saplings, growth rate increased with age, but this relationship did not differ after 1975 (Table 1.2, Figure 1.5a). However, in mature trees, the relationship between growth rate and age did change significantly between the two periods (Table 1.2, Figure 1.5b). Before 1975, growth rate decreased modestly with every additional year in age (B_1 = -0.2 cm^2 $year^{-1}$; Table 1.2, Figure 1.5b), but after 1975, growth rate increased significantly with age by 1.67 cm^2 $year^{-1}$

(z-test, $p < 0.0001$). The RMSE of the sapling and mature tree models are 1.20 and 0.39 $cm^2\ year^{-1}$, respectively.

1.4.4 Tree-ring width and radial stem growth vs. climate

Tree ring-climate analyses

The MNE tree ring chronology echoed the results of radial stem growth in mature trees: After 1975, tree ring width increased by 54% relative to previous decades (Figure 1.6; $p < 0.0001$, Wilcoxon test). The trend in radial stem growth is less prominent (7% increase; $p = 0.64$, Wilcoxon test) in the spline chronology due to the intrinsic nature of the detrending method. The correlations between the MNE tree ring chronology and the monthly climate variables highlighted some prominent trends between annual growth (proxy as TRC) and environmental conditions (Table 1.3). Generally, warmer springs (May) and summers (June, July, August) of the current and previous years were associated with increased annual growth. Additionally, annual growth increased when the spring (May) and early- to mid-summer (June, July) of the current and previous year were drier (higher VPD) and when the previous February was wetter (lower VPD). Precipitation in July of the previous year was positively correlated with annual growth the following year. As SNO decreased in the spring (March, May) and fall (September) of the previous year, annual growth increased. Lastly, the correlation between climate index and TRC was negative ($r = -0.43 \pm 4.6 \times 10^{-7}$, mean ± SEM; p-value < 0.0001, $df = 78$), suggesting that annual growth increased as the climate became warmer and drier.

Temperature divergence

The 31-year running correlations between TRC, current June temperature, and July precipitation revealed some signs of temperature divergence in our tree ring chronology. We

examined the correlations with June temperature and July precipitation specifically because their correlations with the spline chronology from 1900-2015 was statistically significant (see Methods). Overall, the correlation between temperature and TRC weakened over the 20th century but was variable (Figure 1.7). For example, c. 1955, the correlation between TRC and current June temperature decreased and became statistically insignificant after circa 1955. After circa 1965, June temperature correlations began increasing again, only to decrease circa 1988. Meanwhile, the correlation between TRC and current July precipitation increased steadily until circa 1980 before decreasing again. The running correlations between TRC and current July precipitation were never statistically significant.

1.5 Discussion

Our findings reveal that climate at our latitudinal treeline site in Alaska became warmer and drier after circa 1975. Concurrently, the unimodal age structure suggests that forest regeneration decreased circa 1975 relative to previous decades, corroborating our hypothesis that warmer but drier conditions would decrease regeneration. However, in contrast to our hypothesis, our analysis of growth rate before and after 1975 showed that the warmer and drier climate did not appear to affect growth rates in saplings but increased the growth of mature trees substantially. Radial stem growth of mature trees was substantially larger after 1975 despite the overall drying trend, suggesting that mature tree growth was not or was minimally water-limited during the 20th century. However, the tree ring chronology of mature trees exhibited positive correlations with July precipitation as well as temperature divergence starting in mid-1900s, suggesting that a shift towards water-limitation could occur if drying trends continue (Andreu-Hayles et al. 2011, Hofgaard et al. 2019). Together, our results show divergent responses of

regeneration and radial stem growth of white spruce growing at Arctic treeline in response to the same climatic stimuli.

The decrease in regeneration beginning circa 1975 was likely driven by changes in the climate. Success in early life stages relies on adequate water availability during germination (Angell and Kielland 2009), establishment (Walker et al. 2012), and seedling development (Angell and Kielland 2009) because smaller root systems make saplings highly vulnerable to water stress (Smith et al. 2003). Additionally, saplings are more likely to survive when well-covered by snow during winter since the snowpack decouples them from the harsh conditions of the free atmosphere (Körner 2012, 2016, Renard et al. 2016). While we do not have data available for tracking snow depth during the 20th century, we observed significant decreases in precipitation received as snow (SNO) during spring (i.e., -38% decrease in March and -100% decrease May after 1975) and fall (i.e., - 28% decrease in September) in the years after 1975. Such a shift could have decreased the snow depth and therefore exposed seedlings to the free atmosphere earlier, ultimately decreasing survival.

While approximately half of the studied Arctic treeline sites have advanced during periods of warming (Rees et al. 2020), advance seems unlikely at our study site. The observed decrease in population regeneration at this site suggests that the tree population has not grown, and therefore treeline has not advanced. Other stationary treeline sites around the circumarctic had similar responses to climate trends such as warmer springs and summers and drier springs and falls (Rees et al. 2020). Further, the decreasing moisture gradient from western to eastern Alaska (Wilmking and Juday 2005) may explain why treeline has advanced on the Seward Peninsula (Suarez et al. 1999, Lloyd and Fastie 2002) but not at our study site in the Brooks Range. Of course, the decreased regeneration could also be explained by non-climatic factors.

Many seedlings, saplings, and mature trees within the vicinity of and at our study site exhibited mild to severe browsing damage from snowshoe hares *(personal observation*). In multiple cases, snowshoe hare browsing girdled the stem and killed the tree, highlighting the strong control herbivores can have on tree survival and treeline advancement (e.g., see Olnes et al. 2018). Other factors could have affected regeneration but were beyond the scope of this study such as nitrogen-limitation (Gustafson et al. 2021), permafrost thaw (Lloyd 2005, Maher et al. 2021), nutrient availability, and seed dispersal (Kambo and Danby 2018a, 2018b). While we cannot definitively conclude that climate was the main driver in decreasing regeneration after 1975, the striking synchronicity of the shift in climatic conditions and the shift in regeneration, plus the knowledge demonstrated from prior research that climate constrains regeneration in tree populations, strongly suggests a mechanistic link.

In contrast to the decrease in regeneration of saplings, the growth rates of mature trees increased in response to warming and drying after circa 1975. This finding contradicts our hypothesis that both growth and regeneration would decrease in response to warming and drying. However, these differing responses may be explained by studies which show that climate change influences saplings and mature trees differently, often because of their difference in size (Körner 2012, 2016, Stovall et al. 2019). For example, larger, mature trees may be able to grow under drier conditions than saplings because of their more developed root systems which can more easily access deeper water reserves (Körner 2012, Kambo and Danby 2018a, 2018b). While it appears that the growth response of mature trees at our site is not currently water-limited, the presence of temperature divergence in our tree ring chronology suggests that continued drying and warming may cause future water-limitation to impede growth (Hofgaard et al. 2019, Peters et al. 2021).

Surprisingly, our results show that relative to before 1975, the growth of saplings did not change significantly after 1975. At face value, one might conclude that the growth of saplings was not impacted by warming and drying conditions, although seedling and sapling mortality were not measured and may confound this conclusion. This presents a question for future research: How and why would warming and drying conditions affect regeneration but not sapling growth? Recent studies suggest that sapling survival depends on overcoming higher respiratory carbon losses (Griffin et al. 2021) which may in turn affect growth. Furthermore, the carbon balance constraints resulting from high respiratory rates and low photosynthetic rates are exaggerated at treeline relative to the southern range limit of white spruce (Griffin et al. 2022, Schmiege et al. 2022). Future research is necessary to identify the physiological explanations for this finding and might consider investigating the growth and carbon balance of both small and large spruce trees growing in different water regimes.

The age-height model enabled us to predict the age of trees detected by aerial-lidar and therefore expand our scope to the landscape level. Tree height is not typically an accurate proxy for tree age due to several factors which can stunt or accelerate the growth of individuals such as gap dynamics or environmental (Kuuluvainen et al. 2002). However, in this population we validated the relationship and found a strong relationship between age and height ($r^2 = 0.82$, RMSE = 23.8 years). More research is required to understand this unusually strong relationship in trees; however, it is likely because trees at our study site are well spaced, therefore the effects of gap dynamics and competition are limited. We do observe an increase in the variation of age among mature trees, possibly due to variation in environmental stress. When studying other species or older populations, we recommend verifying age-height models, as the mature trees in this study are still relatively young in a general context.

Future research may advance the method presented here by improving the predictive accuracy of the age-height model, diversifying the species in the model, and using lidar with improved vertical accuracy to decrease the height detection threshold of individual trees. Adding other predictor variables to the age-height model, such as diameter at breast height or distance to nearest neighbor, could greatly improve model accuracy. Additionally, developing age-height models for other treeline species would make our methods more widely applicable. Lastly, using higher resolution aerial lidar scans (> 8 returns per m^2) and higher vertical accuracy in future studies would enable the observation of trees below the height detection threshold (i.e., 30 cm) and decrease the possibility that small shrubs (i.e., > 30 cm tall) were misclassified as spruce seedlings and vice versa. If small trees were misclassified as shrubs, then regeneration could be higher than reported. Conversely, if shrubs were misclassified as small trees in the sample population assessed in this study, regeneration was even more negatively affected by climate.

Conclusion

The results of our study show that at our Arctic treeline site in interior Alaska, shifts towards a drier and warmer climate were highly associated with a decrease in regeneration of saplings and increased growth of mature trees. Together, this lends evidence that this section of treeline has remained stationary since circa 1975 while mature tree growth has increased. However, only one or two successful cohorts are necessary to advance treeline position (Körner 2016). Should the many stochastic factors necessary for increased regeneration temporarily align, this section of the Arctic treeline may advance. Therefore, we stress that continued monitoring is necessary to properly assess current treeline behavior. Our novel method for monitoring regeneration offers a means to do so that is less labor-intensive than traditional methods. Wide application of this method has the potential to open research to more less well-

documented locations of the Arctic treeline and clarify the varied responses of Arctic treeline to climate change.

1.6 Acknowledgements and Author Contributions

Funding for this research came from NASA Terrestrial Ecology grant NNX15AT86A and NASA ABoVE grant (Eitel-01). JEJ, KLG, NB, JUHE, and LAV developed the initial framework and objectives of the study. JEJ, KLG, NB, JUHE, LAV, and AJM assisted in data collection in the field. CS extracted tree location and height using the ITD algorithm. Tree ring analysis was led by JEJ and RO. RD and LAH were partly supported by NSF OISE-1743738 and NSF- 2124885. JEJ drafted the initial version of the manuscript. All coauthors contributed to the interpretation of the results and revisions of the manuscript. We thank Hélène Genet at the University of Alaska Fairbanks for providing us with historical climate data of our study site via the Scenarios Network for Alaska and Arctic Planning (SNAP) database. We are also grateful for the support provided by the staff of the ABoVE Fairbanks logistics office, notably Sarah Sackett. We would also like to give a special thanks to Sarah Bruner and Jyoti Jennewein for assistance in the field; Arjan Meddens for assistance with geospatial analysis; Mukund Rao for advice in analyzing tree rings; and Duncan Menge for statistical advice and collaboration.

1.7 Figures and Tables

Table 1.1. Comparison of annual and monthly climate means at Arctic treeline in central Brooks Range, AK before and after 1975. The selected months are presented because they are significantly correlated with the MNE chronology (TRC; see Table 1.3). Terms in bold are statistically different after 1975 (p < 0.01, t-test).

Climate Variable	Annual[1] or Month	Mean ± Standard Deviation		Increase or Decrease	t-statistic	df	p-value[2]
		Before 1975	After 1975				
Temperature	Annual	-10.1 ± 1	-8.8 ± 1	+	6.52	83.2	****
	May	0.3 ± 1.4	1.7 ± 1.9	+	4.15	65.6	****
	Jun	7.6 ± 1.1	8.6 ± 0.9	+	5.02	96.7	****
	Jul	9.7 ± 0.9	10.7 ± 0.9	+	5.63	82.0	****
	Aug	6.9 ± 1.2	7.8 ± 1.3	+	3.81	75.9	***
VPD	Annual	0.14 ± 0.01	0.14 ± 0.01		0.686	73.4	ns
	Feb	0.03 ± 0.03	0.02 ± 0.02	-	-3.14	106.	**
	Apr	0.08 ± 0.02	0.08 ± 0.02		0.07	102.	ns
	May	0.25 ± 0.03	0.28 ± 0.03	+	3.86	65.5	***
	Jun	0.41 ± 0.03	0.43 ± 0.04	+	3.99	75.3	***
	Jul	0.37 ± 0.04	0.38 ± 0.04		1.87	83.2	ns
Precipitation	Growing Year	310.6 ± 49.6	298.9 ± 48.4		-1.23	87.3	ns
	Jul	47.8 ± 23.4	54.8 ± 24.1		1.52	80.5	ns
SNO	Growing Year	162.3 ± 38.6	136.6 ± 43.6	-	-3.17	77.4	**
	Mar	15.1 ± 13.1	9.4 ± 8.5	-	-2.84	110	**
	May	6.2 ± 7.9	3.1 ± 3.6	-	-2.88	110	**
	Sep	36.5 ± 24.9	26.4 ± 32.6		-1.72	63.3	ns
Climate Index	Annual	0.5 ± 1.3	-0.8 ± 1.3	-	-5.40	88.6	****

[1] Annual means were calculated from Jan-Dec and growing year from Aug-Jul.

[2] * p < 0.05, ** p < 0.01, *** p < 0.001, ****p < 0.0001, ns p > 0.05.

Table 1.2. Coefficient estimates, standard error, and significance for fixed effects in the models for growth rate of white spruce saplings and trees at Arctic treeline in the central Brooks Range, AK. Bold terms are significant (p < 0.0001).

Model	Maturity	Fixed Effect	Random Effect	Symbol	Coefficient Estimate	Std. Error	t-value	P-value[1]
Model 1	Saplings	Intercept	-	B_0	-0.73	0.46	-1.60	0.111
		Age		**B_1**	**1.34**	**0.07**	**18.9**	**< 0.0001**
		Period		B_2	0.09	0.69	0.13	0.898
		Age*Period		B_3	0.02	0.10	0.20	0.842
Model 2	Mature Trees	**Intercept**	**Tree ID**	**B_0**	**160.4**	**22.3**	**7.20**	**< 0.0001**
		Age		**B_1**	**-0.196**	**0.035**	**-5.65**	**< 0.0001**
		Period		**B_2**	**-130.6**	**17.6**	**-7.44**	**< 0.0001**
		Age*Period		**B_3**	**1.87**	**0.162**	**11.56**	**< 0.0001**

[1] p-values derived from a t-test for saplings and from a Z-test for mature trees

Table 1.3. Significant Pearson correlation coefficients, r, between monthly climate and the mean negative exponential tree ring chronology (TRC) from 1900-2015 ($p \leq 0.01$) of white spruce trees at Arctic treeline in the central Brooks Range, AK. Months of the previous year are lower case abbreviations, and the current year are in all caps. Values within parentheses indicate the 99% confidence interval around the mean.

Temperature		VPD		Precipitation		SNO	
Month	r	Month	r	Month	r	Month	r
May	0.37 (0.14, 0.53)	Feb	-0.21 (-0.43, -0.02)	Jul	0.21 (0.03, 0.39)	Mar	-0.27 (-0.47, -0.05)
Jun	0.36 (0.05, 0.52)	May	0.31 (0.04, 0.49)			May	-0.25 (-0.38, -0.10)
Aug	0.25 (0.02, 0.42)	Jun	0.30 (0.02, 0.47)			Sep	-0.24 (-0.39, -0.04)
JUN	0.48 (0.23, 0.62)	JUN	0.43 (0.21, 0.61)				
JUL	0.41 (0.12, 0.54)						
AUG	0.27 (0.03, 0.48)						

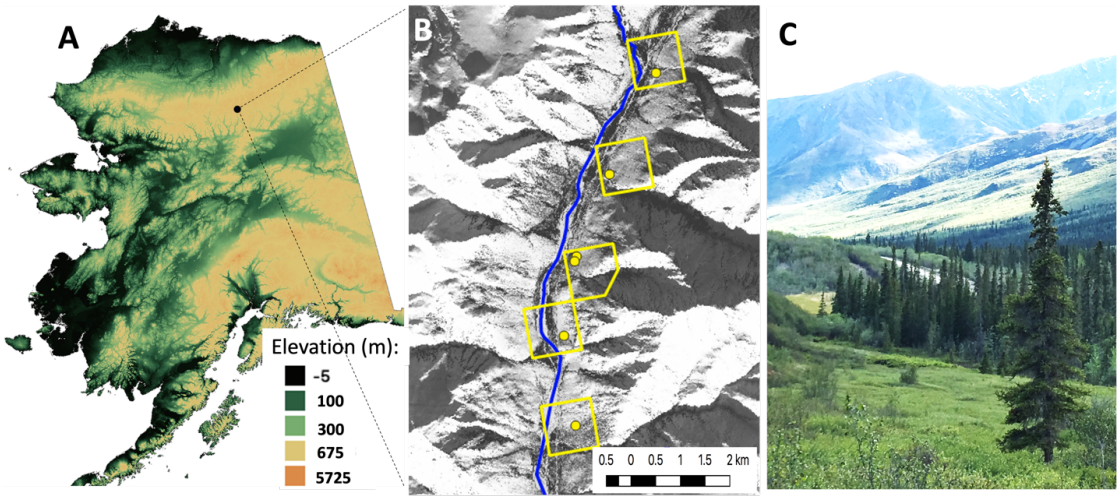

Figure 1.1. The study area at Arctic Treeline in the central Brooks Range, AK, USA. (A) Elevation map of Alaska with site location. (B) Black and white aerial imagery of the study area in winter, highlighting snow covered tundra (white) and tree cover (black). Yellow dots represent the location of six study plots, the Dietrich River as a blue line and the boundaries of the five forest stands as yellow boxes. (C) Photograph of the northernmost study plot looking south at treeline.

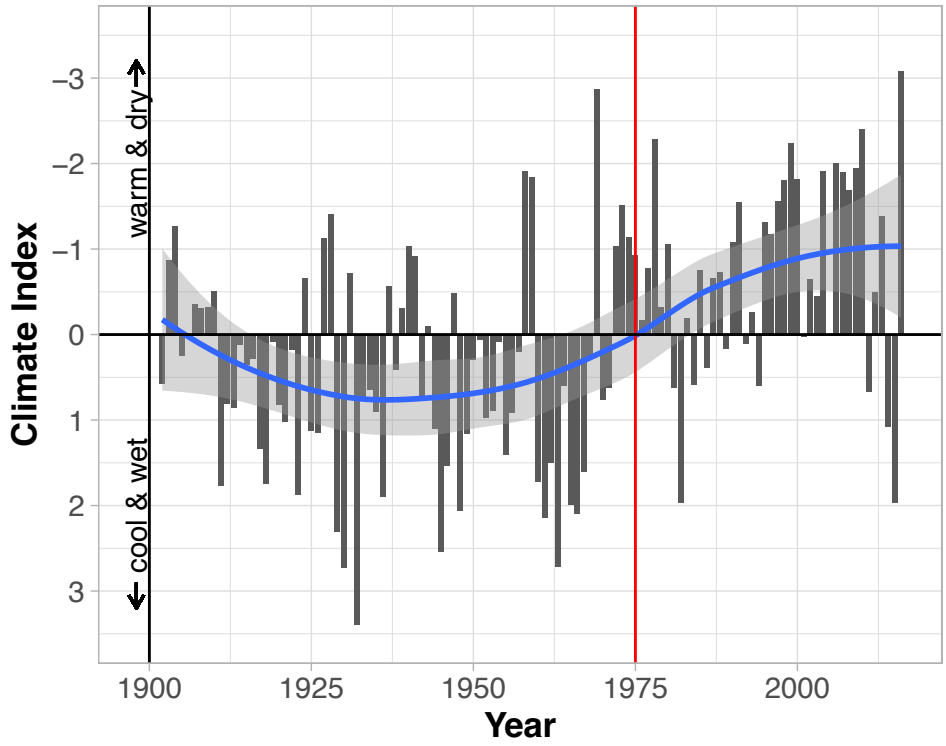

Figure 1.2. Climate trend from 1900-2016 at Arctic treeline in central Brooks Range using the climate index developed by Barber et al (2000). The index differentiates between relatively cool, wet years (positive values) and warm, dry years (negative values). A loess smoothing curve (blue line) with 95% confidence intervals (grey shading) shows the overall trend through time. The vertical red line indicates the year 1975.

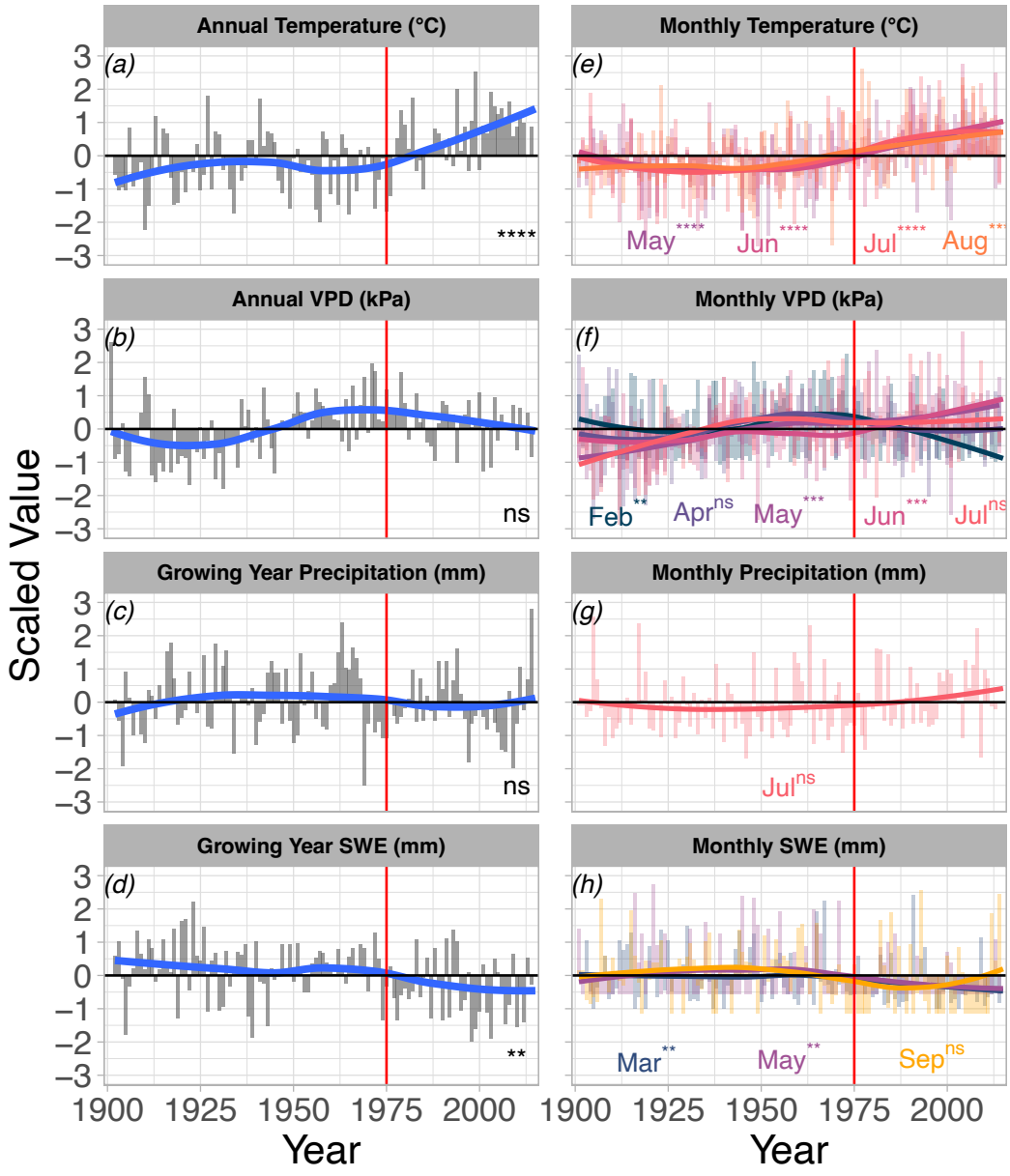

Figure 1.3. Trends in yearly (a, b, c, d) and monthly (e, f, g, h) climate means from 1900 – 2015 at Arctic treeline in central Brooks Range, AK. Annual means were calculated from Jan-Dec and growing year from Aug-Jul. The selected monthly climate variables are presented because of their significant correlations with tree ring width during the 20th century (see Table 1.1). The y-axis of all variables is expressed in scaled units where zero is record mean (1900 – 2015) and units are standard deviation. Loess smoothing curves (blue line for annual means; colors for monthly means, legend on each panel) highlight the overall trend through time. The vertical red line indicates the year 1975. Asterisks show p-values from t-tests of the mean before and after 1975 (* $p < 0.05$, ** $p < 0.01$, *** $p < 0.001$, ****$p < 0.0001$, ^{ns} $p > 0.05$).

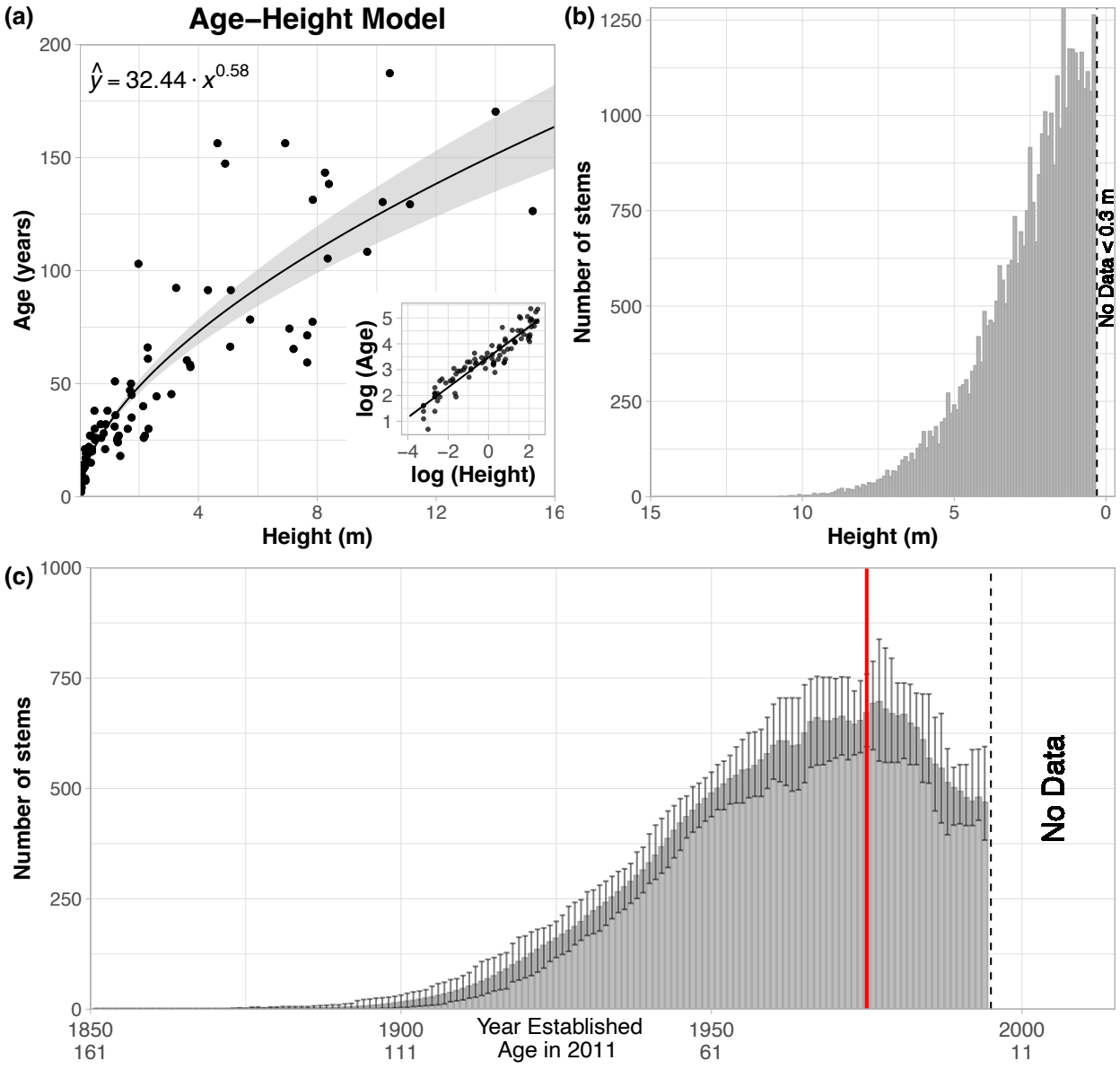

Figure 1.4. Forest structure at Arctic treeline in central Brooks Range, AK. (a) Relationship between age and height for white spruce at the Alaskan treeline (black line is the mean and grey shading is the 95th percent confidence interval; inset is the relationship in log-log space) (n = 94; mean r^2 = 0.89). (b) The lidar-derived height structure for white spruce at the study area (~250 ha). Bin widths are each 0.1 m. (c) Age structure of white spruce trees at the study area in 2011. Columns represent the mean number of individuals in each age class, where error bars represent the 95% confidence interval. The vertical red line indicates the year 1975. Note, that trees below 0.3 meters tall were not detectable (dashed vertical line in b) which limited the age structure to those established before 1995 (dashed vertical line in c).

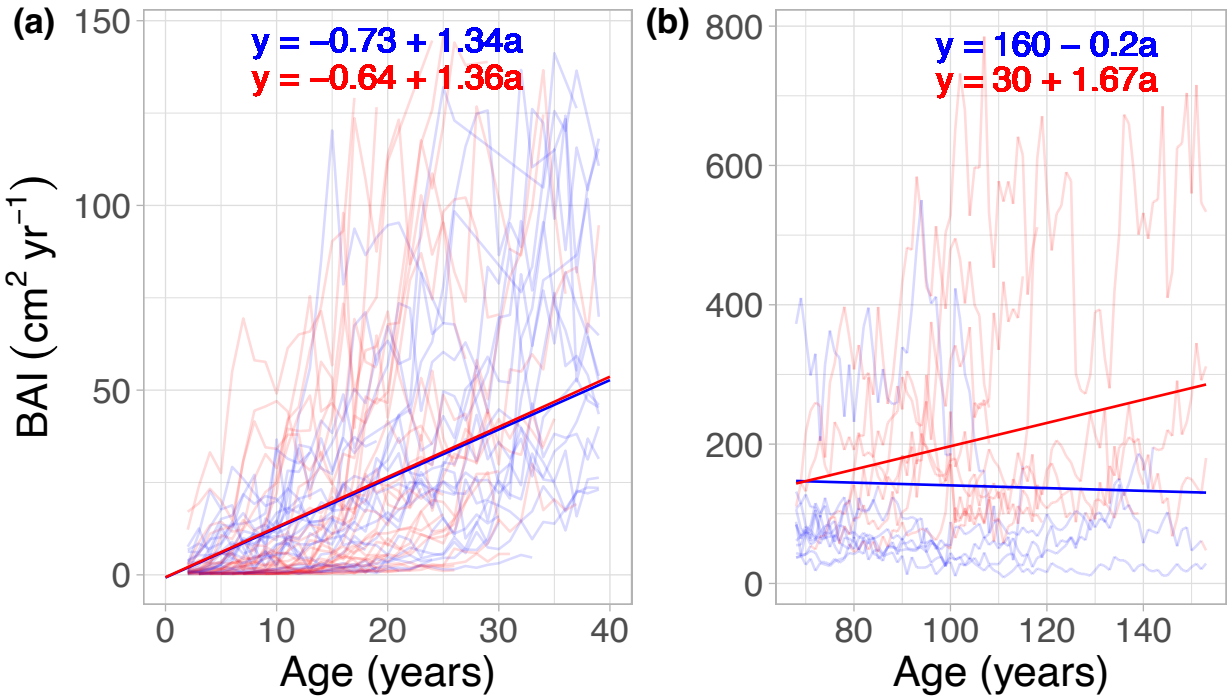

Figure 1.5. The relationship between growth rate (basal area increment, BAI; cm^2 yr^{-1}) and age (years) of white spruce saplings (a) and mature trees (b) before (blue) and after (red) 1975 at Arctic treeline in the central Brooks Range, AK. The equations of the lines (i.e., Equations 2 and 3) are presented on each panel with the colors also corresponding to period. To simplify the figure and highlight the change in slope, the lines/equations present the means of the coefficients (see Table 1.1) and exclude the error and random effects, if applicable. The difference in slope between the two periods was only significant in mature trees ($p < 0.0001$; z-test).

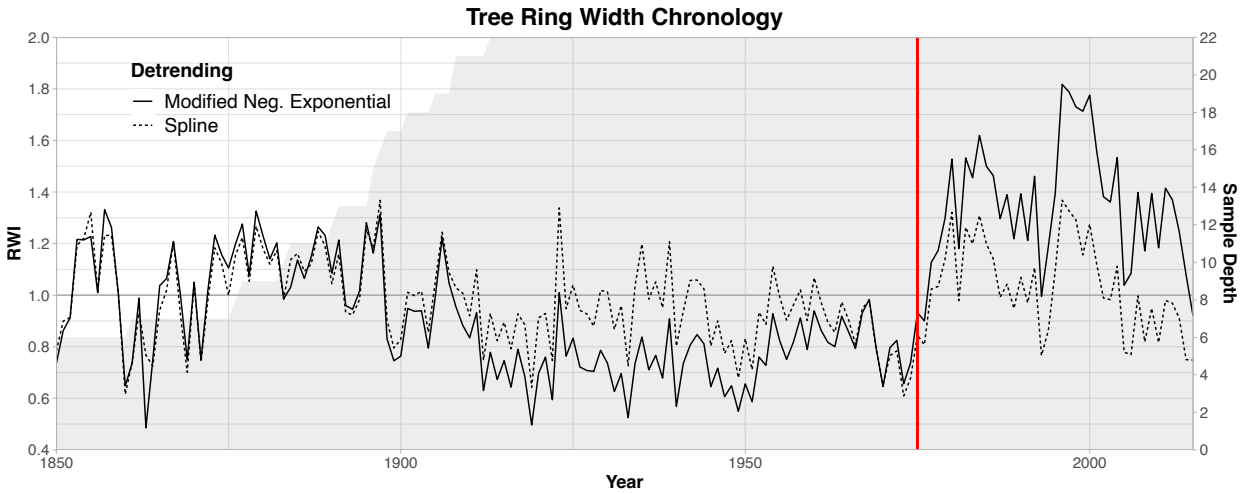

Figure 1.6. Tree ring width chronologies with two types of detrending (modified negative exponential and two-thirds spline) of white spruce trees at Arctic treeline in the central Brooks Range, AK. Y-axis shows the ring-width index (RWI), or standardized ring width after detrending. Grey shading and secondary y-axis indicate the sample depth, or the number of cores in the chronology. The vertical red line indicates the year 1975.

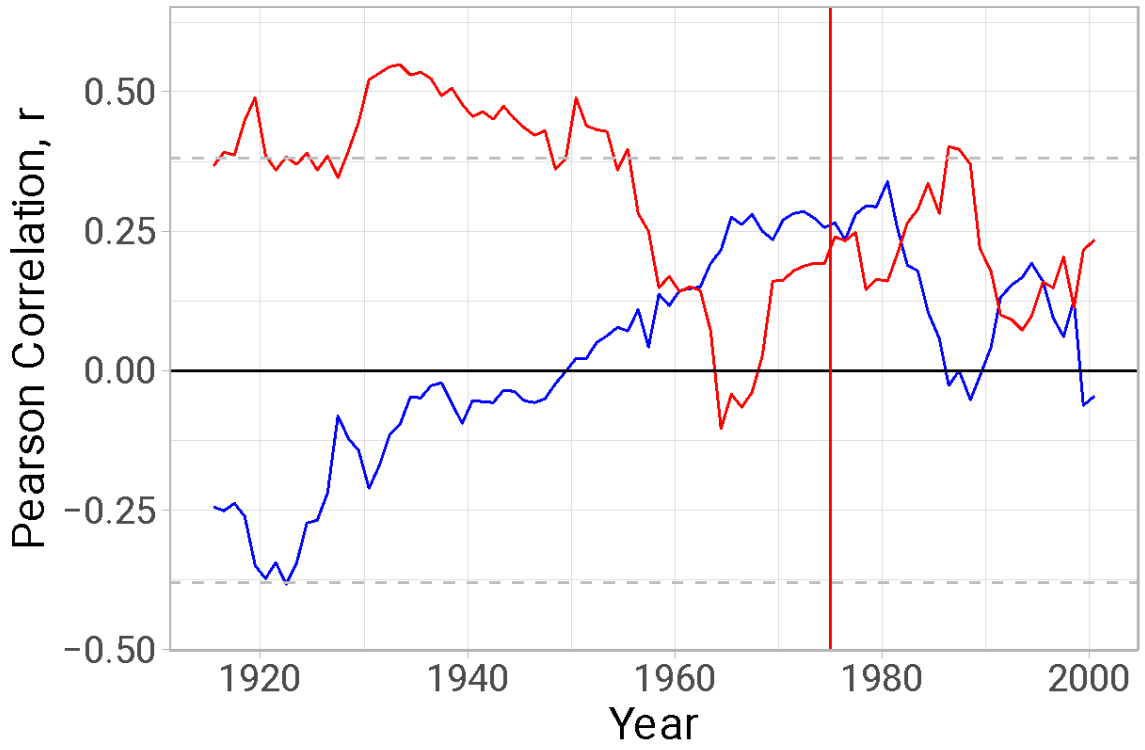

Figure 1.7. Running 31-year Pearson correlation, r, between spline-detrended TRC and mean June temperature (red line) and July precipitation (blue line) demonstrating temperature divergence of white spruce trees at Arctic treeline in the central Brooks Range, AK. The dashed, grey lines represent the 95% confidence limits, outside of which the correlation is significant. The vertical red line highlights the year 1975. Mean June temperature and July precipitation is presented because it was found to be optimal for the tree ring series analysis from 1900-2015 (see Table 1.3).

Chapter 2: Temperature vs moisture: dissecting the relative influence of temperature, vapor pressure deficit, and soil moisture on intra-annual radial stem growth at Arctic treeline

Johanna Jensen, Natalie Boelman, Jan Eitel, Lee Vierling, Andrew Maguire, and Kevin L. Griffin

2.1 Abstract

Individual tree growth at Arctic treeline is expected to increase in response to warming, but evidence of increased growth is mixed, suggesting factors other than temperature may be becoming more limiting as the climate continues to change. Further, chapter 2 concluded that the growth of saplings and mature trees varied in their response to climate change during the 20th century. Therefore, in this study, we ask: (1) How do present-day intra-annual dynamics in air temperature, vapor pressure deficit (VPD), and soil volumetric water content (VWC) interact to influence radial stem growth of white spruce trees at Arctic treeline? and (2) Do the growth rates of saplings and mature trees respond differently to these dynamics in environmental conditions, and if so, in what way? We hypothesize that: (1) the influence of temperature will be moderated by VPD and soil moisture, and that; (2) compared to mature trees, the growth rate of saplings will be more susceptible to low water availability and/or high atmospheric evaporative demand. We obtained near continuous, sub-daily measurements of temperature, VPD, soil moisture, and stem radius using automated point dendrometers from two growing seasons (2018 and 2019) at an Arctic treeline site in the foothills of the central Brooks Range, AK. A generalized linear mixed effects model revealed that VPD, VWC, and tree size were statistically more important to

determining growth rate than air temperature. Lower VPD positively influenced the growth in general but was especially influential in large trees. Further, growth in mature trees benefitted in wetter soil conditions. Our results support that the growth rate of mature trees is more susceptible to low water availability and/or high evaporative demand. Together, these results suggest that while VPD and volumetric water content affect trees of all sizes at this section of Arctic treeline, saplings are less water-stressed than mature trees. We recommend considering life stage and the interactions between temperature and moisture availability when making predictions about growth at treeline in a changing climate.

2.2 Introduction

Arctic treeline is the largest ecotone on the planet (Callaghan et al. 2002a) and represents the northern-most extent of the ecological niche space of tree species (Körner 2012, 2021). The ecotone's northern limit is thought to be primarily delineated by cold temperatures (Körner 2012, 2021, Paulsen and Körner 2014) and thus growth at Arctic treeline serves as a sensitive indicator of climate change as trees are functioning at the limit of their physiological tolerance (Körner 2012, 2021, Griffin et al. 2022). Given that the Arctic has warmed almost four times more rapidly than the global average (Rantanen et al. 2022), it follows that tree growth at Arctic treeline is commonly predicted to increase into the future (ACIA 2005, Callaghan et al. 2005, Pearson et al. 2013, Zhang et al. 2013). However, evidence of increased tree growth due to warming is mixed, with some treeline sites showing increased growth while others have mixed or no response (Briffa et al. 1998, Barber et al. 2000, Wilmking and Juday 2005, D'Arrigo et al. 2008). Additionally, the recent deterioration of positive correlations between air temperature and tree growth at Arctic treeline, commonly known as 'temperature divergence', suggests that

increasing temperatures do not always benefit growth (D'Arrigo et al. 2008). This suggests that other environmental conditions and their interactions (Ellison et al. 2019), as well as genetic (Zacharias et al. 2021), age-related and physiological (Körner 2012) factors are becoming important in limiting local tree growth (Körner 2012, Ellison et al. 2019, Zacharias et al. 2021).

A growing body of evidence suggests that water availability (e.g. vapor pressure deficit and soil moisture) may limit growth once temperature-limitation is alleviated (Barber et al. 2000, Driscoll et al. 2005, Wilmking and Juday 2005, Peng et al. 2011, Wilmking et al. 2012b, Lange et al. 2020, Tumajer et al. 2022). In the southern foothills of the Brooks Range, AK, white spruce (*Picea glauca*) growth responded positively to warming in the 20th century in the wetter, western regions while the response decreased and ceased in the drier central and eastern regions (Wilmking et al. 2004, Wilmking and Juday 2005, Brownlee et al. 2016). In fact, water-limitation is one of the most common hypotheses to explain temperature divergence (Wilmking et al. 2004, 2005, Driscoll et al. 2005, Wilmking and Juday 2005, Lloyd and Bunn 2007, D'Arrigo et al. 2008, Porter and Pisaric 2011, Lange et al. 2020). Exploring the influence of water availability on intra-annual growth may help to elucidate the ways that tree growth is responding to a changing climate.

Tree size also plays a critical role in how trees respond to environmental conditions (Körner 2016, Stovall et al. 2019), and likely influences dynamics in radial stem growth of different sized trees at Arctic treeline (Körner 2012). The physiology of taller, often more mature trees, is more tightly coupled to atmospheric conditions than shorter saplings, making them more susceptible to changes in environmental conditions such as temperature and vapor pressure deficit (Körner 2016). While taller trees have greater water demands (Körner 2016), their larger

root structures allow them access to more belowground water relative to smaller trees, especially under drought conditions (Jackson et al. 1996). Together, these previous studies suggest that predicting how radial stem growth at Arctic treeline will respond to the rapid warming associated with climate change requires an improved understanding of how temperature, vapor pressure deficit, water availability, and tree size interact at Arctic treeline to influence local tree growth. Such an understanding will help elucidate how ongoing climate change shapes the ecotone's ability to store carbon aboveground, extend northward, and thereby mitigate future climate change (Wilmking et al. 2006, Pearson et al. 2013).

In this study, we ask: (1) How do intra-annual dynamics in air temperature, vapor pressure deficit (VPD), and soil volumetric water content (VWC) interact to influence radial stem growth of white spruce trees at Arctic treeline? and (2) Do the growth rates of saplings and mature trees respond differently to these dynamics in environmental conditions, and if so, in what way? To answer these questions we obtained near continuous, sub-daily measurements of temperature, VPD, soil moisture, and stem radius using automated point dendrometers from two growing seasons (2018 and 2019) at an Arctic treeline site in the foothills of the central Brooks Range, AK. We then determined periods of active growth from stem radius measurements using a zero-growth model (Zweifel et al. 2016) and compared patterns of intra-annual relative growth rate between saplings and mature trees. Next, we used a generalized linear mixed effects model to infer the impacts of temperature, VPD, and moisture availability on growth rate. We hypothesized that: (1) the positive influence of increasing temperature will be moderated by VPD and soil moisture, and that; (2) compared to saplings, the growth rate of mature trees will be more susceptible to low water availability and/or high atmospheric evaporative demand (i.e., high temperature, low VPD conditions).

2.3 Methods

2.3.1 Study site

Our study was conducted from June 2016 – Sept 2019 along a 5.5 km north-south transect bordering the Dalton Highway in the foothills of the Brooks Range, AK (67°59′ 40.92’’ N, 149°45′ 15.84’’W, 727 m a.s.l.). According to monthly climate data from the Integrated Ecosystem Model for Alaska and Northwest Canada (McGuire et al. 2016), the mean annual temperature was -8.25 ± 0.65°C and the average precipitation was 304 ± 77.1 mm $year^{-1}$, with approximately half (45%) received as snow between 2000-2015. The site receives 24-hours of daylight from May 27 to July 18. Along the transect, the forest transitions to treeless tundra in patches and is underlain by discontinuous permafrost. The canopy is dominated by white spruce (*Picea glauca*) (Moench) while the understory consists mostly of sedges (e.g., *Eriophorum* spp.) and deciduous shrubs (e.g., *Betula nana* L., *Alnus* spp.) (Eitel et al. 2019).

2.3.2 Radial tree growth rate

In June 2016, we selected 36 white spruce trees along the transect using stratified random sampling with a diameter at breast height (DBH) of 10 cm as the stratification variable. Trees with a 5-10 cm DBH were considered saplings (n = 18) and those with a DBH greater than 10 cm were considered mature trees (n = 18) (Tranquillini 1979, Körner 2012, Griffin et al. 2021). The mean DBH of saplings and mature trees included in this study was 6.62 cm and 18.4 cm, respectively. The average height of saplings was 4.15 m tall while mature trees were more than twice that height at 9.74 m tall. The mean tree age was predicted from height (see Chapter 1) and revealed that saplings were on average 73 years old while mature trees were on average 122 years old.

Measurements of radial stem growth were made from June 2016 to September 2019. Each study tree was fitted with a point dendrometer, fabricated from a linear motion, spring-loaded potentiometer (LP-10F; Midori USA). Dendrometers were placed at a height of 1.37 m on the north side of each tree (to minimize exposure to direct solar radiation) after removing any loose outer bark. Each potentiometer was calibrated at the time of installation with stem DBH to derive the stem radius and basal area (BA), so that:

$$R_0 = \frac{D_0}{2}$$

$$R_t = d_t + R_0$$

$$B_t = \pi {R_t}^2$$

where D_0 and R_0 are the DBH and stem radius at the time of installation, respectively; d_t is the linear distance measured by the dendrometer (0.001 cm) at time *t*; R_t is the stem radius at time *t*; and B_t is basal area at time *t*. Data were recorded on one of two types of dataloggers: a CR300 from Campbell Scientific or an EM50 data logger from METER Group. The linear distance displaced by fluctuations in stem radius was recorded at five- or 20-minute intervals (for EM50 and CR300 data loggers, respectively). A more detailed description of dendrometer measurements can be found in (Eitel et al. 2020).

The onset of annual radial stem growth for each tree was defined as the day (at midnight) that the mean daily stem radius of the current year surpassed the 95th percentile of the mean daily stem radius of the previous year (May – August) (Figure 2.1) (Etzold et al. 2022). Similarly, the cessation of annual radial stem growth was defined as the date at which the 95th percentile of growth for the current year (May – August) was reached. However, if the data in the previous

season lacked >10% of the daily observations, we defined the onset of annual radial stem growth as the day that the mean daily stem radius of the current year surpassed the mean daily stem radius of the previous August. A more detailed description on determination of the onset and cessation of annual radial stem growth can be found in Eitel et al. (2020). The onset and cessation of annual growth demarcated the growing season. It is important to note that we define the cessation of annual radial growth as the cessation of radial expansion; cellular wall thickening continues through August (Cuny et al. 2015) but is not a limitation in answering our question which centers on irreversible radial stem growth.

Within the growing season, we identified periods of irreversible radial stem growth (i.e., production of wood) using the 'zero-growth model,' which assumes that stem expansion beyond the previous maximum is driven by xylogenesis and those below the previous maximum were due to tree-water deficit (Zweifel et al. 2016). Therefore, the raw growth rate was the positive change in stem radius (cm per 20-mins). Following Tumajer et al. (2022), we standardized the raw growth rate at each timestamp by the cumulative annual growth of a specific tree during the growing season to determine the contribution of each timestamp to annual growth, hereafter called 'GRO contribution'.

2.3.3 Microclimate

Alongside changes in stem radius, we measured air temperature, RH, and VWC at each of the 18 mature and 18 saplings studied. Air temperature and RH were measured using VP-4 sensors (METER Group) placed approximately 1.5 m above the ground on the south side of each tree within the dripline but outside of the foliage. VPD was then calculated using RH and air temperature by calculating the difference between saturated vapor pressure and the vapor

pressure of the air (Jones 1992). VWC sensors (ECH_2O 5TM, METER Group) were installed in 18 of the 36 trees at 10 cm depth on the north side of the tree just inside the drip line. All weather data were recorded at five-minute intervals on a EM50 datalogger.

2.3.4 Statistical analysis and visualization of intra-annual growth

We manually reviewed the dendrometer and microclimate data to identify and remove outliers or periods of sensor malfunction. For each tree, we limited our analysis to datasets collected: (1) during days for which growth data were collected for at least 75% of the day (i.e., ≥ 55 observations out of a possible 74 per day), (2) from trees for which growth data were collected for at least 90% of the days between May 1 – Aug 31 (≥110 days of 123 total days) during which stems begin and cease growth (See Section 2.3.2), and (3) from trees that grew during our study period (i.e., stem radius at onset of annual growth was greater than that after cessation). After applying these restrictions, the data included in our analysis were from six saplings and five mature trees across two years of study (Table 2.1). Then, five-minute intervals were averaged over the previous twenty minutes to provide a consistent unit of measurement between the two types of dataloggers (i.e., CR300 from Campbell Scientific or an EM50 data logger from METER Group).

To answer our study questions, we predicted relative growth rate from the environmental conditions and tree size using a generalized linear mixed effect model (GLMM) in R statistical software (R Core Team 2021) with the R package '*nlme'* (Pinheiro et al. 2022). The predictor variables included day of year (DOY), air temperature (airT), VPD, VWC, and tree size (DBH). The full model included additive effects of each predictor variable, the interactions between size and the weather variables, as well as interactions between each weather variable. Correlations

between the continuous predictor variables were examined but none were excluded from the model since each were necessary to answer our study question. This resulted in a model with the form:

$$y_{i,t} \sim \beta_0 + \beta_1 x_{DOY,t} + \beta_2 x_{size,i,t} + \beta_3 x_{airT,i,t} + \beta_4 x_{VPD,i,t} + \beta_5 x_{VWC,i,t} + \beta_6 x_{airT,i,t} x_{size,i,t} + \beta_7 x_{VPD,i,t} x_{size,i,t} + \beta_8 x_{VWC,i,t} x_{size,i,t} + \beta_9 x_{airT,i,t} x_{VPD,i,t} + \beta_{10} x_{airT,i,t} x_{VWC,i,t} + \beta_{11} x_{VPD,i,t} x_{VWC,i,t} + e_i$$

where, $y_{i,t}$ represents the growth rate of tree *i* at time *t*; *x* represents the predictor variable (see subscript); β_0 is the y-intercept, β_1 through β_{11} are coefficients relating the predictor variable(s) of each term to the growth rate; and e_i is the random intercept per tree, *i*.

GLMMs relax the assumptions of normality and homoscedasticity required by linear regression models by specifying the distribution of the dependent variable and a link function (McCullagh and Nelder 1990, Zuur et al. 2009). Because relative growth rate was non-normally distributed, we compared the above model with multiple distributions and link functions using the Akaike Information Criterion (AIC) (Akaike 1973). The distribution and link function that had the lowest AIC, and therefore the best fit to the data, was a gamma distribution with a log link. Because the observations of growth rate were not independent (e.g., we tested the same individuals repeatedly), we tested random effects of tree ID, plot location, and year in our model. In the end, we included only tree ID as a random effect as it produced a model with the lowest AIC and including any combination of the three potential random effects made the model singular. Laplace estimation (Gelfand and Dey 1994) for the model converged easily.

The quality of the models was assessed by marginal (R^2_m) and conditional (R^2_c) pseudo-R^2 statistics (Nakagawa and Schielzeth 2013). We then interpreted the relationships between

growth rate and the predictor variables. Individual terms within the model were deemed significant predictors of growth rate if $p < 0.05$ in a z-test. We interpreted the effect of each predictor variable on relative growth rate with the aid of a heat map. The heat map was created by predicting relative growth rate at every possible combination of weather conditions for a sapling (DBH = 6.6 cm) and a mature tree (DBH = 18.4 cm) in the early growing season (June 10; DOY= 162).

2.4 Results

2.4.1 Environmental conditions

Environmental conditions during the growing season of 2019 were warmer and drier than those of 2018 (Figure 2.2). The mean, maximum and minimum growing season air temperatures were significantly warmer in 2019 (14.6°C, 31.7°C, and 0.2 °C, respectively) compared to in 2018 (11.6°C, 27°C, and -7.18°C, respectively) (Wilcoxon test, $p < 0.0001$). Conditions were also significantly more arid in 2019 than in 2018, with the mean VPD of 0.78 and 0.46 kPa, respectively (Wilcoxon test, $p < 0.0001$). VWC was significantly lower in 2019 than in 2018 (Wilcoxon test, $p < 0.0001$). We found statistically significant correlations among the day of year (DOY) and all the weather variables in the model (Figure 2.3). Despite these correlations, we retained all variables in the model to answer our hypothesis.

2.4.2 Radial stem growth

At the annual scale (i.e., the total width of the tree ring grown between onset and cessation of annual growth), growth rate of saplings and mature trees was statistically identical when quantified as basal area increment (BAI, cm^2; Table 2.1). However, when annual growth

was quantified as the percent increase relative to starting basal area, we found that saplings grew 3.6 and 4.1 times more than mature trees in 2018 and 2019, respectively (Wilcoxon test, $p < 0.05$; Table 2.1). The growth rate as GRO contribution (percent grown of the total annual growth per timestamp) was significantly higher in mature trees compared to saplings (Wilcoxon test, $p < 0.001$) (Figure 2.4). The time during which growth occurred for saplings and mature trees significantly differed between tree size and year (Wilcoxon, $p < 0.0001$ for all comparisons; Figure 2.5). Mature trees most frequently grew in the early morning hours (4:00 – 8:00), whereas saplings tended to grow throughout the day, with modest peaks in the early morning hours.

Environmental conditions vs. radial tree growth.

Radial stem growth most commonly occurred when air temperature was 7-14°C, VPD was 0–0.5 kPa and VWC was 30 – 45%. Saplings more commonly grew at slightly warmer temperatures than mature trees (11.4°C on average compared to 9.8°C, respectively; Wilcoxon, $p < 0.0001$; Figure 2.6 *left*). Mature trees grew at a narrower range of VPD than saplings, with 75% of growth occurring at VPD between 0-0.33 kPa in mature trees compared to 0 – 0.65 kPa in saplings (Wilcoxon, $p < 0.0001$; Figure 2.6 *middle*). Growth occurred at a wide range of soil moisture (14-70 % VWC). No discernible optima were found for saplings or mature trees, however, the distributions were significantly different (Wilcoxon, $p < 0.0001$; Figure 2.6 *right*).

The fixed effects of the model captured 6.8% of the variance in the relative growth rate data (marginal R^2). Including random effects of tree ID (Supplementary Material Table 2.1 and 2.2) increased the variance captured to 42% (conditional R^2). The only significant terms in the model were those for VPD, the interaction between VPD and tree size, and the interaction between VWC and tree size (Table 2.2). In general, GRO contribution decreased significantly

with increasing VPD in trees of all sizes (VPD, β_4), but higher VPD particularly affected larger, mature trees (VPD:DBH, β_7). While VWC alone was not a significant predictor of relative growth rate (VWC, β_5), higher VWC positively influenced the growth response of larger, mature trees (VWC:DBH, β_8).

Interpreting the overall effect of the variables on relative growth rate is complicated by the multiple interaction terms. Figure 2.7 helps to illustrate the effect of these interactions on relative growth rate. Trees generally grew more than saplings however, the range of environmental conditions beneficial for growth is narrower. Barring changes in VWC, growth rate of mature trees responded more positively to decreased VPD than saplings (i.e., relative growth rate increases mainly along the y-axis). Increasing VWC increased growth rate in mature trees but decreased growth rate of saplings (i.e., relative growth rate increases across panel columns), especially under warmer temperatures. Increasing temperature alone did not have a significant effect on either saplings or mature trees, as it was not a significant term in the model. While both saplings and mature trees grew most when conditions were moderately cool (8-12°C) and VPD was low (<0.5 kPa), saplings grew most when the soil was dry (10-30%) (Figure 2.7 *top, left*) and mature trees grew most when the soil was wet (50-70%) (Figure 2.7 *bottom, right*).

2.5 Discussion

The results of our study suggest that VPD, VWC, and tree size were statistically more important to determining growth rate than air temperature. This confounds our first hypothesis, which expected our variables of water availability to moderate the influence in temperature. Lower vapor pressure deficit positively influenced the growth in general but was especially influential in large trees. Further, growth in mature trees benefitted in wetter soil conditions.

These support our second hypothesis that the growth rate of mature trees is more susceptible to low water availability and/or high evaporative demand. Together, these results suggest that while VPD and volumetric water content affect trees of all sizes at this section of Arctic treeline, saplings are less water-stressed than mature trees. As Arctic treeline continues to become warmer and drier (Overland et al. 2019, Rantanen et al. 2022), we can expect the radial growth in trees of all sizes to decrease but mature trees will likely be first to be negatively affected.

In addition to the results of our model, the timing of growth during the day suggests that mature trees are more water-limited than saplings at Arctic treeline (Wilmking et al. 2004, Wilmking and Juday 2005, Brownlee et al. 2016). Mature tree growth mainly occurred in the early morning hours (4:00- 5:00) when VPD is lowest (*data not shown*), whereas sapling growth occurred throughout the day. Tree stem radius growth usually occurs at night when VPD is low, and stems have overcome daily water deficits enough to continue growth (Zweifel et al. 2021). The physiological explanation behind why saplings appear less water-limited than mature trees may lie in the structural difference between these two life stages. Taller, mature trees are more coupled to the atmosphere than shorter saplings which are protected by the surrounding canopy and boundary layer (Körner 2012, 2016). As a result, mature trees experience more variation in climate conditions than saplings, including larger fluctuations in temperature and VPD (Körner 2006, 2016). Further, drier conditions at the top of the canopy may create a larger evaporative demand on mature trees than saplings, increasing the likelihood of cavitation and embolism of xylem cells (Maruta et al. 2020). Therefore, growth in mature trees at our Arctic treeline site may be limited to conditions during which VPD is lowest, and evaporative demand and risk of cavitation is minimized. In contrast, saplings may be able to exhibit a riskier growth response compared to their larger conspecifics.

By including tree size and interactions between climate variables in our model, we were able explain more variance in growth rate ($R_m^2 = 0.07$) than those which only included temperature and VPD ($R_m^2 = 0.01$) but analyzed trees together, regardless of variation in their size (Tumajer et al. 2022). The remaining unexplained variance in relative growth rate could be due to several other abiotic and biotic conditions at the Arctic treeline. These include but are not limited to mean wind velocity (Lyu et al. 2019), evapotranspiration (Lyu et al. 2019), sunlight (Lyu et al. 2019), nutrient limitation (Ellison et al. 2019, Möhl et al. 2019, Gustafson et al. 2021), nutrient cycling from denning animals (Lang 2019), structure damage from browsing (Olnes and Kielland 2017, Olnes et al. 2017), and mycorrhizal associations (Ellison et al. 2019). We recommend future studied which implement logistic regression or random forest to differentiate which climatic/environmental conditions stimulate irreversible radial growth from fluctuations in radius due to tree water status (e.g., Ziaco and Biondi 2016).

Our results support that climate warming is alleviating temperature-limitation while increasing water-limitation in Arctic treeline and boreal ecosystems (Barber et al., 2000; Driscoll et al., 2005; Lange et al., 2020; Peng et al., 2011; Wilmking et al., 2012; Wilmking & Juday, 2005) but stresses that tree size plays an influential role in growth response to these new conditions (Körner 2016). In addition, our findings help to temperature divergence at Arctic treeline (Briffa et al. 1998, Barber et al. 2000, Wilmking and Juday 2005, D'Arrigo et al. 2008) by showing that changes in VPD and soil moisture play a dominant role in growth rate at Arctic treeline, especially in mature trees which are commonly used for dendrochronological studies. As increasingly warm and dry conditions are expected throughout Arctic and boreal regions because of climate change (Overland et al. 2019, Rantanen et al. 2022), growth in mature trees may decrease relative to previous decades. However, saplings may continue to respond

positively to these conditions until reaching maturity and becoming more coupled with the atmosphere (Körner 2016).

2.6 Acknowledgements

Funding for this research came from NASA Terrestrial Ecology grant NNX15AT86A and NASA ABoVE grant (Eitel-01). We would also like to acknowledge and thank the Toolik Lake Long-term Ecological Research Station (LTER) from which we staged our research. We are also particularly for the support provided by the staff of the ABoVE Fairbanks logistics office, notably Sarah Sackett, and Toolik Lake Field Station. We also thank Jyoti Jennewein, William Weygint, and Kathryn Baker for their help in the field.

2.7 Figures and Tables

Table 2.1. Structural characteristics and annual growth for white spruce growing at Arctic treeline, AK. Annual growth is shown in basal area increment and percent increase in basal area relative to the basal area at the onset of growth.

Size Category	Tree ID*	DBH (cm)	Height** (m)	Predicted Age (years)** Mean ± SD (min, max)	Annual Growth Basal Area Increment, cm^2 (% increase of Basal Area)	
					2018	2019
Saplings (< 10 cm DBH)	1E	5.0	3.00	61 ± 2 (56, 65)	1.2 (5.9)	2.1 (9.3)
	1F	6.5	3.82	70 ± 2 (64, 76)	2.7 (6.8)	4.7 (10.9)
	2E	8.7	5.81	90 ± 3 (81, 1)	1.5 (2.2)	1.8 (2.7)
	2F	5.8	3.5	67 ± 3 (61, 72)	-	0.4 (1.5)
	4A	7.85	4.88	81 ± 2 (74, 88)	1.1 (2.0)	-
	6B	5.9	3.86	71 ± 2 (65, 76)	0.5 (1.5)	0.9 (2.5)
Mature Trees (≥ 10 cm DBH)	1A	20.6	7.84	107 ± 4 (96, 117)	2.3 (0.7)	3.7 (1.0)
	1F	19.1	11.86	137 ± 5 (121, 151)	-	3.2 (1.2)
	4D	23.1	10.71	129 ± 5 (114, 142)	3.5 (0.9)	5.6 (1.4)
	6A	16.0	10.13	125 ± 4 (111, 137)	2.3 (1.1)	2.9 (1.3)
	6D	13.5	8.17	110 ± 4 (98, 120)	2.2 (1.5)	2.4 (1.6)

* Tree ID corresponds to the ID's assigned in the data published in Eitel et al. (2020).
**Height was measured in 2016, therefore predicted age (from height) is the age in 2016.

Table 2.2. Coefficient Estimates, standard error, and significance for the model predicting GRO contribution of white spruce growing at Arctic treeline, AK. P-value was determined using a z-test. Bolded terms indicate significance (p < 0.05). *Note*: Coefficient estimates are scaled to the data (see Supplementary Material Table 2.3) and in log-space due to the log-link in the model.

Predictor Variable	Coefficient Abbreviation	Estimate	Std. Error	t value	p-value[1]
(Intercept)	β_0	-0.12	0.28	-0.43	
DOY	β_1	-0.01	0.02	-0.73	
DBH	β_2	-0.25	0.28	-0.87	
airT	β_3	0.01	0.02	0.51	
VPD	$\boldsymbol{\beta_4}$	**-0.09**	**0.03**	**-2.94**	**
VWC	β_5	0.03	0.02	1.25	
airT:DBH	β_6	0.02	0.02	0.93	
VPD:DBH	$\boldsymbol{\beta_7}$	**-0.08**	**0.02**	**-4.34**	****
VWC:DBH	$\boldsymbol{\beta_8}$	**0.08**	**0.03**	**3.2**	**
airT:VPD	β_9	0	0.01	-0.2	
airT:VWC	β_{10}	-0.02	0.02	-0.97	
VWC:VPD	β_{11}	0.03	0.02	1.46	

[1]Significance codes: * p < 0.05, ** p < 0.01, *** p < 0.001, ****p < 0.0001

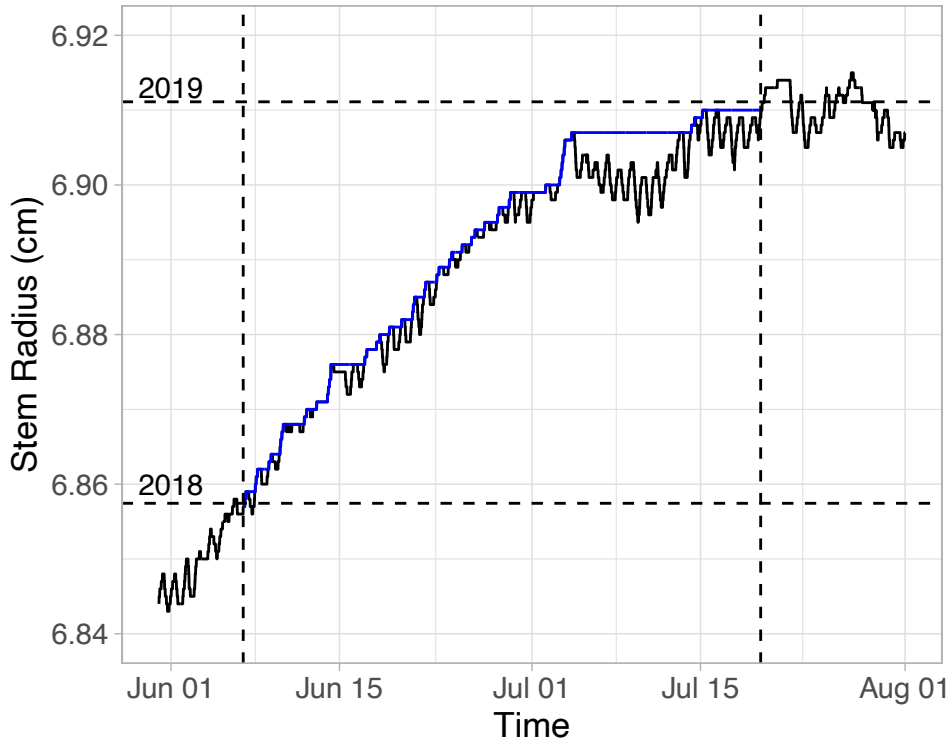

Figure 2.1. Visualization of intra-annual growth periods and irreversible radial stem growth of a white spruce tree (Tree 6D) growing at Arctic treeline, AK from Jun - Aug 2019. Irreversible stem growth (blue) is detected from stem radius (black) using the 'zero-growth approach' (Zweifel et al., 2016). Vertical dashed lines represent the onset date (left) and cessation date (right) of annual growth and horizontal dashed lines represent the equivalent starting (bottom; 95th percentile of 2018 stem radius) and ending (top; 95th percentile of 2019 stem radius) stem radius for those times.

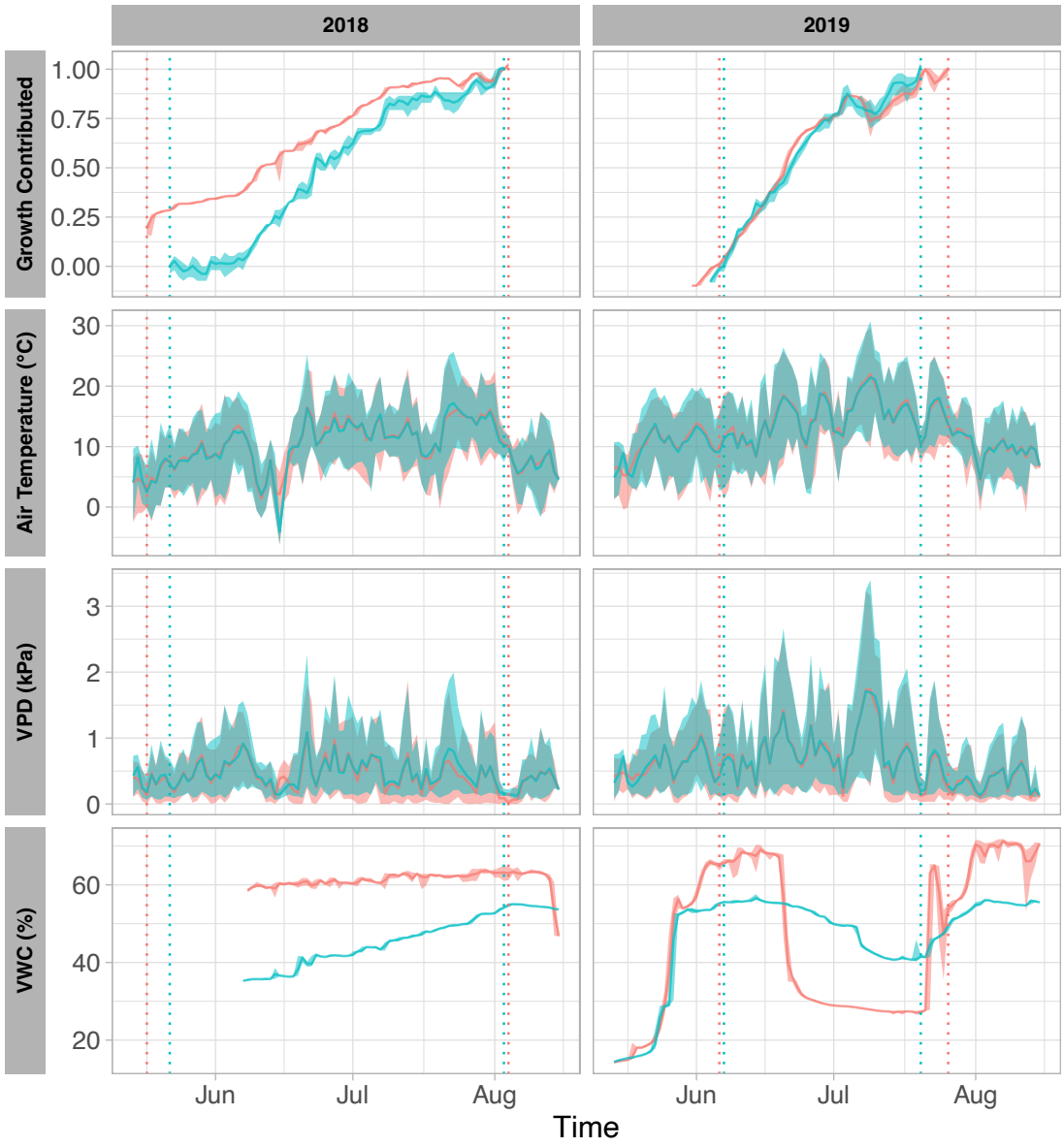

Figure 2.2. Timeseries of white spruce radial stem growth and weather during the growing seasons of 2018 and 2019 at the Arctic treeline, AK. (*first row*) Daily mean stem size as the percent change in basal area for one sapling (red; Tree 2E) and one mature white spruce tree (blue; Tree 6D) in 2018 (left column) and 2019 (right column). Vertical dashed and dotted lines represent the onset and cessation of radial stem growth, respectively, and are extended across all panels for reference. Site-level climate throughout the growing season includes (*second row*) air temperature, (*third row*) vapor pressure deficit (VPD), and (*fourth row*) volumetric water content (VWC) where solid lines represent the daily mean and shading represents the daily minimum and maximum. Note: VWC sensors were installed in early June 2018, hence no data for VWC is presented before this period.

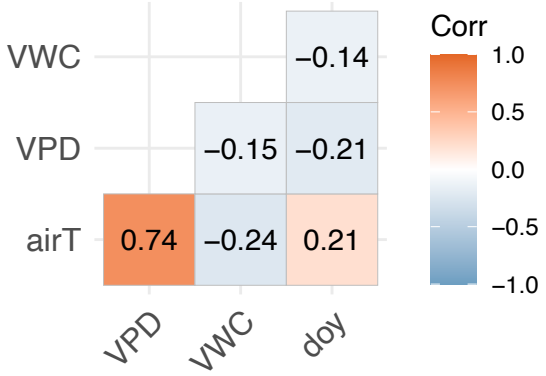

Figure 2.3. Relationships between climate variables and day of year during active growth of white spruce growing at Arctic treeline, AK, USA. Pearson correlation matrix of air temperature (airT), day of year (doy), VPD, and VWC. All correlations were statistically significant (Pearson correlations alpha < 0.01).

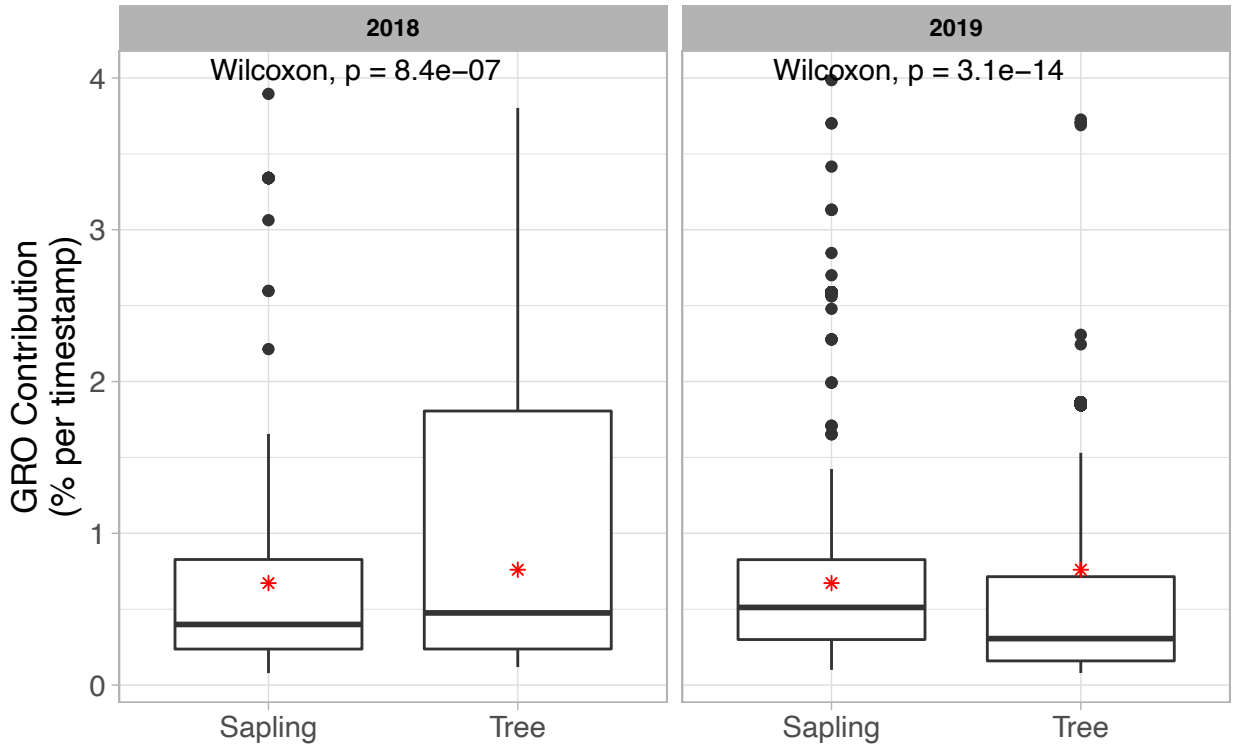

Figure 2.4. Growth rate as GRO contribution (% grown of annual growth per timestamp) for white spruce saplings and trees growing at Arctic treeline, AK in 2018 and 2019. The box represents the first and third quartiles; the bold line as the median. The arithmetic mean is represented by a red asterisk. The whiskers extend from the hinge to the smallest/largest value no further than 1.5 * IQR from the hinge (where IQR is the inter-quartile range, or distance between the first and third quartiles). Outlying points beyond this range are plotted individually. Results of a Wilcoxon test of growth rate in saplings and trees within each year are shown as text on the top of the panel.

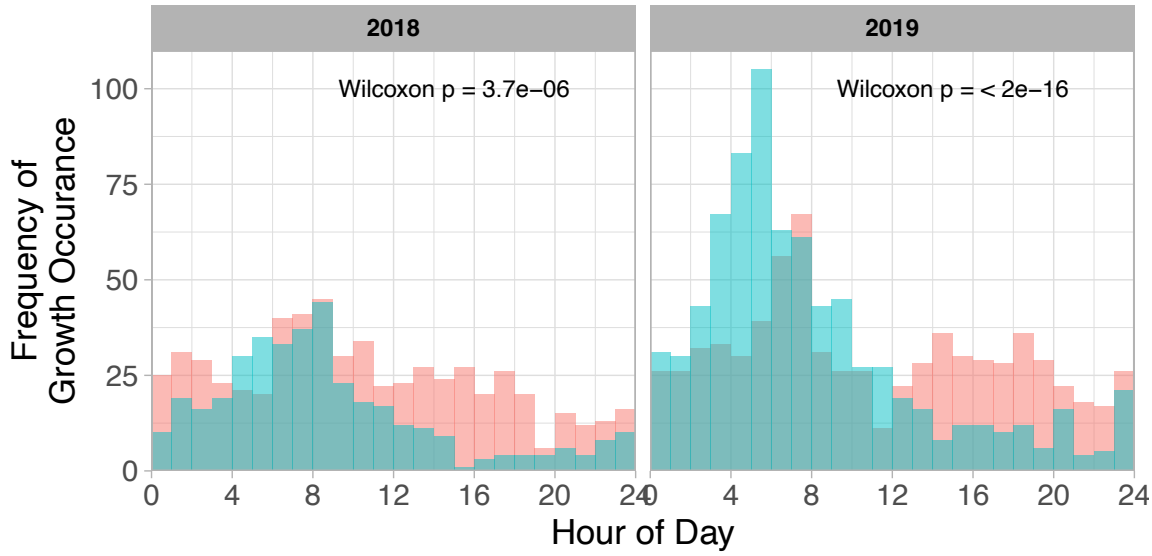

Figure 2.5. Frequency of growth occurrence in saplings (red) and mature trees (blue) during each hour of the day for 2018 (left) and 2019 (right). Results of a Wilcoxon test between saplings and trees within each year are shown as text on the top of the panel.

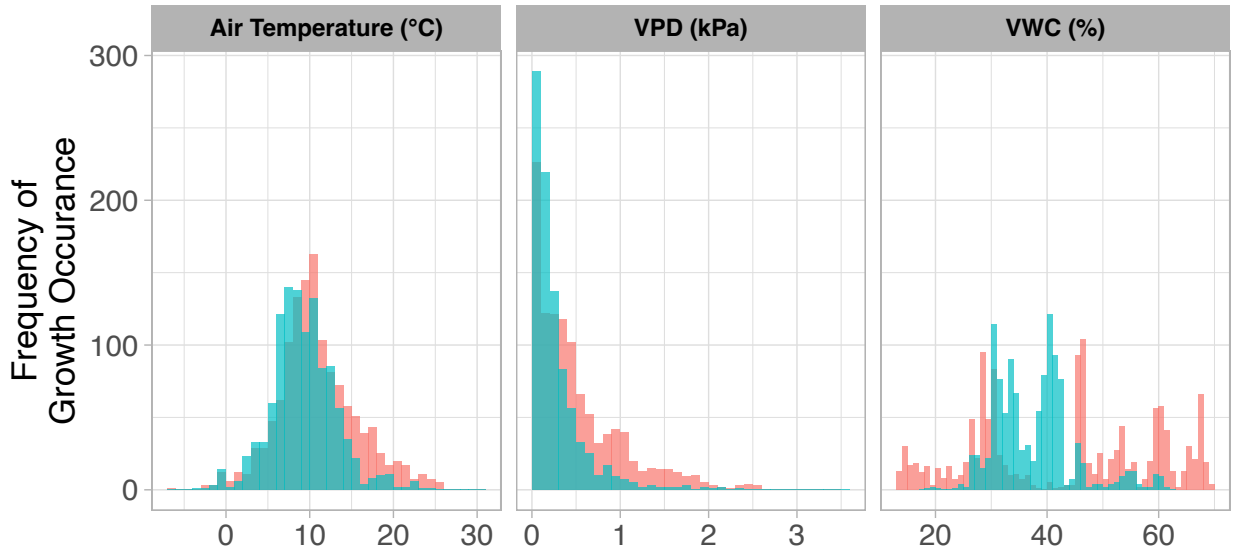

Figure 2.6. The number of timestamps with growth occurrence during specific intervals of environmental conditions. Air temperature is shown in 1°C intervals; VPD in 0.1 kPa intervals, and VWC in 1% intervals. Occurrence of saplings growth is shown in red, and mature trees growth in blue. All distributions differed significantly between saplings and trees (Wilcoxon, $p < 0.0001$).

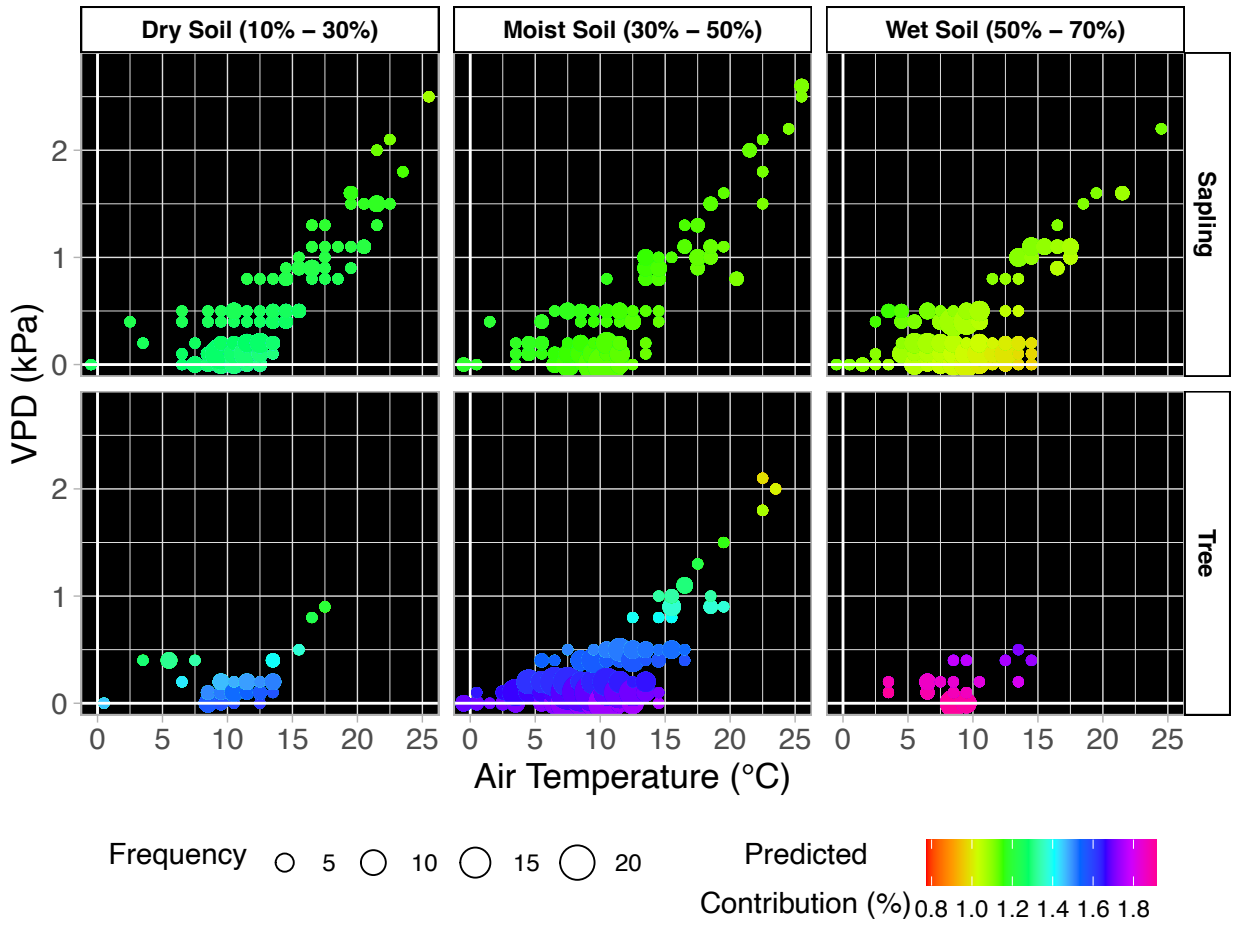

Figure 2.7. Heat map of the model showing the relationships between white spruce growth rate and the weather variables at Arctic treeline, AK. Interactions between predicted growth rate (color; GRO contribution), temperature (x-axis; °C), relative humidity (y-axis; %), and three levels of soil moisture (columns; % VWC) impact white spruce saplings (top row; DBH = 6.6 cm) and trees (bottom row; DBH = 18.4 cm) differently. Relationships are shown for growth early in June 10 (DOY 162) but were similar throughout the growing season. Low, moderate, and high values for soil moisture were chosen to represent the range of conditions experienced during the growing season. The size of the points describes the frequency (number of 20-min timestamps) that combination of weather conditions occurred during the growing seasons of 2018 and 2019.

Chapter 3: Extreme cold and subsequent thermal accumulation provide the environmental cues for initiating radial stem growth at the Arctic treeline: A dendrometer study of white spruce (*Picea glauca*) in central Alaska, USA

Johanna Jensen, Natalie Boelman, Jan U. H. Eitel, Lee Vierling, and Kevin L. Griffin

3.1 Abstract

Climate change is expected to advance the seasonal onset of radial stem growth and lengthen the duration of the growing season. Such a change could potentially increase radial stem growth and above-ground carbon accumulation at Arctic treeline. Here, we identify the main environmental cues that initiate radial stem growth in spring for white spruce (*Picea glauca*) growing at Arctic treeline in the Brooks Range, AK, USA. We then simulate how additional warming may alter the timing of onset in radial stem growth. We hypothesize that the onset of radial stem growth of white spruce trees at our Arctic treeline site is triggered by winter chilling and spring heat accumulation, as found at slightly lower latitudes. Further, we expect soil temperature to play an important role in the onset of radial growth as soil temperature controls the presence of liquid water in permafrost and is necessary for radial growth. Therefore, we expect that soil temperature thresholds will predict onset more accurately than air temperature. To that end, we made continuous measurements of air temperature, soil temperature, and stem radius using automated point-dendrometers from 2016-2019. Our results confirm our first hypothesis: winter chilling interacts with warming spring temperature to initiate radial stem growth in spring. However, air temperature was a better predictor of onset than soil temperature. The extremely cold winter chilling threshold compared to studies elsewhere in the

boreal forest suggest that environmental conditions initiating radial stem growth may be species, site, and/or regionally specific, complicating predictions of radial growth onset in a changing climate. The simulation to predict onset of radial growth in a warming climate suggest that the onset of radial stem growth could occur one to two weeks earlier with 1-4°C warming.

3.2 Introduction

Trees synchronize their lives to the environment, relying on environmental signals to cue critical physiological functions (Purnell 2003). This adaptation is particularly important in cold climates where the growing season lasts only 100-110 days (Deslauriers et al. 2008, Körner 2012, Rossi et al. 2014a) and most radial stem growth occurs within only the first 60-70 days (Rossi et al. 2008). To take advantage of such a short growing season, it is critical for trees to synchronize the onset of radial stem growth with the first availability of suitable environmental conditions (Körner 2012). Climate change is expected to advance the seasonal onset of radial stem growth and lengthen the duration of the growing season (Piao et al. 2007, Wang et al. 2019). This is particularly important at Arctic treeline as longer growing seasons could substantially increase radial stem growth, woody biomass, and thus above-ground carbon accumulation and storage which in turn would mitigate climate change (Rahman et al. 2020). Determining the species-specific environmental conditions that cue the onset of radial stem growth at Arctic treeline is therefore an important variable for forest research (Delpierre et al. 2019).

Environmental conditions cue the onset of radial stem growth. Observational studies have found that the spring onset of radial stem growth in cold environments is often driven by photoperiod and air temperature in some way (e.g. Moser et al. 2010, Delpierre et al. 2016,

Begum et al. 2018). As such, these factors are the primary focus for the three most widely supported models being tested to understand how environmental conditions trigger radial stem growth: the temperature threshold model, the heat sum model, and the chilling-induced heat sum model (Chuine et al. 2013, Chuine and Régnière 2017). The temperature threshold model suggests that the onset of radial stem growth occurs once a critical temperature threshold is reached (Deslauriers et al. 2008, Rossi et al. 2008, 2011) The heat sum model, also known as the 'cambial reactivation index' (Begum et al. 2010, Li et al. 2017), is a degree day model that suggests that the onset of radial stem growth occurs after sufficient exposure to temperatures above a critical threshold (Wang 1960, Seo et al. 2008, Swidrak et al. 2011, Rahman et al. 2020). Lastly, the chilling-induced heat sum model suggests that the onset of radial stem growth is determined by winter chilling below a threshold temperature and spring heat sum above a different threshold temperature (Ford et al. 2016, Delpierre et al. 2019). In each model, photoperiod is used to define the days during which warming and/or chilling can occur. A comparison of these models, Delpierre et al. (2019) concluded that while the chilling-induced heat sum model determined the onset of radial stem growth in four species of high latitude conifers (*Picea mariana* Mill., *Pinus sylvestris* L., *Picea abies* L. Karst., and *Larix decidua* Mill.), the environmental thresholds were species-specific.

In addition to air temperature and photoperiod, soil temperature may also be an important environmental cue in triggering the onset of radial stem growth at Arctic treeline, as it is an important influence on the reactivation of the vascular cambium in spring (Vaganov et al. 1999, Hoch and Körner 2003, Körner and Paulsen 2004, Körner and Hoch 2006). Since this ecotone is underlain by discontinuous permafrost, soil water remains biologically unavailable throughout the winter and into spring (Chabot and Mooney 1985). This contributes to winter desiccation of

tree stems until the active layer thaws, at which point liquid water becomes available and stems are able to rehydrate (Maruta et al. 2020). Stem rehydration is essential for cambial reactivation to occur (Sanmiguel-Vallelado et al. 2021) and for turgor pressure to be sufficient for radial stem growth (Cabon et al. 2020, Peters et al. 2021). Therefore, research aimed at understanding environmental cues that trigger the onset of radial stem growth at Arctic treeline should consider both air and soil temperatures (Turcotte et al. 2009).

Determining the onset of radial stem growth in remote locations. To study the onset of radial stem growth, precise measurements of either cell division or stem diameter are needed. Micro-cores can detect the onset of radial stem growth if taken at regular, frequent intervals (i.e., daily to weekly) throughout the spring (i.e., late April to June at Arctic treeline) (Turcotte et al. 2009). However, the need for high temporal resolution in measurement intervals over the course of several consecutive weeks renders this method difficult to implement at remote locations such as most pan-Arctic treeline sites. In addition, micro-coring is difficult to master and requires substantial post-processing to produce a dataset of radial stem growth (Tardif et al. 2001). Alternatively, autonomous point dendrometers continuously record tree diameter with high spatial and temporal precision (i.e., <3 μm at 5- to 20-minute intervals), making them ideal for studies of Arctic treeline (Eitel et al. 2020).

After dendrometer measurements have been collected, a post-processing technique must be used to detect when the expansion of newly formed xylem, and thus radial stem growth, begins each year. The prevailing technique, hereafter referred to as the '95th percentile method', considers the onset of radial stem growth to be the day on which stem radius of the current spring surpasses the 95th percentile of the previous year's radial stem growth (Zweifel et al. 2016, Eitel

et al. 2020, Nezval et al. 2021, Etzold et al. 2022). However, this method requires the previous season's data, which limits its accuracy and utility in two ways. First, it is sensitive to the inclusion of commonly incomplete records of stem radius that are due to sensor malfunction. Incomplete records will skew the value of the 95th percentile and therefore provide erroneous dates of onset. Second, this method cannot be used to detect the onset of growth in the *first* year that stem radius measurements were made. A new technique is needed that provides statistically indistinguishable dates of onset to the 95th percentile method but that circumvents these limitations.

The overall goal of our study is to gain better understanding of the main environmental cues that initiate radial stem growth in spring for trees at Arctic treeline, and how additional warming may alter the timing of onset in radial stem growth. We focus on the dominant tree species (white spruce, *Picea glauca*) at our study site, which is located in the southern foothills of the central Brooks Range, AK, USA. We made continuous measurements of air and soil temperature, as well as stem radius using automated point-dendrometers from 2016-2019. We create and validate alternative to the '95th percentile method' to detect the onset of radial stem growth, hereafter referred to as the 'plateau method', that both accounts for incomplete records of stem radius and leverages patterns present in the current year's stem radius only. We then use a Bayesian analysis to test our hypothesis that the onset of radial stem growth of white spruce trees at our Arctic treeline site is triggered by winter chilling and spring heat accumulation. We expect that modifying the chilling-induced heat sum model to incorporate soil temperature during spring warming will predict onset most accurately. Then we conduct a simple simulation

to test our second hypothesis that onset of radial stem growth will occur earlier if temperature increases due to climate warming.

3.3 Methods

3.3.1 Site Description

We conducted our field work along a ~5 km long, latitudinal transect at Arctic treeline bordering the Dalton Highway just south of the Brook Range in Alaska, USA (67°59′ 40.92″ N latitude, 149°45′ 15.84″ W longitude) from June 2016 to September 2019. Along this transect, trees become increasingly sparse until the landscape transitions into treeless tundra. The site is underlain by discontinuous permafrost and dominated by white spruce (*Picea glauca*). The understory is populated by tundra and boreal sedges (e.g., *Eriophorum* spp.) and deciduous shrubs (e.g., *Betula nana* L., *Alnus spp*.) (Eitel et al. 2020). We established six plots at the forest-tundra transition where canopy trees were ≥ 2 m tall.

Based on *in situ* weather stations (VP-4 air temperature and EM50 data loggers; METER Group, Inc., Pullman, WA 99163), the average annual air temperature is -3.16°C. Air temperatures reach as low as -40.0°C in the winter and as high as 31.3°C in the growing season. Soil temperatures are buffered by the insulating snowpack in winter but still vary annually from -3.8°C to 12.2°C. Average annual soil temperature is -1.90°C. As an Arctic ecosystem, there is 24 hours of darkness between Dec 10th - Jan 3rd (24 days) and 24 hours of light from May 27th - July 18th (52 days) (data based on GPS position; local topography from the Brooks Range may affect these numbers). Local weather data from three nearby stations (Wiseman, Atigun Pass, and Chandalar Shelf) indicate that the area receives 521 mm of precipitation on average with 44% received as snow (Eitel et al. 2020).

3.3.2 Environmental Data

Each tree was equipped with a micro-meteorological station which recorded air and soil temperature at five-minute intervals on a datalogger (VP-4 air temperature; 5TM soil temperature and moisture; and EM50 data loggers; METER Group, Inc., Pullman, WA 99163). Air temperature sensors were installed at approximately 130 cm from the soil surface, just within the canopy perimeter. Soil temperature sensors were installed 10 cm into the active layer just within the drip line. The environmental data were manually checked for sensor malfunctions, outliers were removed, and daily averages were calculated from days with ≥ 90% data coverage. Daily photoperiod (hours of sunlight per day) was computed from the date and the geographic coordinates in the 'geosphere' package (Hijmans 2019). All statistical analyses were conducted using the open-source software package R version 3.6.2 (R Core Team 2021).

3.3.3 Onset of Radial Stem Growth

Measurement of radial stem growth

At each plot we selected six white spruce trees to monitor (n = 36). To select for trees with a wide range of structural characteristics we used a stratified random sampling approach with diameter at breast height (DBH, 1.37 m above the ground) as the stratification variable; half the trees selected at each site had a DBH between 5 and 10 cm and half with DBH > 10 cm. The diameter at breast height of trees included in the study ranged from 5.1 to 25.0 cm in 2016. High precision point dendrometers were installed on each tree at breast height following the methods outlined in Eitel et al. (2020). Each dendrometer was calibrated and related to the DBH at installation to derive the linear changes in stem radius from the voltage difference signal. The dendrometers had a spatial and temporal resolution of <3 μm and 20 minutes, respectively.

Dendrometer data were quality-checked using methods for data treatment in Zweifel et al. (2016) and manually reviewed before any calculations or statistical analyses were performed. We excluded trees from the study that did not grow during that season (i.e., missing rings, dead trees, etc.). We also excluded and those whose sensors malfunctioned or had insufficient data (i.e., < 90% of the daily observations recorded) around the time of onset (i.e., May 14 – June 14).

Detecting of the onset of radial stem growth

In this study, we developed the 'plateau method' to detect the onset of radial stem growth which capitalizes on the following general pattern in the temporal dynamics in stem radius data collected by the point dendrometers. This pattern is also observed in several species of conifers growing in cold environments (Tardif et al. 2001, King et al. 2013) that we discuss later in the text. During the winter, the stem shrinks and rapidly swells in the spring (Zweifel and Häsler 2000, Tardif et al. 2001). Swelling lasts approximately 10 - 14 days (Tardif et al. 2001) beginning around May 1st each year at our site and should not be confused with radial stem growth (see Discussion) (Tardif et al. 2001). After this initial swelling, the stem radius plateaus for two-weeks at the end of May; the stem radius then begins to increase once again and continues to do so through the growing season (e.g., see Figure 3 in Eitel et al 2020, and Figures 1 and 2 in Tardif et al., 2001). This pattern was present in the data collected for each of the study trees (Supplementary Material Figures 3.1 and 3.2). The following describes the plateau method, which is visualized in Figure 3.1a. First, the mean and standard deviation of the stem radius during the last two weeks of May were calculated. The date of growth onset was defined as the first day that the stem radius exceeded the mean + 3 standard deviations of the stem radius during the last two weeks of May.

To assess the performance of plateau method, we compared the dates of growth onset predicted for each study tree to those predicted by the widely used 95th percentile method (Zweifel et al. 2016, Eitel et al. 2020, Nezval et al. 2021). According to this method, the onset of radial stem growth occurs when the stem radius of the current year exceeds the 95th percentile of the stem radius of the previous growing season (May 14 – Aug 1). Using the 95th percentile instead of the maximum stem radius is less affected by sporadic outliers and therefore provides a more stable approach in detecting the onset of radial stem growth (Eitel et al. 2020). Because the 95th percentile method requires a complete growing season of stem radius measurements from the previous year to detect onset of the current year (data in 2016 began part-way through the growing season), growth onset could only be detected in 18 tree-years using the 95th percentile method. As a result, dates of growth onset for each tree, as predicted by each of the two methods, were compared for the stem radius data collected during the years of 2018 and 2019. A paired Wilcoxon rank sum test for non-parametric data confirmed that the two methods provided statistically identical dates of onset in 2018 ($n = 11$, $p = 0.052$) or 2019 ($n = 7$, $p = 0.171$, Wilcoxon test), indicating that the plateau method could be used to predict the onset of radial stem growth for each tree in all of the years (i.e. including the first year, 2017) in which measurements of radial stem growth were made. As such, our study included 9,748 observations of daily stem radius yielding 56 observations of radial stem growth onset (tree-years) across 27 white spruce trees and three years.

3.3.4 Models relating environment to onset of radial stem growth

Model Descriptions

The following is a summary of the three models whose equations are explained in detail in Delpierre et al. (2019). The three models build upon one another to become increasingly

complex. The temperature threshold model (Tt model) assumes that the onset of radial stem growth occurs when thresholds of photoperiod, DL^*, and temperature, T^*, have been crossed (Chuine et al. 2013, Chuine and Régnière 2017). The heat accumulation model (HS model) is a degree day model which assumes that after surpassing DL^*, heat accumulates above T^* until it reaches a heat accumulation threshold, F^*, and triggers the onset of radial stem growth (Seo et al. 2008, Delpierre et al. 2019). The chilling-induced heat sum model (CiHS model) suggests that F^* is modified by the severity of winter. The severity of the winter is measured by the number of 'chilling days', C_{tot}, defined as the number of days below a chilling temperature threshold, T_c^*, occurring between two photoperiod thresholds, DL_{cstart} and DL_{cend}. The heat accumulation threshold, F^*, necessary to trigger radial stem growth is then linearly modified by the number of days below the chilling threshold, C_{tot}, so that

$$F^*(d) = g * C_{tot} + h$$

where g (°C-days/chill day) is the slope of the relationship between winter severity and heat accumulation and h is the heat accumulation necessary to trigger onset in the absence of chilling (Cannell and Smith 1983, Delpierre et al. 2019). Similar to the HS model, the period of heat accumulation begins once a threshold of photoperiod, DL_{fstart}, is reached and accumulates above a temperature threshold, T_f^*. In this model, the periods of winter chilling and heat accumulation are representative of endo- and ecodormancy, respectively (Delpierre et al. 2019). Therefore, to encompass the possibilities that endo- and ecodormancy can be sequential or parallel (Cooke et al. 2012, Chuine et al. 2013, Delpierre et al. 2016, Chuine and Régnière 2017), the model allows the DL_{cstart}, DL_{cend}, and DL_{fstart} to vary widely and overlap (i.e., between 0 and 24 hours of light).

Parameter estimation and model comparisons

The model parameters for the three models discussed above were estimated via Bayesian inference. This method produces estimates of the parameters and their uncertainties in the form of a posterior distribution. The global mode of the posterior distribution, or point of maximum likelihood, represents the most likely value of the parameter. All models used a gaussian likelihood and uniform prior distributions bounded by the natural extremes of the photoperiod, temperature, or soil temperature of the dataset depending on the environmental variables used by the model. The posterior distributions were calculated using a differential evolution Markov Chain Monte Carlo (MCMC) in the R package 'BayesianTools' (Hartig et al. 2019). For each model, we ran 300,000 MCMC iterations. To confirm proper chain convergence, we required the Gelman-Rubin criterion (*psrf*) to be less than 1.05 after burn-in (Gelman et al. 1996).

To compare the models, we calculated the mean of the residuals (the mean difference between the predicted onset calculated at the point of maximum likelihood and the observed onset), the root mean square error (RMSE; calculated at the point of maximum likelihood), the Akaike information criterion corrected for small sample biases (AIC_C; Akaike 1973), the deviance information criterion (DIC; Spiegelhalter et al. 2002), and the widely-applicable information criterion (WAIC; Watanabe 2010) for Bayesian analyses. According to the information criterion, the model with the lowest value is the model of best fit. The model of best fit as represented by RMSE and the mean of the residuals is the model whose value is closest to zero.

Onset of growth in a changing climate

We explored how onset of radial stem growth may differ in a changing climate by following methods established in Rahman et al. (2020). We calculated onset using the model of best fit after adding 1, 2, 3, or 4 °C to the observed temperature data from 2017-2019. We chose these scenarios to replicate the predicted 4°C increase in global temperature by 2050 under the ambitious low emission scenario, RCP 2.6) (IPCC 2013, Taylor et al. 2013). We compared the calculated onset for each warming scenario to the observed onset using a paired Wilcoxon rank sum test grouped by year.

3.4 Results

3.4.1 Onset of radial stem growth

During the study period, the median onset of radial stem growth occurred on June 7 with statistically significant year-to-year variation (Figure 3.2). The median radial onset in 2019 occurred on June 4, which was five days earlier than in 2017 ($p < 0.001$) and four days earlier than in 2018 ($p < 0.0001$; Wilcoxon test). There was no significant difference between the radial stem growth onset between 2017 and 2018. Of the sampled trees, the earliest onset observed occurred on June 2 in 2018 and 2019, and June 3 in 2017. The latest observed onset occurred on Jun 16, 2017, June 14, 2018, and June 9, 2019. Therefore, all the studied trees began growing within the two weeks of each other in 2017 and 2018, and within the one week in 2019. The onset of radial stem growth did not vary with tree size (DBH, Pearson's product-moment correlation, $p = 0.11$).

3.4.2 Environmental conditions before and during growth onset

Figure 3.3 illustrates the changes in air and soil temperature alongside stem radius and onset of radial stem growth during the study period for Tree 5D. Mean daily air temperature

ranged between -36.5°C and 17.1°C from the winter solstice to the date of onset and did not differ significantly year-to-year (Figure 3.4a; Wilcoxon test). However, soil temperature before onset became significantly warmer each year ($p < 0.0001$; Wilcoxon test) increasing from an average of -4.77°C in 2017 to -2.77°C and -1.85°C in 2018 and 2019, respectively (Figure 3.4c).

During onset, mean daily soil temperature was significantly warmer in 2019 (3.10°C) when compared to 2017 (1.50°C; $p < 0.01$) and 2018 (1.63°C; $p < 0.0001$; Wilcoxon test) and ranged from 0.3 to 5.1°C (Figure 3.4d). Mean daily air temperature during onset was 11.5°C when averaged across the study period and ranged from 1.9 to 16.2°C (Figure 3.4b). Air temperature during onset was coolest in 2018 (10.1 ± 3.18°C), however this difference was only significant between 2017 and 2018 ($p < 0.01$; Wilcoxon test).

3.4.3 Model performance for detecting environmental controls of growth onset

The models generally improved with increasing model complexity so that the most complex model, CiHS, outperformed the simpler HS and Tt models (Table 3.1). Further, models with air temperature as the predicting variable outperformed those with soil temperature as they yielded mean residuals and RMSE closer to zero and the lower information criteria scores. Mean residuals showed that all models except for CiHS with air temperature tended to predict onset three to six days earlier than was observed.

The chilling-induced heat-sum model with air temperature had the best mean residual, RMSE, DIC, and WAIC values, signaling it as the best performing model when compared with these criteria. While the HS model had the lowest AIC_C score, the CiHS model's AIC_C score was within 1 unit, suggesting they were not significantly different when compared with this criterion (Akaike 1973). Therefore, the CiHS model with air temperature was identified as the best-supported model for predicting the onset of radial stem growth at our Arctic treeline site.

3.4.4 Posterior distributions of parameters reveal environmental thresholds

The parameter estimates of the CiHS model revealed multiple environmental cues which lead to onset of radial stem growth (Figure 3.5). First, according to our model, the winter chilling associated with triggering the onset of radial stem growth occurs on days with 10.4 – 13 hours of daylight (DL_{cstart} and DL_{cend}, respectively), corresponding to March 7 and March 27. During this time, 'chilling days' are those with daily average air temperatures below -19.2°C (T_c^*). Spring warming begins when there is at least 10 hours of daylight per day (DL_{fstart}), corresponding to March 4 and ends at the onset of radial stem growth. Heat accumulates when the daily average air temperatures (T_f^*) is above 1.4°C. The heat accumulation threshold (F^*) necessary to trigger radial stem growth is at least 172 degree-days (h) and increases by 6.9 degree-days per chilling day (g). There was a median of nine chilling days in 2017, two days in 2018 and zero chilling days in 2019.

3.4.5 Onset of radial stem growth under 1-4°C of warming

Under the hypothetical conditions where current mean daily air temperature was 1-4°C warmer, the average onset of radial stem growth varied anywhere from 2 – 13 days earlier than the actual date of onset depending on the degree of warming (Figure 3.6). Apart from 2017 under +1°C of warming, the earlier onset dates were significantly different for all years and climate scenarios tested (paired Wilcoxon test, $p < 0.01$). For example, when 4°C was added to the observed mean daily air temperature at Tree 5B, the CiHS model predicted that the onset of radial stem growth would begin 10 – 18 days earlier (Figure 3.6) on May 28, 26, and 24 in 2017, 2018, and 2019, respectively (Figure 3.7). At the current conditions, heat accumulation above T_f^* mainly began in early May. However, adding 4°C to the daily mean temperature caused heat

accumulation to begin an average of 2, 12, and 44 days earlier in 2017, 2018, and 2019, respectively. For example, when 4°C was added to the air temperature observed in 2019, heat accumulation began as early as March 18 but was modest until late April (Figure 3.7 *bottom*). In addition, when 4°C were added to the observed air temperature the number of chilling days below T_f^* decreased from an average of 10.6 days to six days in 2017 and 1.5 to zero days in 2018 (Figure 3.7 *middle*), decreasing the heat accumulation threshold from 244 °C-days to 213°C-days in 2017 and from 182 °C-days to 172°C-days in 2018. This combined with the earlier heat accumulation caused the calculated onset of radial stem growth to occur two weeks earlier than under the current conditions. When three or more degrees were added to the observed air temperature during the study period, no chilling days were observed in 2018 or 2019, and decreased the number of chilling days in 2017 by an average of 4 days (range 2-8 days).

3.5 Discussion

Our results partially confirm our hypothesis: the onset of radial stem growth of white spruce trees at our Arctic treeline site between 2018 and 2019 was best described by the chilling-induced heat sum model. However, air temperature alone was found to be a better predictor of onset than models including soil temperature or a combination of air and soil temperature. These results support similar studies of high latitude and alpine treeline conifers which suggest a common mechanism for the onset of radial growth of conifers in cold environments (Körner 2012, Delpierre et al. 2019). The chilling-induced heat sum model with air temperature revealed that extreme chilling below -19.2°C in winter (during days with 10.4 - 13 hours of light per day) increased the spring heat accumulation above ≥ 1.4°C (on days with ≥ 10 hours of light per day) necessary to trigger radial stem growth at our Arctic treeline site. Our simple simulation of

climate warming decreased the chilling in winter and increased the warming in spring so that the onset of radial stem growth was earlier in all scenarios. Together, these results suggest the onset of radial stem growth of white spruce growing at Arctic treeline is largely driven by air temperature and photoperiod.

Winter and Spring temperatures combine to trigger the onset of radial stem growth.

Our study adds to mounting evidence suggesting that both winter chilling and spring heating of air temperature trigger the onset of radial stem growth in conifers in cold climates (Cannell and Smith 1983, Körner 2012, Delpierre et al. 2019). However, two things make our results stand out. First, the specific chilling threshold (-19.2°C) and heat accumulation threshold (+1.4°C) for white spruce at our Arctic treeline site is far colder than the chilling threshold identified for all four conifer species growing in western Canada describe in Delpierre et al. (2019) (ranging from -5.6°C to +6.1°C). Second, we found that warmer winters decrease heat accumulation threshold necessary to trigger the onset of radial stem growth at Arctic treeline. These results directly contrast the findings of Delpierre et al. (2019) and Cannell and Smith (1983). According to their theory, temperatures below the chilling temperature threshold signal the passage of winter so that even low quantities of heat accumulation indicate the oncoming spring and trigger radial stem growth (Cannell and Smith 1983). Our conflicting results may be explained by local adaptation as the trees at Arctic treeline are located at comparatively higher latitudes and experience colder winter temperatures (68°N and -40°C) compared to those studies in boreal western Canada (47.54°N - 50.68°N and -10°C) (Delpierre et al. 2019).

A possible explanation for why the soil temperature models did not perform as well as air temperature models may be because soil temperature is a trigger for stem rehydration *prior* to growth. This is supported by patterns in the stem radius from winter to onset. As described in the

plateau method, the stem shrinks in winter due to desiccation and rapidly swells as it is rehydrated in spring (Tardif et al. 2001). Winter desiccation can be so severe that conifer trees experienced complete loss of xylem conductivity in winter due to excessive winter drought stress at comparable sites at alpine treeline in Japan (Maruta et al. 2020). But approximately two weeks prior to the onset of radial growth, xylem conductivity rapidly recovered, and stem radius swelled once soil temperatures were warm enough to hold liquid water (>0°C; Maruta et al. 2020). Importantly, this initial swelling due to rehydration in spring should not be confused with radial stem growth (Fraser 1956, Tardif et al. 2001), but instead represents the rehydration of the cambium which always precedes the onset of radial growth by 'several' weeks (Fraser 1956, Kozlowski and Peterson 1962, Kozlowski and Winget 1964, Tardif et al. 2001). Thus, because rehydration must occur prior to growth, soil temperature is still important to physiological processes leading to onset but may not be identified as a trigger of onset itself (Lupi et al. 2012a, 2012b). To identify a clear physiological link, we recommend further research investigating the changes in stem radius from winter to onset alongside measurements of xylem conductivity, air temperature, water stress, wind speed, and cellular development using histological analyses (i.e., microcores). Additionally, we recommend developing a model which incorporates winter chilling alongside the spring warming of both soil and air temperature.

The plateau method: Pros and cons

The plateau method for the detection of onset in radial growth presented here is a valuable tool for understanding the growth of trees in remote locations. For example, the plateau method provided quantitatively similar estimates to those of the 95th percentile method but detected onset in three times the number of tree-years. However, because the plateau method is based on an observed feature of our dataset, it cannot necessarily be applied to other species

growing in different environments. Instead, the plateau method may be uniquely suited for detecting onset in cold environments where trees experience severe winter desiccation and rapid spring rehydration prior to growth. For example, severe winter desiccation, rapid spring hydration, and a plateau prior to radial stem growth occurred ubiquitously in 40 trees of seven boreal tree species growing in northwestern Quebec including white spruce, black spruce (*Picea mariana*), jack pine (*Pinus banksiana*), red pine (*Pinus resinosa*), northern white cedar (*Thuja occidentalis*), and North American fir (*Abies balsamea*) (Tardif et al. 2001). The pattern can also be observed in the dendrometer series in European larch (*Larix decidua*) and Norway spruce (*Picea abies*) in the central Swiss Alps (see Figure 4 in King et al. 2013).

However, the plateau pattern is not observed in white spruce trees growing in temperate conditions of New York, USA (Griffin et al. 2020). While white spruce stems in temperate conditions desiccated during the winter and stem radii contracted sharply when air temperature decreased below -5°C (Griffin et al. 2020), the degree of desiccation was less severe (~ 250-400 um in Figure 6 of Griffin et al., 2020 compared to ~ 700-800 um at our sites) and rehydration was not rapid, extending throughout several weeks compared to the 10-14 days observed at our sites and in other cold environments (Tardif et al. 2001). Therefore, this pattern in stem radius may be unique to trees growing in very cold environments such as at high latitudes or altitudes. Local adaptation is common in phenology of other tree organs, such as for budburst (see, e.g., Chuine, Mignot, & Belmonte, 2000; Osada et al., 2018; Vitasse, Delzon, Bresson, Michalet, & Kremer, 2009; von Wuehlisch, Krusche, & Muhs, 1995). As a result, we suggest that the plateau method be used as a tool to detect the onset of radial stem growth in cold environments where these patterns are distinct and reliable.

Continued warming could advance the onset of radial stem growth.

Our results suggest that if the mean daily air temperature increased by ≥ 3° C, the onset of radial stem growth in white spruce growing at Arctic treeline would occur one to two weeks earlier. Under the ambitious low emission scenario (RCP 2.6), +4°C of warming in the Arctic will occur by 2050 (IPCC 2013). Our results echo those of Rossi et al. (2011) and Rahman et al. (2020), who found that spring warming would cause earlier onset over the next decades. The earlier onset date from our model can be attributed to the combination of both fewer chilling days in winter and earlier heat accumulation in spring. In fact, in the case of 4°C warming air temperature rarely (1-2 times over the three years studied) occurred below the chilling threshold and the onset of radial stem growth was only driven by heat accumulation. However, these conclusions assume the chilling and heat accumulation thresholds are static within species. Future research identifying these threshold temperatures for white spruce growing in warmer conditions (like those at the southern range of the species distribution) would elucidate if these thresholds are locally adapted.

An earlier onset date may lengthen the brief growing season and thus potentially increase radial stem growth at Arctic treeline (Rossi et al. 2011). However, the degree of radial stem growth – and therefore the degree of carbon sequestration – will also depend on the weather conditions during the summer (Rossi et al. 2011). Chapter 2 suggested that radial stem growth during the growing season relied on water availability as much as temperature. Therefore, while onset of radial stem growth is earlier, the potential to sequester more carbon depends on climate conditions remaining adequate throughout the growing season to effectively use the additional time (Deslauriers et al. 2014, Rossi et al. 2014a, 2014b).

Conclusion

We found that the process triggering the onset of radial stem growth of white spruce at the Arctic treeline is similar to that observed at alpine treeline (Körner 2012) and the boreal forest (Delpierre et al. 2019): winter chilling interacts with warming spring air temperature to initiate radial stem growth in spring. However, the extremely cold winter chilling threshold compared to studies elsewhere in the boreal forest suggest that environmental conditions initiating radial stem growth may be species, site, and/or regionally specific, complicating predictions of radial growth onset in a changing climate. As winters and springs at Arctic treeline become warmer due to climate change (Overland et al. 2019, Rantanen et al. 2022), our results suggest onset of radial stem growth significantly earlier. Such a change could increase the aboveground C sink at Arctic treeline if growing season conditions remain appropriate for radial growth (Rossi et al. 2011).

3.6 Acknowledgements

Funding for this research came from NASA Terrestrial Ecology grant NNX15AT86A and NASA ABoVE grant (Eitel-01). We are grateful for the support of the ABoVE Fairbanks logistics office, particularly Sarah Sackett. We also thank the Theodore Gordon Flyfishers, Inc. Founders Fund Scholarship for their generous contribution in supporting this research. We thank Dr. Nicolas Delpierre and Dr. Florian Hartig for their valuable guidance in the analysis used and for sharing their code in modeling the ecophysiological models presented in Delpierre et al (2019). We would like to thank Dr. Jyoti Jennewein, Dr. Kathryn Baker, William Weygint, Elizabeth Min, Elisabeth Hiers, Sarah Bruner, and Dr. Stephanie Schmiege for their assistance in the field. The authors have no conflict of interest to declare.

3.7 Figures and Tables

Table 3.1. Comparison of model performance between the models tested to understand how environmental conditions trigger radial stem growth in white spruce at Arctic treeline, AK. Model criteria include the mean of the residuals (days; i.e., the mean difference between the predicted onset calculated at the point of maximum likelihood and observed onset); root mean squared error (RMSE; days; calculated at the point of maximum likelihood); the differential Akaike information criterion corrected for small sample sizes (Δ AIC_C); the differential deviance information criterion (ΔDIC); and the differential widely-applicable information criterion (ΔWAIC). The information criterions are calculated as the difference (Δ) from the minimum across all models. According to the information criteria metrics, the best performing model has a score of zero and models within two points are not considered significantly different. Bolded terms indicate the best performing model according to that criterion.

Model Category	Temperature Variable Included in Model [a]	Mean of Residuals (days)	RMSE (days)	Δ AIC_C	ΔDIC	ΔWAIC
CiHS	Air	**0**	**3.1**	0.5	**0**	**0**
HS	Air	-3.5	4.8	**0**	31.8	1.3
CiHS	Air & Soil	-3.6	4.7	7.0	45.2	10
Tt	Air	-3.0	4.3	18.0	47.7	18.4
HS	Soil	-3.7	5.3	18.9	49.3	18.6
Tt	Soil	-6.6	8.2	71.8	101.6	73.8

[a] all models include photoperiod.

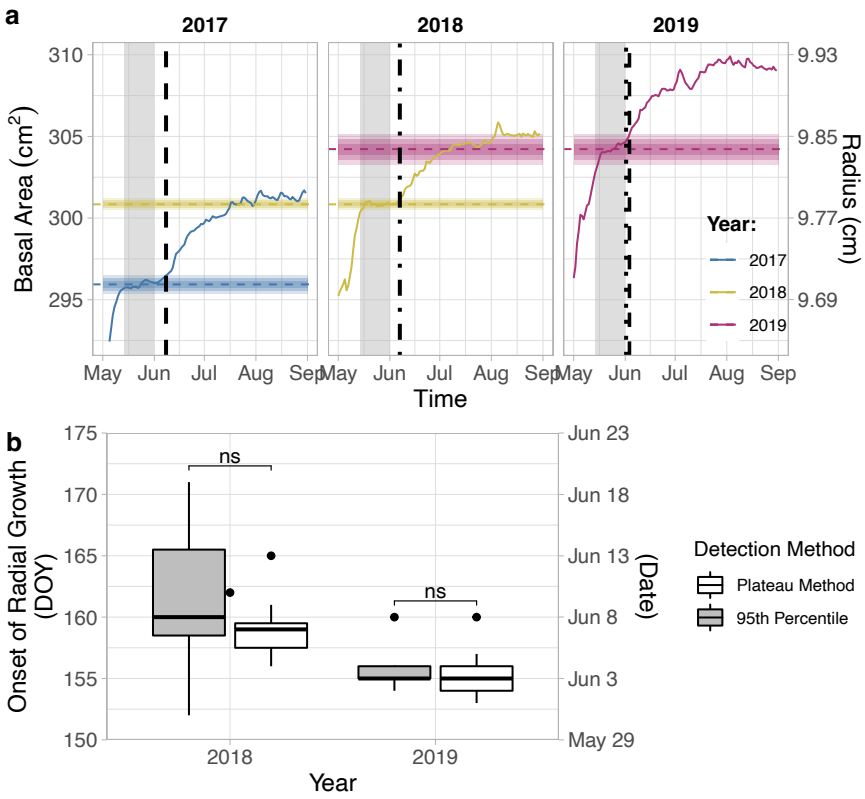

Figure 3.1. Visualization of the plateau method for detecting onset in radial stem growth at Arctic treeline, AK, and comparison to the 95th percentile method. (a) Visualization of the plateau method for detecting the onset of radial stem growth via point dendrometers in white spruce (*Picea glauca*) trees growing at the Arctic treeline in central Alaska, USA. Solid lines show basal area (cm^2 on primary y-axis; stem radius in cm on secondary y-axis) as measured by point dendrometers at Arctic treeline in AK (Tree 1C) over three growing seasons (panels). The last two weeks of May are shaded in grey to highlight the plateau in basal area before beginning radial stem growth during the growing season. The colored, horizontal dashed lines and shading represent the mean stem radius and three standard deviations, respectively, during the plateaued period for the corresponding year (colors); Lines are extended into the panel of the previous year to highlight the equivalence to the end of last year's growth. Onset derived via the 95th percentile method (vertical dashed lines) and the plateau method (vertical dotted lines) are identical in 2018 and differ by one day 2019 for Tree 1C. Note, onset derived via the 95th percentile method was not possible in 2017 as this was the first year with a complete growing season of data. (b) Onset of radial stem growth as detected by the plateau method did not differ significantly in either 2018 (n = 11, p = 0.052) or 2019 (n = 7, p = 0.171, Wilcoxon test). Primary y-axis shows day of year (DOY) while secondary y-axis shows corresponding date. Boxes represent the first and third quartiles, the bold line as the median. The whiskers extend from the box hinge to the smallest/largest value no further than 1.5 * inter-quartile range. Outlying points beyond this range are plotted individually.

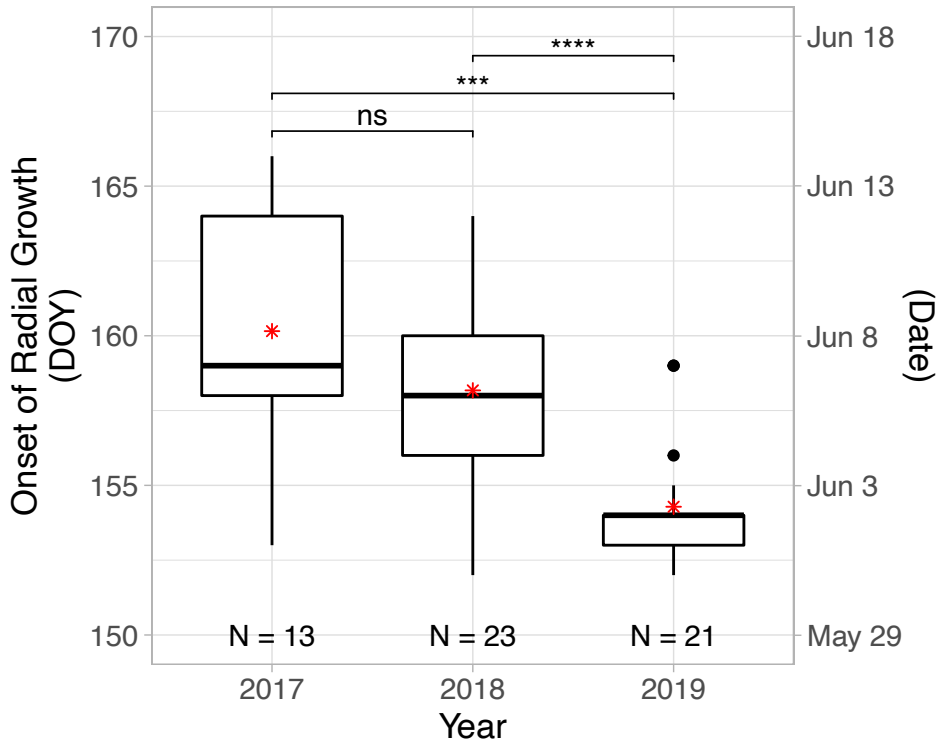

Figure 3.2. Onset of radial stem growth in white spruce growing at the Arctic treeline, AK from 2017 - 2019. Primary y-axis shows day of year (DOY) while secondary y-axis shows corresponding date. Boxes represent the first and third quartiles. Median and mean date of onset are represented by bold horizontal lines and red stars, respectively. The whiskers extend from the box hinge to the smallest/largest value no further than 1.5 * inter-quartile range from the hinge. Outlying points beyond this range are plotted individually. Brackets indicate Wilcoxon test results for non-parametric data (ns $p > 0.05$; *** $p < 0.001$; **** $p < 0.0001$).

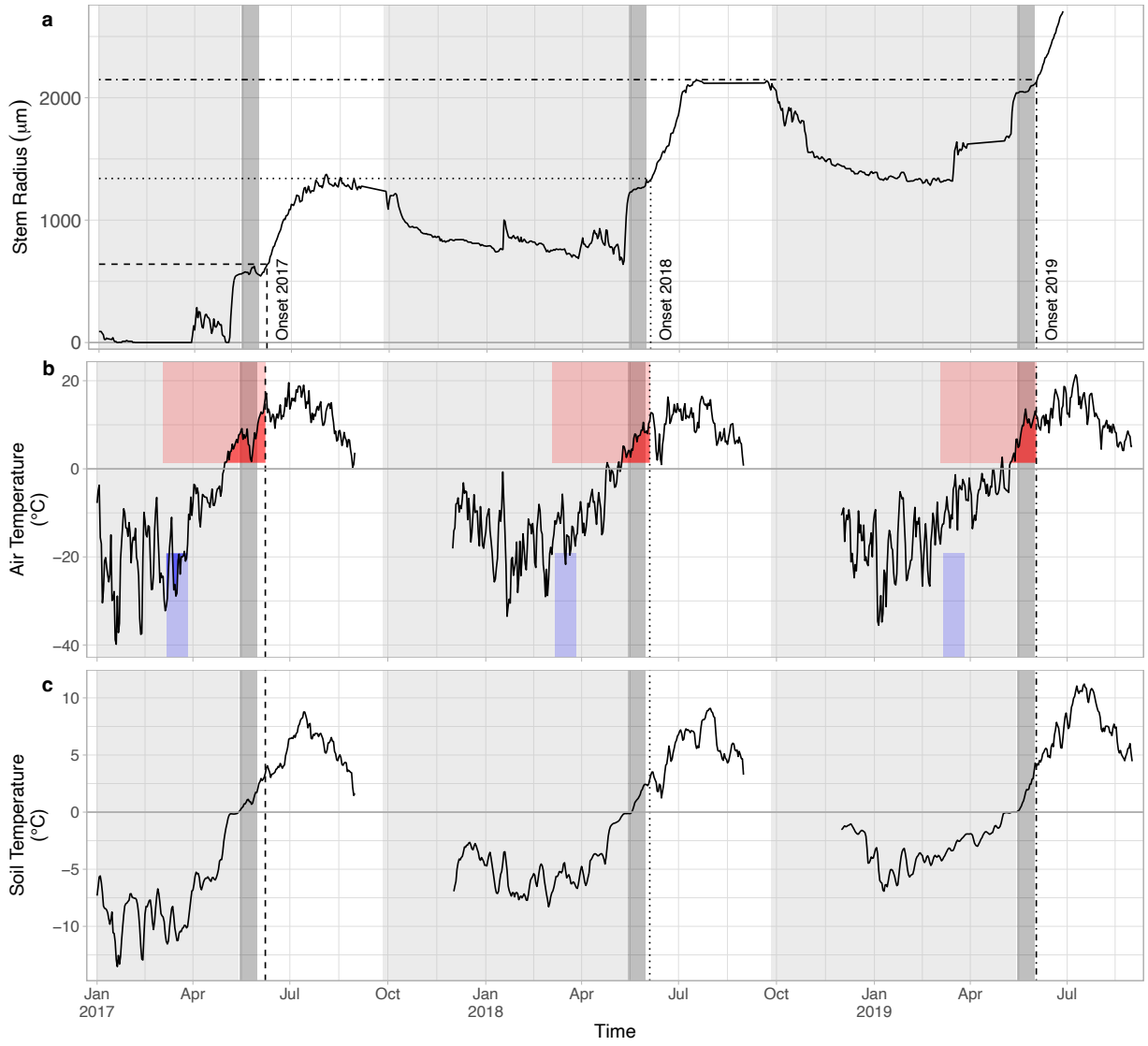

Figure 3.3. Time series of mean daily stem radius (a), air temperature (b), and soil temperature (c) from a white spruce tree (Tree 5D) growing at the Arctic treeline, AK from Jan 2017 – Oct 2019. Generally, the stem radius goes through three periods each year (Turcotte et al. 2009): a period of winter desiccation followed by rapid rehydration (light grey regions), plateau (dark grey regions), and radial stem growth (white region). Vertical lines represent the onset of radial stem growth on June 8, 2017 (dashed), June 4, 2018 (dotted), and June 2, 2019 (dash-dotted); horizontal lines represent the corresponding stem radius at onset. Gaps in data are missing data due to sensor malfunction but did not interfere with the calculations of onset. (*b*) The blue rectangle highlights the chilling period (bounded by DL_{cstart} and DL_{cend}) where days with mean daily temperature below T_c^* (-19.2°C, top of blue rectangle) accumulate according to the best fit model (CiHS with air temperature only). Similarly, the red rectangle highlights the heat accumulation period (bounded by $DL_{fstart}$and the onset of radial stem growth) where heat accumulates above T_f^* (1.4°C, bottom of red rectangle). Dark red or blue shading within these periods highlight the accumulation of heat or extreme chilling, respectively.

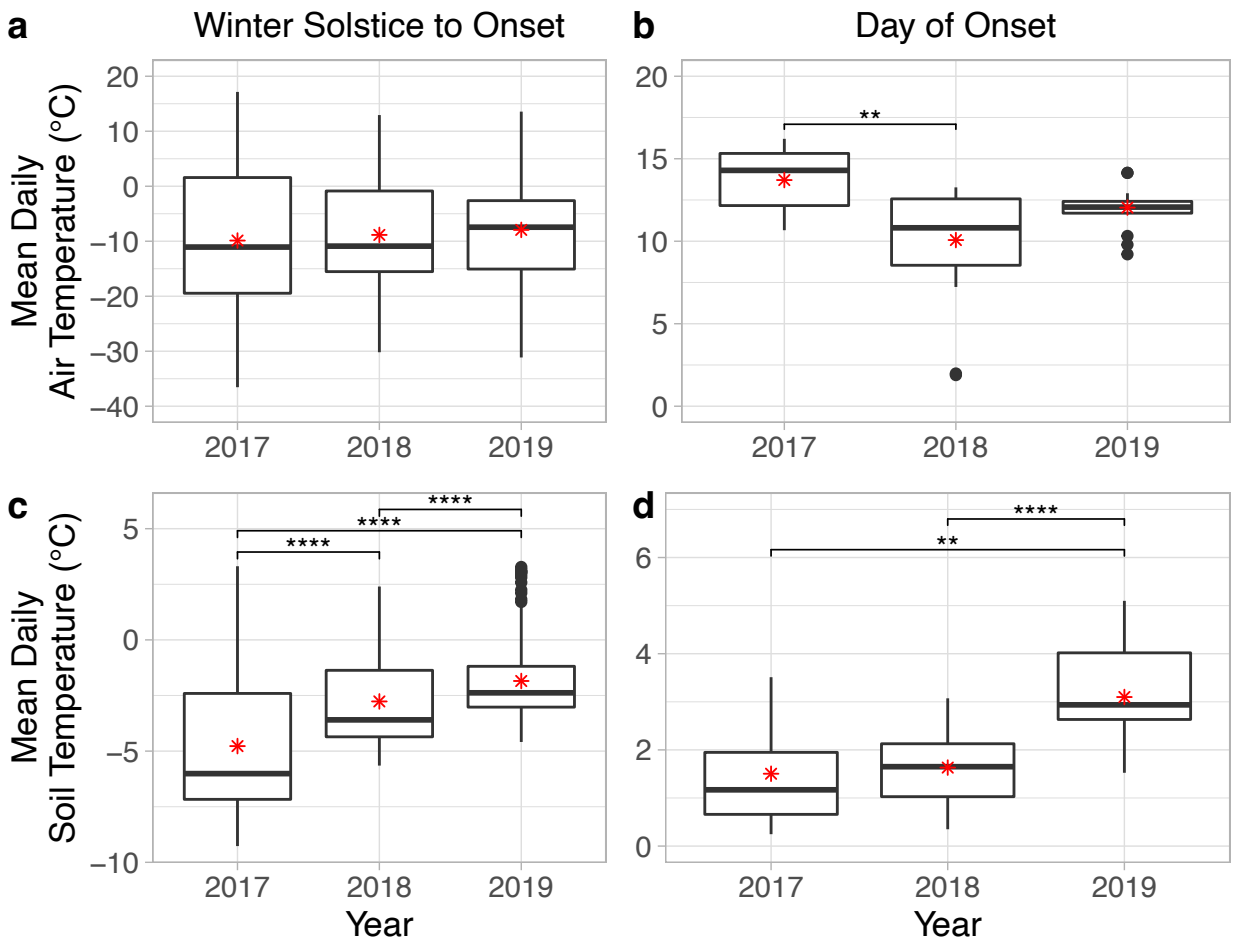

Figure 3.4. Mean daily air temperature (*top row*) and soil temperature (*bottom row*) conditions on the day of onset (*left column*) and from the winter solstice to the onset of radial stem growth (*right column*) in white spruce growing at the Arctic treeline, AK. The box represents the first and third quartiles. Median and mean values are represented by bold horizontal lines and red stars, respectively. The whiskers extend from the box hinge to the smallest/largest value no further than 1.5 * inter-quartile range from the hinge. Outlying points beyond this range are plotted individually. Brackets indicate Wilcoxon test results for non-parametric data; only significant differences are shown ($p < 0.01$; *** $p < 0.001$; **** $p < 0.0001$).**

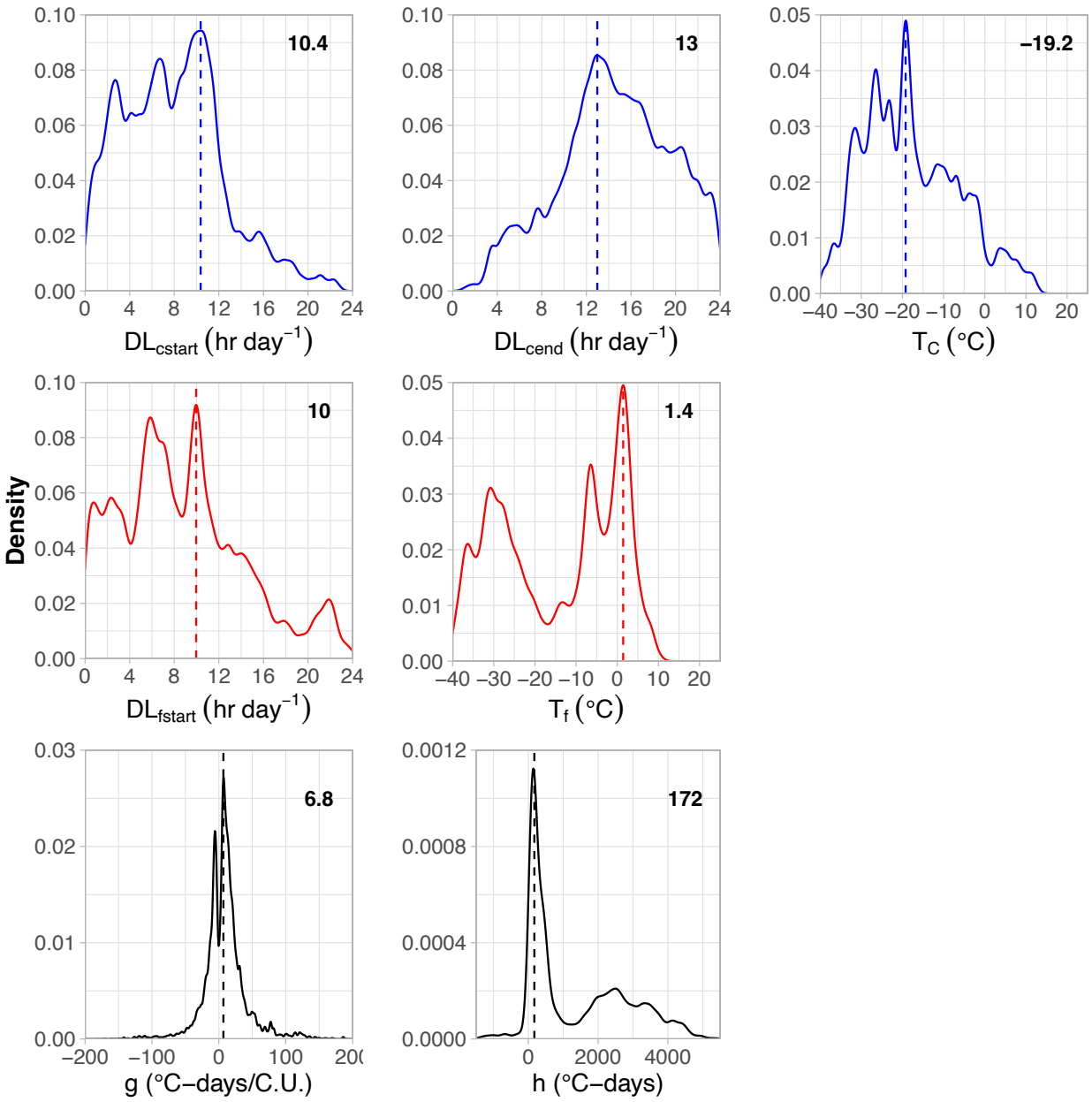

Figure 3.5. Posterior distributions of parameters in the best performing model (CiHS) with air temperature fit to white spruce growing at the Arctic treeline, AK. Parameters associated with winter chilling (*top row*) are in blue, spring warming (*middle row*) in red. The parameters in black (*g* and *h*; *bottom row*) are used in the linear model to determine the heat accumulation threshold, F^*, as predicted by the number of chilling days below the chilling threshold, T_c^*. The point of maximum likelihood of each distribution appears in the top right corner and as a vertical dashed line on the panel.

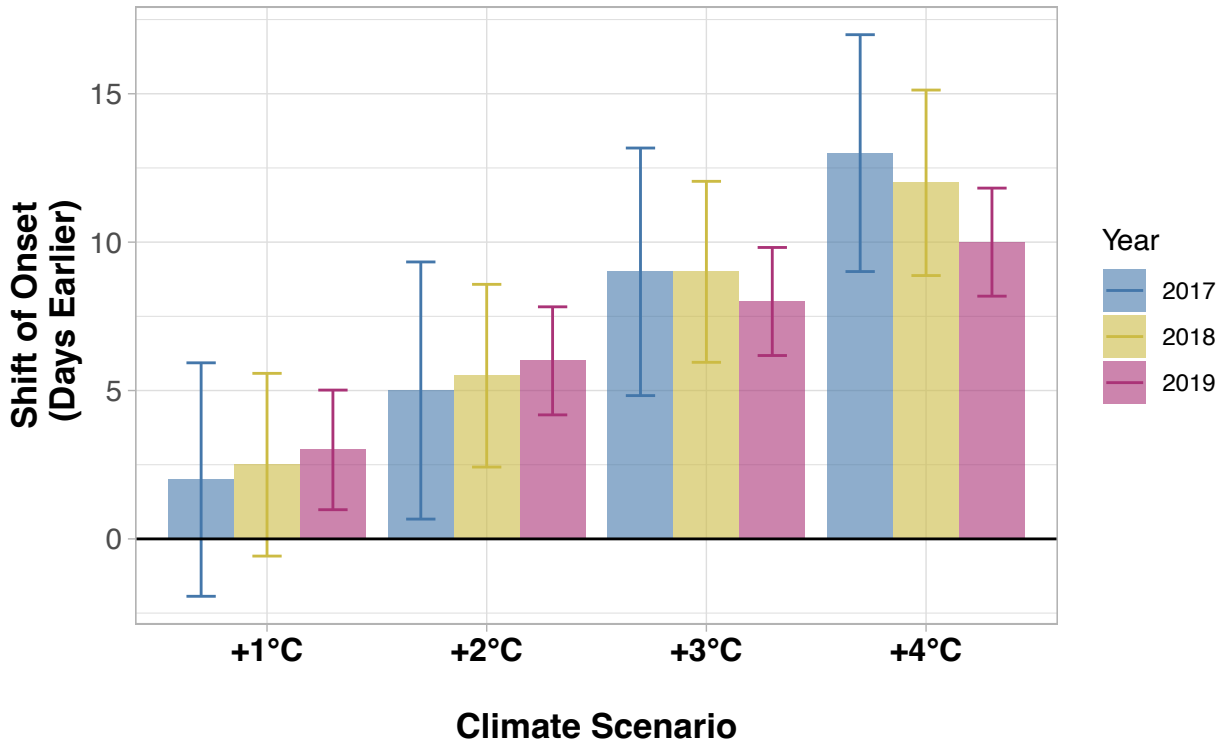

Figure 3.6. The changes in the onset of radial stem growth of white spruce growing at Arctic treeline, AK for the various climate scenarios. Climate scenarios were (ACIA 2005) calculated by the addition of 1-4 °C to the temperatures experienced in 2017-2019 (colors). Columns show the mean and error bars show the standard deviation. All predicted dates of onset were significantly different (paired Wilcoxon test, $p < 0.01$) except for those in 2017 under +1°C of warming ($p = 0.09$).

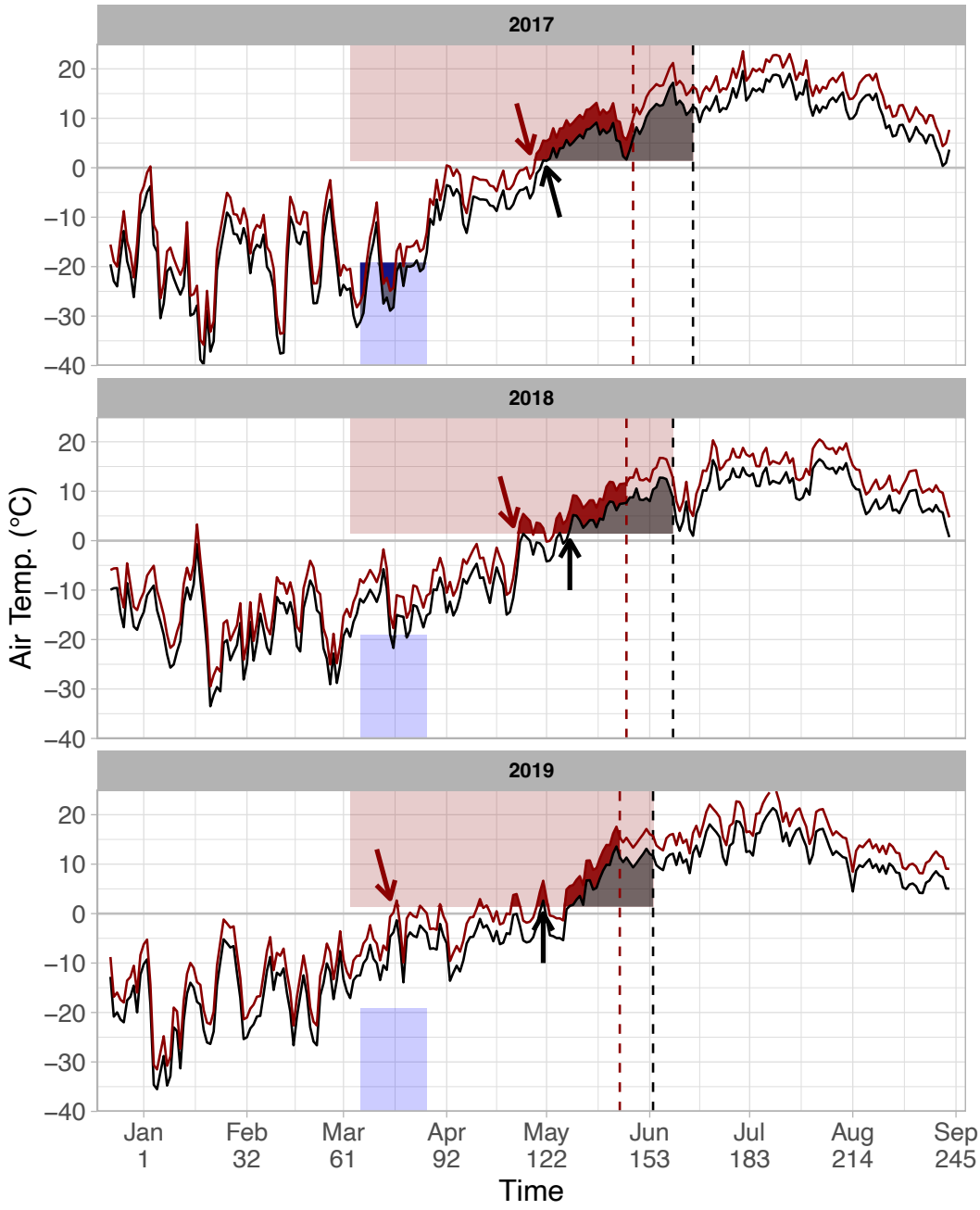

Figure 3.7. Graphical representation of the difference in onset of radial stem growth in a white spruce tree (Tree 5B) after the addition of 4°C (dark red line) to the actual daily mean temperature (black line) in 2017 (*top*), 2018 (*middle*), and 2019 (*bottom*). Onset of radial stem growth is represented by vertical dashed lines. Heat accumulation period is represented by the red shaded region and the chilling period by the blue shaded region. Red shaded areas under the temperature lines represent the accumulated temperature above the threshold, T_f^*, until onset of radial stem growth is triggered. Heat accumulation under 4°C warmer climate begins earlier (red arrows) than under current conditions (black arrows). Meanwhile, the number of days below the chilling threshold, T_c^*, during the chilling period (blue shaded areas above the temperature lines, *top row*) decreases with 4°C warmer climate.

Conclusion

As the northern edge of the largest terrestrial biome on Earth (Apps et al. 2006, Brown et al. 2010), the dynamics of Arctic treeline in response to climate change have global importance (Callaghan et al. 2002a, 2002b, Skre et al. 2002). The position and growth of trees at Arctic treeline will continue to have significant impacts on the global carbon cycle (Kurz and Apps 1993, Wilmking et al. 2006, Pearson et al. 2013), human resources (Callaghan et al. 2002a, Brown et al. 2010) and much more (Harding et al. 2002, Skre et al. 2002, Zhang et al. 2013). Until recently, research suggested that temperature-limitation on tree growth has delineated the global position of Arctic treeline (Körner and Paulsen 2004, Paulsen and Körner 2014). However, the predictions of treeline position and actual treeline position are different (Rees et al. 2020), suggesting a knowledge gap in our understanding of the limiting factors on tree growth when temperature-limitation is alleviated. A secondary control of water availability on growth at Arctic treeline may be critical to understanding this surprising behavior. As tree seedlings and saplings are the future of Arctic treeline, it is also critical to examine how water availability affects all tree life stages. Studies examining growth in response to air temperature alongside measurements of water availability will test this hypothesis and provide the foundation on which to assess the future of Arctic treeline in a rapidly changing climate.

This dissertation examined the relationships between climate (i.e., air temperature and water availability) and growth in the past and present in order to help examine the diverse

responses of treeline behavior and growth in white spruce growing at Arctic treeline. First, I examined recruitment and the long-term growth response to temperature and precipitation in saplings and mature trees during the 20th century (Chapter 1). The decrease in sapling recruitment was strongly associated with a warming but drying climate, however sapling growth remained unaffected. Mature tree growth initially increased but showed signs of water limitation towards the end of the century. I delved further into this finding by exploring how vapor pressure deficit, soil moisture, and air temperature drive the present-day growth response (Chapter 2). Results showed that vapor pressure deficit and VWC had a more prominent influence on growth than air temperature, especially in mature trees. Together, my first and second chapters show that radial stem growth at this section of Arctic treeline has recently become significantly affected by water availability. Finally, I identified the environmental cues triggering the onset of growth in spring to ascertain how future climate change may affect the duration of the growing season (Chapter 3). I found that a combination of extreme chilling and thermal accumulation of air temperature triggers the onset of growth at Arctic treeline. While the onset of growth is triggered mainly by air temperature, the capacity for trees to capitalize on longer growing seasons may still be limited by moisture. The results of these three studies lead me to conclude that the secondary control of water availability is strongly linked to the divergent responses of treeline behavior and growth in the Arctic.

In addition to increasing the understanding of the complex drivers of treeline position these studies have additional implications and highlight critical areas of research. These findings suggest decreases in regeneration and growth at Arctic treeline from water limitation may become more widespread as drier conditions in the Arctic become more frequent and intense (Overland et al., 2019). Therefore, I hypothesize that water limitation will be critical in

determining carbon storage capacity in boreal forests. Together these findings lay the groundwork for a better understanding of the dynamics at Arctic treeline and, more broadly, for understanding the distribution of the boreal forest biome. Even so, much remains to be understood, particularly regarding the physiological mechanisms driving these associations and the long-term impacts water-limitation. For example, while my work provides key information on the past and present dynamics between regeneration, growth, temperature-, and water-limitation at a section of Arctic treeline in interior Alaska, the long-term impacts at local and circumpolar scales remain to be elucidated.

My work indicates that temperature isotherm models predicting treeline position no longer provide accurate assessments in the rapidly changing Arctic. Future research that incorporates variables such as precipitation, vapor pressure deficit, and soil moisture/temperature into models of northern forests will greatly improve our estimates of how changes at Arctic treeline will affect global carbon cycling, nutrient cycling, and future climate change. Additionally, future research identifying the physiological mechanisms explaining the strong associations between water availability, regeneration, and growth at Arctic treeline are critical. Future research may consider investigating growth and carbon balance of saplings and mature trees in different water regimes. Lastly, future research must continue to explore the factors affecting seedling establishment and survival in a drier Arctic environment, such as herbivory (Olnes and Kielland 2016, Olnes et al. 2017, 2018), boundary layer dynamics (e.g., changes in snowpack), and microenvironment (Maguire et al. 2019).

At the broadest definition, terrestrial biomes are defined by their temperature and precipitation regimes (Whittaker 1970). However, up until now, temperature has been the dominant driver of Arctic treeline position and growth (Körner 2012). But as the climate rapidly

warms and the isotherm, which previously delineated treeline position so ubiquitously, shifts northward (Körner 2012), precipitation and other plant water sources now limit the northern distribution of boreal forest biome. This dissertation links past and present climate, growth, and regeneration of white spruce growing Arctic treeline and paves the way for exploring the physiological mechanisms driving this link. Through these new findings, I believe that this dissertation advances our understanding of Arctic treeline dynamics and will help to predict the future of Arctic treeline more accurately in a changing climate.

References

ACIA. 2005. Arctic Climate Impact Assessment. Cambridge University Press, Cambridge, UK.

Akaike, H. 1973. Information theory and an extension of the maximum likelihood principle. International Symposium on Information Theory:267–281.

Andreu-Hayles, L., R. D'Arrigo, K. J. Anchukaitis, P. S. A. Beck, D. Frank, and S. Goetz. 2011. Varying boreal forest response to Arctic environmental change at the Firth River, Alaska. Environmental Research Letters 6.

Angell, A. C., and K. Kielland. 2009. Establishment and growth of white spruce on a boreal forest floodplain: Interactions between microclimate and mammalian herbivory. Forest Ecology and Management 258:2475–2480.

Apps, M. J., A. Z. Shvidenko, and E. A. Vaganov. 2006. Boreal Forests and the Environment: A Foreword. Mitigation and Adaptation Strategies for Global Change 2006 11:1 11:1–4.

Axelsson, P. 2000. DEM generation from laser scanner data using adaptive TIN models. International Archives of Photogrammetry and Remote Sensing 33:110–117.

Barber, V. A., G. P. Juday, and B. P. Finney. 2000. Reduced growth of Alaskan white spruce in the twentieth century from temperature-induced drought stress. Nature 405:668–673.

Bates, D., M. Mächler, B. Bolker, and S. Walker. 2015. Fitting Linear Mixed-Effects Models Using lme4. Journal of Statistical Software 67:1–48.

Begum, S., K. Kudo, M. H. Rahman, S. Nakaba, Y. Yamagishi, E. Nabeshima, W. D. Nugroho, Y. Oribe, P. Kitin, H.-O. O. Jin, R. Funada, Md, H. Rahman, Satoshi Nakaba, Y. Yamagishi, Eri Nabeshima, Widyanto, D. Nugroho, Y. Oribe, Peter Kitin, H.-O. O. Jin, and

• Ryo Funada. 2018. Climate change and the regulation of wood formation in trees by temperature. Trees - Structure and Function 32:3–15.

Begum, S., S. Nakaba, Y. Oribe, T. Kubo, and R. Funada. 2010. Cambial sensitivity to rising temperatures by natural condition and artificial heating from late winter to early spring in the evergreen conifer Cryptomeria japonica. Trees - Structure and Function 24:43–52.

Van Bogaert, R., K. Haneca, J. Hoogesteger, C. Jonasson, M. De Dapper, and T. V. Callaghan. 2011. A century of tree line changes in sub-Arctic Sweden shows local and regional variability and only a minor influence of 20th century climate warming. Journal of Biogeography 38:907–921.

Briffa, K. R., F. H. Schweingruber, P. D. Jones, T. J. Osborn, S. G. Shiyatov, and E. A. Vaganov. 1998. Reduced sensitivity of recent tree-growth to temperature at high northern latitudes. Nature 391:678–682.

Brodersen, C. R., M. J. Germino, D. M. Johnson, K. Reinhardt, W. K. Smith, L. M. Resler, M. Y. Bader, A. Sala, L. M. Kueppers, G. Broll, D. M. Cairns, F. K. Holtmeier, and G. Wieser. 2019. Seedling Survival at Timberline Is Critical to Conifer Mountain Forest Elevation and Extent. Frontiers in Forests and Global Change 2.

Brown, M., T. A. Black, Z. Nesic, V. N. Foord, D. L. Spittlehouse, A. L. Fredeen, N. J. Grant, P. J. Burton, and J. A. Trofymow. 2010. Impact of mountain pine beetle on the net ecosystem production of lodgepole pine stands in British Columbia. Agricultural and Forest Meteorology 150:254–264.

Brownlee, A. H., P. F. Sullivan, A. Z. Csank, B. Sveinbjörnsson, and S. B. Sarah. 2016. Drought- induced stomatal closure probably cannot explain divergent white spruce growth

in the Brooks Range, Alaska, USA. Ecology 97:145–159.

Bunn, A., M. Korpela, F. Biondi, F. Campelo, P. Mérian, F. Qeadan, and C. Zang. 2010. A dendrochronology program library in R (dplR). Dendrochronologia 26:115–124.

Cabon, A., R. L. Peters, P. Fonti, J. Martínez-Vilalta, and M. De Cáceres. 2020. Temperature and water potential co-limit stem cambial activity along a steep elevational gradient. New Phytologist 226:1325–1340.

Callaghan, T. V, L. O. Björn, and F. S. Chapin III. 2005. Arctic Tundra and Polar Desert Ecosystems. Page ACIA 2005: Arctic Climate Impact Assessment. Cambridge, UK.

Callaghan, T. V, R. M. M. Crawford, M. Eronen, A. Hofgaard, S. Payette, W. G. Rees, O. Skre, B. Sveinbjörnsson, T. K. Vlassova, and B. R. Werkman. 2002a. The dynamics of the tundra-taiga boundary: an overview and suggested coordinated and integrated approach to research. Ambio Special Report 12, Tundra-Taiga Treeline Research 12:3–5.

Callaghan, T. V, B. R. Werkman, and R. M. M. Crawford. 2002b. The Tundra-Taiga Interface and Its Dynamics: Concepts and Applications. Ambio Special Report:6–14.

Camarero, J. J., A. Gazol, R. Sánchez-Salguero, A. Fajardo, E. J. B. McIntire, E. Gutiérrez, E. Batllori, S. Boudreau, M. Carrer, J. Diez, G. Dufour-Tremblay, N. P. Gaire, A. Hofgaard, V. Jomelli, A. V. Kirdyanov, E. Lévesque, E. Liang, J. C. Linares, I. E. Mathisen, P. A. Moiseev, G. Sangüesa-Barreda, K. B. Shrestha, J. M. Toivonen, O. V. Tutubalina, and M. Wilmking. 2021. Global fading of the temperature–growth coupling at alpine and polar treelines. Global Change Biology 27:1879–1889.

Cannell, M. G. R., and R. I. Smith. 1983. Thermal Time, Chill Days and Prediction of Budburst in Picea sitchensis. Journal of Applied Ecology 20:951–963.

Chabot, B. F., and H. A. Mooney. 1985. Physiological Ecology of North American Plant Communities. Page (B. F. Chabot and H. A. Mooney, Eds.) Physiological Ecology of North American Plant Communities. First edition. New York, NY.

Chuine, I., I. G. de Cortazar-Atauri, K. Kramer, and H. Hänninen. 2013. Plant Development Models. Pages 275–293 *in* M. D. Schwartz, editor. Phenology: An Integrative Environmental Science. 2nd edition. Springer Netherlands, Dordrecht.

Chuine, I., and J. Régnière. 2017. Process-Based Models of Phenology for Plants and Animals. Annual Review of Ecology, Evolution, and Systematics 48:159–182.

Cook, E. R. 1985. A time series analysis approach to tree-ring standardiation. University of Arizona, Tuscon.

Cook, E. R., K. R. Briffa, D. M. Meko, D. A. Graybill, and G. Funkhouser. 1995. The 'segment length curse' in long tree-ring chronology development for palaeoclimatic studies. The Holocene 5:229–237.

Cook, E. R., and L. A. Kairiukstis. 1990. Methods of Dendrochronology. Page (E. R. Cook and L. A. Kairiukstis, Eds.). Springer Netherlands, Dordrecht.

Cooke, J. E. K., M. E. Eriksson, and O. Junttila. 2012. The dynamic nature of bud dormancy in trees: Environmental control and molecular mechanisms. Plant, Cell and Environment 35:1707–1728.

Cuny, H. E., C. B. K. Rathgeber, D. Frank, P. Fonti, H. Makinen, P. Prislan, S. Rossi, E. M. Del Castillo, F. Campelo, H. Vavrčík, J. J. Camarero, M. V. Bryukhanova, T. Jyske, J. Gricar, V. Gryc, M. De Luis, J. Vieira, K. Cufar, A. V. Kirdyanov, W. Oberhuber, V. Treml, J. G. Huang, X. Li, I. Swidrak, A. Deslauriers, E. Liang, P. Nojd, A. Gruber, C. Nabais, H.

Morin, C. Krause, G. King, and M. Fournier. 2015. Woody biomass production lags stem-girth increase by over one month in coniferous forests. Nature Plants 1:1–6.

D'Arrigo, R., R. Wilson, B. Liepert, and P. Cherubini. 2008. On the "Divergence Problem" in Northern Forests: A review of the tree-ring evidence and possible causes. Global and Planetary Change 60:289–305.

Delpierre, N., S. Lireux, F. Hartig, J. J. Camarero, A. Cheaib, K. Čufar, H. Cuny, A. Deslauriers, P. Fonti, J. Gričar, J. Huang, C. Krause, G. Liu, M. de Luis, H. Mäkinen, E. M. del Castillo, H. Morin, P. Nöjd, W. Oberhuber, P. Prislan, S. Rossi, S. M. Saderi, V. Treml, H. Vavrick, and C. B. K. Rathgeber. 2019. Chilling and forcing temperatures interact to predict the onset of wood formation in Northern Hemisphere conifers. Global Change Biology 25:1089–1105.

Delpierre, N., Y. Vitasse, I. Chuine, J. Guillemot, S. Bazot, T. Rutishauser, and C. B. K. Rathgeber. 2016. Temperate and boreal forest tree phenology: from organ-scale processes to terrestrial ecosystem models. Annals of Forest Science 73:5–25.

Deslauriers, A., M. Beaulieu, L. Balducci, A. Giovannelli, M. J. Gagnon, and S. Rossi. 2014. Impact of warming and drought on carbon balance related to wood formation in black spruce. Annals of Botany 114:335–345.

Deslauriers, A., S. Rossi, T. Anfodillo, and A. Saracino. 2008. Cambial phenology, wood formation and temperature thresholds in two contrasting years at high altitude in southern Italy. Tree Physiology 28:863–871.

Driscoll, W. W., G. C. Wiles, R. D. D'Arrigo, and M. Wilmking. 2005. Divergent tree growth response to recent climatic warming, Lake Clark National Park and Preserve, Alaska.

Geophysical Research Letters 32:1–4.

Eitel, J., A. Maguire, N. Boelman, L. Vierling, K. L. Griffin, J. Jensen, T. Magney, P. Mahoney, A. Meddens, C. Silva, and O. Sonnentag. 2019. Remotely sensing tree physiology at northern treeline: Do late-season changes in the photochemical reflectance index (PRI) respond to climate or photoperiod? Remote Sensing of Environment 221:340–350.

Eitel, J. U. H., K. L. Griffin, N. T. Boelman, A. J. Maguire, A. J. H. Meddens, J. Jensen, L. A. Vierling, S. C. Schmiege, and J. S. Jennewein. 2020. Remote sensing tracks daily radial wood growth of evergreen needleleaf trees. Global Change Biology:0–3.

Ellison, S. B. Z., P. F. Sullivan, S. M. P. Cahoon, and R. E. Hewitt. 2019. Poor nutrition as a potential cause of divergent tree growth near the Arctic treeline in northern Alaska. Ecology 100:1–18.

Etzold, S., F. Sterck, A. K. Bose, S. Braun, N. Buchmann, W. Eugster, A. Gessler, A. Kahmen, R. L. Peters, Y. Vitasse, L. Walthert, K. Ziemińska, and R. Zweifel. 2022. Number of growth days and not length of the growth period determines radial stem growth of temperate trees. Ecology Letters 25:427–439.

Ford, K. R., C. A. Harrington, S. Bansal, P. J. Gould, and J. B. St. Clair. 2016. Will changes in phenology track climate change? A study of growth initiation timing in coast Douglas-fir. Global Change Biology 22:3712–3723.

Fraser, D. A. 1956. II . Ecological Conditions and Radial Increment. Ecology 37:777–789.

Gelfand, A. E., and D. K. Dey. 1994. Bayesian Model Choice: Asymptotics and Exact Calculations. Journal of the Royal Statistical Society. Series B (Methodological) 56:501–514.

Gelman, A., X.-L. Meng, and H. Stern. 1996. Posterior predictive assessment of model fitness via realized discrepancies. Statistica Sinica 6:733–760.

Griffin, K. L., Z. M. Griffin, S. C. Schmiege, S. G. Bruner, N. T. Boelman, L. A. Vierling, and J. U. H. Eitel. 2022. Variation in White spruce needle respiration at the species range limits: A potential impediment to Northern expansion. Plant Cell and Environment 45:2078–2092.

Griffin, K. L., S. C. Schmiege, S. G. Bruner, N. T. Boelman, L. A. Vierling, and J. U. H. Eitel. 2021. High Leaf Respiration Rates May Limit the Success of White Spruce Saplings Growing in the Kampfzone at the Arctic Treeline. Frontiers in Plant Science 12.

Griffin, K. L., H. G. Thomas, S. Bruner, P. Mckenzie, and J. Hise. 2020. Novel insights from point-dendrometers in an urban setting: linking environmental variation to fluctuations in stem radius:0–31.

Gustafson, A., P. A. Miller, R. G. Björk, S. Olin, and B. Smith. 2021. Nitrogen restricts future sub-Arctic treeline advance in an individual-based dynamic vegetation model. Biogeosciences 18:6329–6347.

Hansen, A. M. C., P. V Potapov, R. Moore, M. Hancher, S. A. Turubanova, D. Tyukavina, AThau, S. V Stehman, S. J. Goetz, T. R. Loveland, A. Kommareddy, A. Egorov, L. Chini, C. O. Justice, and J. R. G. Townshend. 2013. High-Resolution Global Maps of 21st-Century Forest Cover Change. Science 342:850–853.

Harding, R., P. Kuhry, T. R. Christensen, M. T. Sykes, R. Dankers, and S. van der Linden. 2002. Climate feedbacks at the tundra-taiga interface. Ambio Special Report:47–55.

Harsch, M. A., P. E. Hulme, M. S. McGlone, and R. P. Duncan. 2009. Are treelines advancing? A global meta-analysis of treeline response to climate warming. Ecology Letters 12:1040–

1049.

Hartig, F., F. Minunno, and S. Paul. 2019. BayesianTools:General-Purpose MCMC and SMC Samplers and Tools for Bayesian Statistics. R package version 0.1.7.

Hijmans, R. J. 2019. geosphere: Spherical Trigonometry. R package version 1.5-10.

Hoch, G., and C. Körner. 2003. The carbon charging of pines at the climatic treeline: a global comparison. Oecologia 135:10–21.

Hofgaard, A., C. Ols, I. Drobyshev, A. J. Kirchhefer, S. Sandberg, and L. Söderström. 2019. Non-stationary Response of Tree Growth to Climate Trends Along the Arctic Margin. Ecosystems 22:434–451.

Holtmeier, F.-K. 2009. Mountain Timberlines: Ecology, Patchiness, and Dynamics. Springer, Berlin, Heidelberg, New York.

Holtmeier, F.-K., and G. Broll. 2019. Treeline Research—From the Roots of the Past to Present Time. A Review. Forests 11:38.

Hubbard, T. D., R. D. Koehler, and R. A. Combellick. 2011. High-resolution lidar data for Alaska infrastructure corridors.

IPCC. 2013. Climate Change 2013: the Physical Science Basis. Conrtribution of Working Group I to the Fifth Assesment Report of the Intergovernmental Panel on Climate Change. Cambridge, UK.

Isenburg, M. 2017. Efficient tools for LiDAR Processing.

Jackson, R. B., J. Canadell, J. R. Ehleringer, H. A. Mooney, O. E. Sala, and E. D. Schulze. 1996. A global analysis of root distributions for terrestrial biomes. Oecologia 108:389–411.

Jacoby, G. C., and N. K. Davi. 2000. NOAA/WDS Paleoclimatology - Jacoby - Dalton Highway - PCGL - ITRDB AK104. NOAA National Centers for Environmental Information.

Jones, H. G. 1992. Plants and microclimate: a quantitative approach to environmental plant physiology. 2nd Editio. Cambridge University Press, Cambridge.

Kambo, D., and R. K. Danby. 2018a. Factors influencing the establishment and growth of tree seedlings at Subarctic alpine treelines. Ecosphere 9.

Kambo, D., and R. K. Danby. 2018b. Constraints on treeline advance in a warming climate: A test of the reproduction limitation hypothesis. Journal of Plant Ecology 11:411–422.

King, G., P. Fonti, D. Nievergelt, U. Büntgen, and D. Frank. 2013. Climatic drivers of hourly to yearly tree radius variations along a 6°C natural warming gradient. Agricultural and Forest Meteorology 168:36–46.

Körner, C. 2006. Significance of temperature in plant life. Pages 48–69 *in* J. I. L. Morison and M. D. Morecroft, editors. Plant growth and climate change. Blackwell, Oxford.

Körner, C. 2012. Alpine Treelines: Functional Ecology of the Global High Elevation Tree Limits. Springer, Basel, Switzerland.

Körner, C. 2016. When it gets cold, plant size matters - a comment on tree line. Journal of Vegetation Science 27:6–7.

Körner, C. 2021. The cold range limit of trees. Trends in Ecology and Evolution 36:979–989.

Körner, C., D. Basler, G. Hoch, C. Kollas, A. Lenz, C. F. Randin, Y. Vitasse, and N. E. Zimmermann. 2016. Where, why and how? Explaining the low-temperature range limits of temperate tree species. Journal of Ecology 104:1076–1088.

Körner, C., and G. Hoch. 2006. A Test of Treeline Theory on a Montane Permafrost Island. Arctic, Antarctic, and Alpine Research 38:113–119.

Körner, C., and J. Paulsen. 2004. A world-wide study of high altitude treeline temperatures. Journal of Biogeography 31:713–732.

Kozlowski, T., R. Kramer, and S. Pallardy. 2008. The physiological ecology of woody plants. Third edition. Elesvier, San Diego, California.

Kozlowski, T. T., and T. A. Peterson. 1962. Seasonal Growth of Dominant, Intermediate, and Suppressed Red Pine Trees. Botanical Gazette 124:146–154.

Kozlowski, T. T., and C. H. Winget. 1964. Diurnal and Seasonal Variation in Radii of Tree Stems. Ecology 45:149–155.

Kurz, W. A., and M. J. Apps. 1993. Conntribution of northern forests to the global C cycle: Canada as a case study. Water, Air, & Soil Pollution 70:163–176.

Kuuluvainen, T., J. Mäki, L. Karjalainen, and H. Lehtonen. 2002. Tree age distributions in old-growth forest sites in Vienansalo wilderness, eastern Fennoscandia. Silva Fennica 36:169–184.

Lang, J. A. 2019. Red foxes engineer the boreal forest: impacts of denning on vegetation near the Arctic treeline.

Lange, J., M. Carrer, M. F. J. Pisaric, T. J. Porter, J. W. Seo, M. Trouillier, and M. Wilmking. 2020. Moisture-driven shift in the climate sensitivity of white spruce xylem anatomical traits is coupled to large-scale oscillation patterns across northern treeline in northwest North America. Global Change Biology 26:1842–1856.

Larsson, L. 2016. CooRecorder and Cdendro Programs of the Coorecorder/Cdendropackage

Version 8.1.

Leland, C., J. Hom, N. Skowronski, F. T. Ledig, P. J. Krusic, E. R. Cook, D. Martin-Benito, J. Martin-Fernandez, and N. Pederson. 2016. Missing rings, synchronous growth, and ecological disturbance in a 36-year pitch pine (pinus rigida) provenance study. PLoS ONE 11:1–17.

Li, X., E. Liang, J. Gričar, S. Rossi, K. Čufar, and A. M. Ellison. 2017. Critical minimum temperature limits xylogenesis and maintains treelines on the southeastern Tibetan Plateau. Science Bulletin 62:804–812.

Lloyd, A. H. 2005. Ecological Histories from Alaskan Tree Lines Provide Insight into Future Change. Ecology 86:1687–1695.

Lloyd, A. H., and A. G. Bunn. 2007. Responses of the circumpolar boreal forest to 20th century climate variability. Environmental Research Letters 2.

Lloyd, A. H., and C. L. Fastie. 2002. Spatial and temporal variability in the growth and climate response of treeline trees in Alaska. Climatic Change 52:481–509.

Lupi, C., H. Morin, A. Deslauriers, and S. Rossi. 2012a. Xylogenesis in black spruce: Does soil temperature matter? Tree Physiology 32:74–82.

Lupi, C., H. Morin, A. Deslauriers, S. Rossi, and D. Houle. 2012b. Increasing nitrogen availability and soil temperature: Effects on xylem phenology and anatomy of mature black spruce. Canadian Journal of Forest Research 42:1277–1288.

Lyu, L., Q. Bin Zhang, M. G. Pellatt, U. Büntgen, M. H. Li, and P. Cherubini. 2019. Drought limitation on tree growth at the Northern Hemisphere's highest tree line. Dendrochronologia 53:40–47.

Maguire, A. J. A. J., J. U. H. J. U. H. Eitel, L. A. L. A. Vierling, D. M. D. M. Johnson, K. L. K. L. Griffin, N. T. K. Boelman, J. E. J. E. Jensen, H. E. H. E. Greaves, and A. J. H. A. J. H. Meddens. 2019. Terrestrial lidar scanning reveals fine-scale linkages between microstructure and photosynthetic functioning of small-stature spruce trees at the forest-tundra ecotone. Agricultural and Forest Meteorology 269–270:157–168.

Maher, C. T., R. J. Dial, N. J. Pastick, R. E. Hewitt, M. T. Jorgenson, and P. F. Sullivan. 2021. The climate envelope of Alaska's northern treelines: implications for controlling factors and future treeline advance. Ecography 44:1710–1722.

Mamet, S. D., and G. P. Kershaw. 2012. Subarctic and alpine tree line dynamics during the last 400 years in north-western and central Canada. Journal of Biogeography 39:855–868.

Maruta, E., M. Kubota, and T. Ikeda. 2020. Effects of xylem embolism on the winter survival of Abies veitchii shoots in an upper subalpine region of central Japan. Scientific Reports 10:6594.

McCullagh, P., and J. A. Nelder. 1990. Generalized Linear Models. Page Monographs on Statistics and Applied Probability. Second. Chapman & Hall, London.

McGuire, A. D., T. S. Rupp, A. Breen, E. S. Euskirchen, S. Marchenko, V. Romanovsky, A. Bennett, W. R. Bolton, T. Carman, H. Genet, T. Kurkowski, M. Lara, D. Nicolsky, R. Rutter, and K. Timm. 2016. Final Report: Integrated Ecosystem Model (IEM) for Alaska and Northwest Canada Project. Fairbanks, AK.

Möhl, P., M. A. Mörsdorf, M. A. Dawes, F. Hagedorn, P. Bebi, D. Viglietti, M. Freppaz, S. Wipf, C. Körner, F. M. Thomas, and C. Rixen. 2019. Twelve years of low nutrient input stimulates growth of trees and dwarf shrubs in the treeline ecotone. Journal of Ecology

107:768–780.

Moser, L., P. Fonti, U. Buntgen, J. Esper, J. Luterbacher, J. Franzen, and D. Frank. 2010. Timing and duration of European larch growing season along altitudinal gradients in the Swiss Alps. Tree Physiology 30:225–233.

Naesset, E., and R. Nelson. 2007. Using airborne laser scanning to monitor tree migration in the boreal-alpine transition zone. Remote Sensing of Environment 110:357–369.

Nakagawa, S., and H. Schielzeth. 2013. A general and simple method for obtaining R2 from generalized linear mixed-effects models. Methods in Ecology and Evolution 4:133–142.

Nezval, O., J. Krejza, M. Bellan, and J. Světlík. 2021. Asynchrony and time-lag between primary and secondary growth of Norway spruce growing in different elevations. Forests 12.

Novak, K., M. de Luis, M. A. Saz, L. A. Longares, R. Serrano-Notivoli, J. Raventós, K. Čufar, J. Gričar, A. Di Filippo, G. Piovesan, C. B. K. Rathgeber, A. Papadopoulos, and K. T. Smith. 2016. Missing rings in pinus halepensis - The missing link to relate the tree-ring record to extreme climatic events. Frontiers in Plant Science 7:1–11.

Olnes, J., and K. Kielland. 2016. Stage-dependent effects of browsing by snowshoe hares on successional dynamics in a boreal forest ecosystem. Ecosphere 7:e01475.

Olnes, J., and K. Kielland. 2017. Asynchronous recruitment dynamics of snowshoe hares and white spruce in a boreal forest. Forest Ecology and Management 384:83–91.

Olnes, J., K. Kielland, H. Genet, G. P. Juday, and R. W. Ruess. 2018. Functional responses of white spruce to snowshoe hare herbivory at the treeline. PLOS ONE 13:e0198453.

Olnes, J., K. Kielland, G. P. Juday, D. H. Mann, H. Genet, and R. W. Ruess. 2017. Can snowshoe hares control treeline expansions? Ecology 98:2506–2512.

Overland, J., E. Dunlea, J. E. Box, R. Corell, M. Forsius, V. Kattsov, M. S. Olsen, J. Pawlak, L. O. Reiersen, and M. Wang. 2019. The urgency of Arctic change. Polar Science 21:6–13.

Paulsen, J., and C. Körner. 2014. A climate-based model to predict potential treeline position around the globe. Alpine Botany 124:1–12.

Pearson, R. G., S. J. Phillips, M. M. Loranty, P. S. A. Beck, T. Damoulas, S. J. Knight, and S. J. Goetz. 2013. Shifts in Arctic vegetation and associated feedbacks under climate change. Nature Climate Change 3:673–677.

Peng, C., Z. Ma, X. Lei, Q. Zhu, H. Chen, W. Wang, S. Liu, W. Li, X. Fang, and X. Zhou. 2011. A drought-induced pervasive increase in tree mortality across Canada's boreal forests. Nature Climate Change 1:467–471.

Peters, R. L., K. Steppe, H. E. Cuny, D. J. W. De Pauw, D. C. Frank, M. Schaub, C. B. K. Rathgeber, A. Cabon, and P. Fonti. 2021. Turgor – a limiting factor for radial growth in mature conifers along an elevational gradient. New Phytologist 229:213–229.

Piao, S., P. Friedlingstein, P. Ciais, N. Viovy, and J. Demarty. 2007. Growing season extension and its impact on terrestrial carbon cycle in the Northern Hemisphere over the past 2 decades. Global Biogeochemical Cycles 21:n/a-n/a.

Pinheiro, J., D. Bates, and R Core Team. 2022. nmle: Linear and Nonlinear Mixed Effects Models. R package version 3.1-157.

Politis, D. N., and H. White. 2004. Automatic block-length selection for the dependent bootstrap. Econometric Reviews 23:53–70.

Porter, T. J., and M. F. J. Pisaric. 2011. Temperature-growth divergence in white spruce forests of Old Crow Flats, Yukon Territory, and adjacent regions of northwestern North America.

Global Change Biology 17:3418–3430.

Purnell, B. 2003. To Every Thing There Is a Season. Science 301:325–325.

QGIS Development Team. 2022. QGIS Geographic Information System. Open Source Geospatial Foundation Project.

R Core Team. 2021. R: A language and environment for statistical computing. Foundation for Statistical Computin, Vienna, Austria.

Rahman, M. H., K. Kudo, Y. Yamagishi, Y. Nakamura, S. Nakaba, S. Begum, W. D. Nugroho, I. Arakawa, P. Kitin, and R. Funada. 2020. Winter-spring temperature pattern is closely related to the onset of cambial reactivation in stems of the evergreen conifer Chamaecyparis pisifera. Scientific Reports 10:1–12.

Ranson, K. J., P. M. Montesano, and R. Nelson. 2011. Object-based mapping of the circumpolar taiga-tundra ecotone with MODIS tree cover. Remote Sensing of Environment 115:3670–3680.

Rantanen, M., A. Y. Karpechko, A. Lipponen, K. Nordling, O. Hyvärinen, K. Ruosteenoja, T. Vihma, and A. Laaksonen. 2022. The Arctic has warmed nearly four times faster than the globe since 1979. Communications Earth & Environment 3:168.

Rees, W. G. G., A. Hofgaard, S. Boudreau, D. M. Cairns, K. Harper, S. Mamet, I. Mathisen, Z. Swirad, and O. Tutubalina. 2020. Is subarctic forest advance able to keep pace with climate change? Global Change Biology 26:3965–3977.

Renard, S. M., E. J. B. Mcintire, and A. Fajardo. 2016. Winter conditions - not summer temperature - influence establishment of seedlings at white spruce alpine treeline in Eastern Quebec. Journal of Vegetation Science 27:29–39.

Rossi, S., A. Deslauriers, J. Griçar, J. W. Seo, C. B. K. Rathgeber, T. Anfodillo, H. Morin, T. Levanic, P. Oven, and R. Jalkanen. 2008. Critical temperatures for xylogenesis in conifers of cold climates. Global Ecology and Biogeography 17:696–707.

Rossi, S., A. Deslauriers, C. Lupi, and H. Morin. 2014a. Control Over Growth in Cold Climates. Pages 191–219 *in* M. Tausz and N. Grulke, editors. Trees in a Changing Environment: Ecophysiology, Adaptation, and Future Survival. First edition. Springer, New York, NY.

Rossi, S., M. J. Girard, and H. Morin. 2014b. Lengthening of the duration of xylogenesis engenders disproportionate increases in xylem production. Global Change Biology 20:2261–2271.

Rossi, S., H. Morin, A. Deslauriers, and P. Y. Plourde. 2011. Predicting xylem phenology in black spruce under climate warming. Global Change Biology 17:614–625.

Sanmiguel-Vallelado, A., J. J. Camarero, E. Morán-Tejeda, A. Gazol, M. Colangelo, E. Alonso-González, and J. I. López-Moreno. 2021. Snow dynamics influence tree growth by controlling soil temperature in mountain pine forests. Agricultural and Forest Meteorology 296:108205.

Schmiege, S. C., K. L. Griffin, N. T. Boelman, L. A. Vierling, S. G. Bruner, E. Min, A. J. Maguire, J. Jensen, and J. U. H. Eitel. 2022. Vertical gradients in physiological function and resource allocation of white spruce diverge at the northern- and southern-most range extremes. bioRxiv.

Seo, J. W., D. Eckstein, R. Jalkanen, S. Rickebusch, and U. Schmitt. 2008. Estimating the onset of cambial activity in Scots pine in northern Finland by means of the heat-sum approach. Tree Physiology 28:105–112.

Silva, C. A., A. T. Hudak, L. A. Vierling, E. L. Loudermilk, J. J. O'Brien, J. K. Hiers, S. B. Jack, C. Gonzalez-Benecke, H. Lee, M. J. Falkowski, and A. Khosravipour. 2016. Imputation of Individual Longleaf Pine (Pinus palustris Mill.) Tree Attributes from Field and LiDAR Data. Canadian Journal of Remote Sensing 42:554–573.

Simpson, J. J., G. L. Hufford, M. D. Fleming, J. S. Berg, and J. B. Ashton. 2002. Long-term climate patterns in Alaskan surface temperature and precipitation and their biological consequences. IEEE Transaction on Geoscience and Remote Sensing 40:1164–1184.

Skre, O., R. Baxter, R. M. M. Crawford, T. V Callaghan, and A. Fedorkov. 2002. How will the tundra-taiga interface respond to climate change? Ambio Special Report:37–46.

Smith, T. B., R. K. Wayne, D. J. Girman, and M. W. Bruford. 1997. A Role for Ecotones in Generating Rainforest Biodiversity. Science 276:1855–1857.

Smith, W. K., M. J. Germino, T. E. Hancock, and D. M. Johnson. 2003. Another perspective on altitudinal limits of alpine timberlines. Tree Physiology 23:1101–1112.

Spiegelhalter, D. J., N. G. Best, B. P. Carlin, and A. van der Linde. 2002. Bayesian measures of model complexity and fit. Journal of the Royal Statistical Society. Series B: Statistical Methodology 64:583–616.

Stockton Maxwell, R., and L.-A. Larsson. 2021. Measuring tree-ring widths using the CooRecorder software application. Dendrochronologia 67:1125–7865.

Stovall, A. E. L., H. Shugart, and X. Yang. 2019. Tree height explains mortality risk during an intense drought. Nature Communications 10:1–6.

Streutker, D. R., and N. F. Glenn. 2006. LiDAR measurement of sagebrush steppe vegetation heights. Remote Sensing of Environment 102:135–145.

Suarez, F., D. Binkley, M. W. Kaye, R. Stottlemyer, and P. Taylor. 1999. Expansion of forest stands into tundra in the Noatak National Preserve, northwest Alaska. Ecoscience 6:465–470.

Sveinbjörnsson, B., A. Hofgaard, and A. Lloyd. 2002. Natural causes of the tundra-taiga boundary. Ambio Special Report 12, Tundra-Taiga Treeline Research:23–29.

Swidrak, I., A. Gruber, W. Kofler, and W. Oberhuber. 2011. Effects of environmental conditions on onset of xylem growth in Pinus sylvestris under drought. Tree Physiology 31:483–493.

Tardif, J., M. Flannigan, and Y. Bergeron. 2001. An analysis of the daily radial activity of 7 boreal tree species, northwestern Quebec. Environmental Monitoring and Assessment 67:141–160.

Taylor, P. C., M. Cai, A. Hu, J. Meehl, W. Washington, and G. J. Zhang. 2013. A decomposition of feedback contributions to polar warming amplification. Journal of Climate 26:7023–7043.

Timoney, K. P., and S. Mamet. 2020. No Treeline Advance over the Last 50 Years in Subarctic Western and Central Canada and the Problem of Vegetation Misclassification in Remotely Sensed Data. Ecoscience 27:93–106.

Tranquillini, W. 1979. Physiological Ecology of the Alpine Timberline. Page (W. D. Billings, F. Golley, O. L. Lange, and J. S. Olson, Eds.). Springer Berlin Heidelberg, Berlin, Heidelberg.

Tumajer, J., T. Scharnweber, M. Smiljanic, and M. Wilmking. 2022. Limitation by vapour pressure deficit shapes different intra-annual growth patterns of diffuse- and ring-porous temperate broadleaves. New Phytologist 233:2429–2441.

Turcotte, A., H. Morin, C. Krause, A. Deslauriers, and M. Thibeault-Martel. 2009. The timing of

spring rehydration and its relation with the onset of wood formation in black spruce. Agricultural and Forest Meteorology 149:1403–1409.

Vaganov, E. A., M. K. Hughes, A. V Kirdyanov, F. H. Schweingruber, and P. P. Silkin. 1999. Influence of snowfall and melt timing on tree growth in subarctic Eurasia. Nature 400:149–151.

Vlam, M., P. van der Sleen, P. Groenendijk, and P. A. Zuidema. 2017. Tree Age Distributions Reveal Large-Scale Disturbance-Recovery Cycles in Three Tropical Forests. Frontiers in Plant Science 7:1984.

Walker, X., G. H. R. Henry, K. McLeod, and A. Hofgaard. 2012. Reproduction and seedling establishment of Picea glauca across the northernmost forest-tundra region in Canada. Global Change Biology 18:3202–3211.

Wang, J. Y. 1960. A Critique of the Heat Unit Approach to Plant Response Studies. Ecology 41:785–790.

Wang, X., J. Xiao, X. Li, G. Cheng, M. Ma, G. Zhu, M. Altaf Arain, T. Andrew Black, and R. S. Jassal. 2019. No trends in spring and autumn phenology during the global warming hiatus. Nature Communications 10:1–10.

Watanabe, S. 2010. Asymptotic equivalence of Bayes cross validation and widely applicable information criterion in singular learning theory. Journal of Machine Learning Research 11:3571–3594.

Whittaker, R. 1970. Communities and ecosystems. Macmillan, New York, NY.

Wilmking, M., R. D'Arrigo, G. C. Jacoby, and G. P. Juday. 2005. Increased temperature sensitivity and divergent growth trends in circumpolar boreal forests. Geophysical Research

Letters 32:2–5.

Wilmking, M., M. Hallinger, R. Van Bogaert, T. Kyncl, F. Babst, W. Hahne, G. P. Juday, M. De Luis, K. Novak, and C. Völlm. 2012a. Continuously missing outer rings in woody plants at their distributional margins. Dendrochronologia 30:213–222.

Wilmking, M., J. Harden, and K. Tape. 2006. Effect of tree line advance on carbon storage in NW Alaska. Journal of Geophysical Research: Biogeosciences 111:1–10.

Wilmking, M., and G. P. Juday. 2005. Longitudinal variation of radial growth at Alaska's northern treeline—recent changes and possible scenarios for the 21st century. Global and Planetary Change 47:282–300.

Wilmking, M., G. P. Juday, V. A. Barber, and H. S. J. Zald. 2004. Recent climate warming forces contrasting growth responses of white spruce at treeline in Alaska through temperature thresholds. Global Change Biology 10:1724–1736.

Wilmking, M., T. G. M. Sanders, Y. Zhang, S. Kenter, S. Holzkämper, and P. D. Crittenden. 2012b. Effects of Climate, Site Conditions, and Seed Quality on Recent Treeline Dynamics in NW Russia: Permafrost and Lack of Reproductive Success Hamper Treeline Advance? Ecosystems 15:1053–1064.

Zacharias, M., T. Pampuch, K. Heer, C. Avanzi, D. G. Würth, M. Trouillier, M. Bog, M. Wilmking, and M. Schnittler. 2021. Population structure and the influence of microenvironment and genetic similarity on individual growth at Alaskan white spruce treelines. Science of The Total Environment 798:149267.

Zang, C., and F. Biondi. 2015. treeclim: an R package for the numerical calibration of proxy-climate relationships. Ecography 38:431–436.

Zhang, W., P. A. Miller, B. Smith, R. Wania, T. Koenigk, and R. Döscher. 2013. Tundra shrubification and tree-line advance amplify arctic climate warming: results from an individual-based dynamic vegetation model. Environmental Research Letters 8:1–10.

Ziaco, E., and F. Biondi. 2016. Tree growth, cambial phenology, and wood anatomy of limber pine at a Great Basin (USA) mountain observatory. Trees - Structure and Function 30:1507–1521.

Zuur, A. F., E. N. Ieno, N. J. Walker, A. A. Saveliev, and G. M. Smith. 2009. Mixed effects models and extensions in ecology with R. Page (M. Gail, K. Krickeberg, J. M. Samet, A. Tsiatis, and W. Wong, Eds.). Springer New York, New York, NY.

Zweifel, R., M. Haeni, N. Buchmann, and W. Eugster. 2016. Are trees able to grow in periods of stem shrinkage? New Phytologist 211:839–849.

Zweifel, R., and R. Häsler. 2000. Frost-induced reversible shrinkage of bark of mature sub alpine conifers. Agricultural and Forest Meteorology 102:213–222.

Zweifel, R., F. Sterck, S. Braun, N. Buchmann, W. Eugster, A. Gessler, M. Häni, R. L. Peters, L. Walthert, M. Wilhelm, K. Ziemińska, and S. Etzold. 2021. Why trees grow at night. New Phytologist 231:2174–2185.

Appendix A. Supporting Information for Chapter 1

Supplementary Material Table 1.1. Variance of Random Effects in Growth Rate v.s. tree age model in mature trees before and after 1975.

Groups	Name	Variance	Std. Dev.
Tree ID	Intercept	2273.7	47.7
Residual		0.16	0.40

Appendix B. Supporting Information for Chapter 2

Supplementary Material Table 2.1. Variance of Random Effects in the model.

Groups	Name	Variance	Std. Dev.
Tree ID	Intercept	0.1225	0.3500
Residual		0.8114	0.9008

Supplementary Material Table 2.2. Estimates and standard deviation of random intercepts for the 11 studied trees in the model.

Tree ID (Intercept)	Estimate	Standard deviation
1A	0.18	0.14
1E	-0.35	0.16
1F	-0.03	0.16
2E	-0.61	0.12
2F	0.51	0.20
4A	-0.05	0.10
4B	0.10	0.14
4D	-0.19	0.12
6A	0.25	0.12
6B	0.40	0.17
6D	-0.27	0.13

Supplementary Material Table 2.3. Center and scaling factors for transforming x-variables.

Variable	Center	Scale
DOY	178.5594	16.33805
Air Temperature	11.79463	4.01741
Vapor Pressure Deficit	0.3687728	0.431494
Vol. Water Content	0.4025955	0.1221045
Tree Size (DBH)	13.15693	5.880221

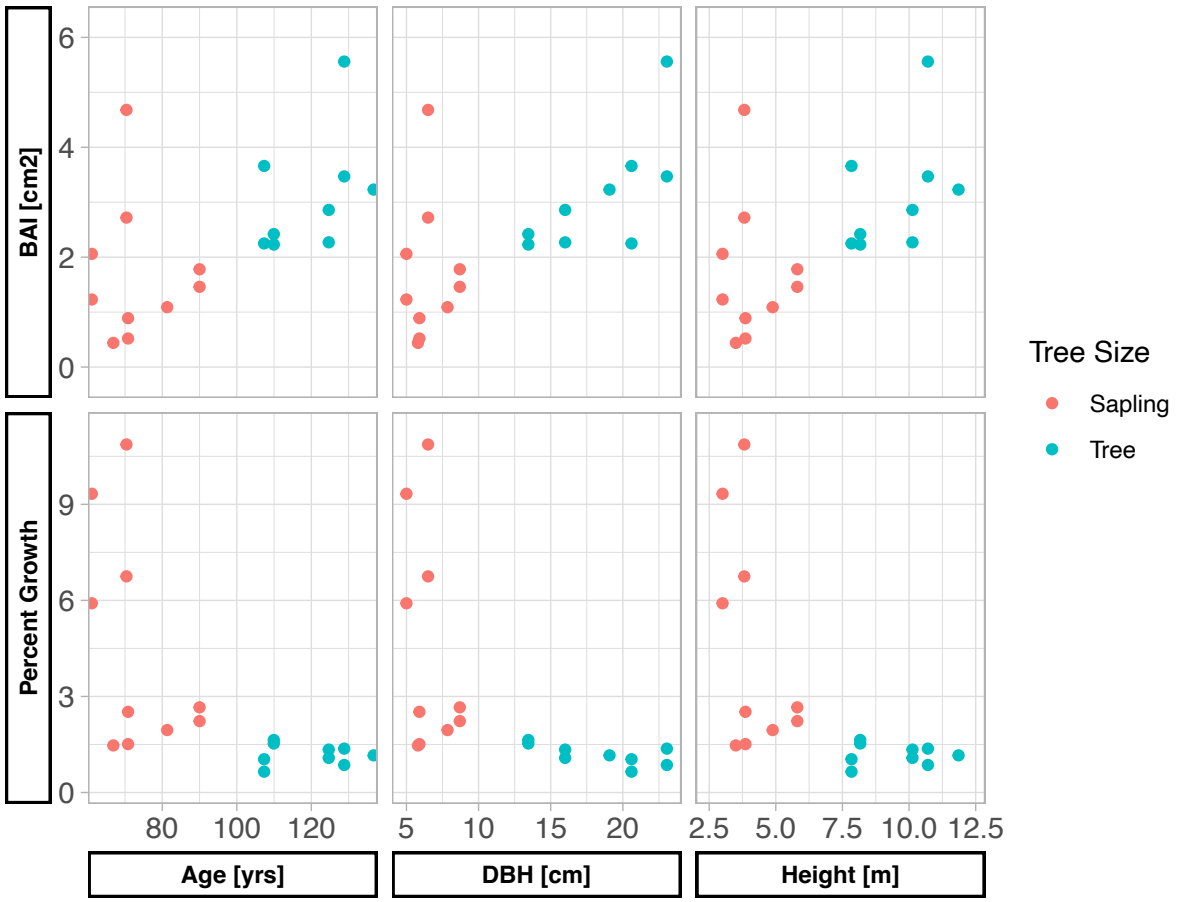

Supplementary Material Figure 2.1. Relationship between tree age, DBH, or height (x-axes) with annual growth (y-axis) in terms of magnitude (*top row*, BAI, cm^2) and percent relative to tree size at the start of the growing season (*bottom row*).

Appendix C. Supporting Information for Chapter 3

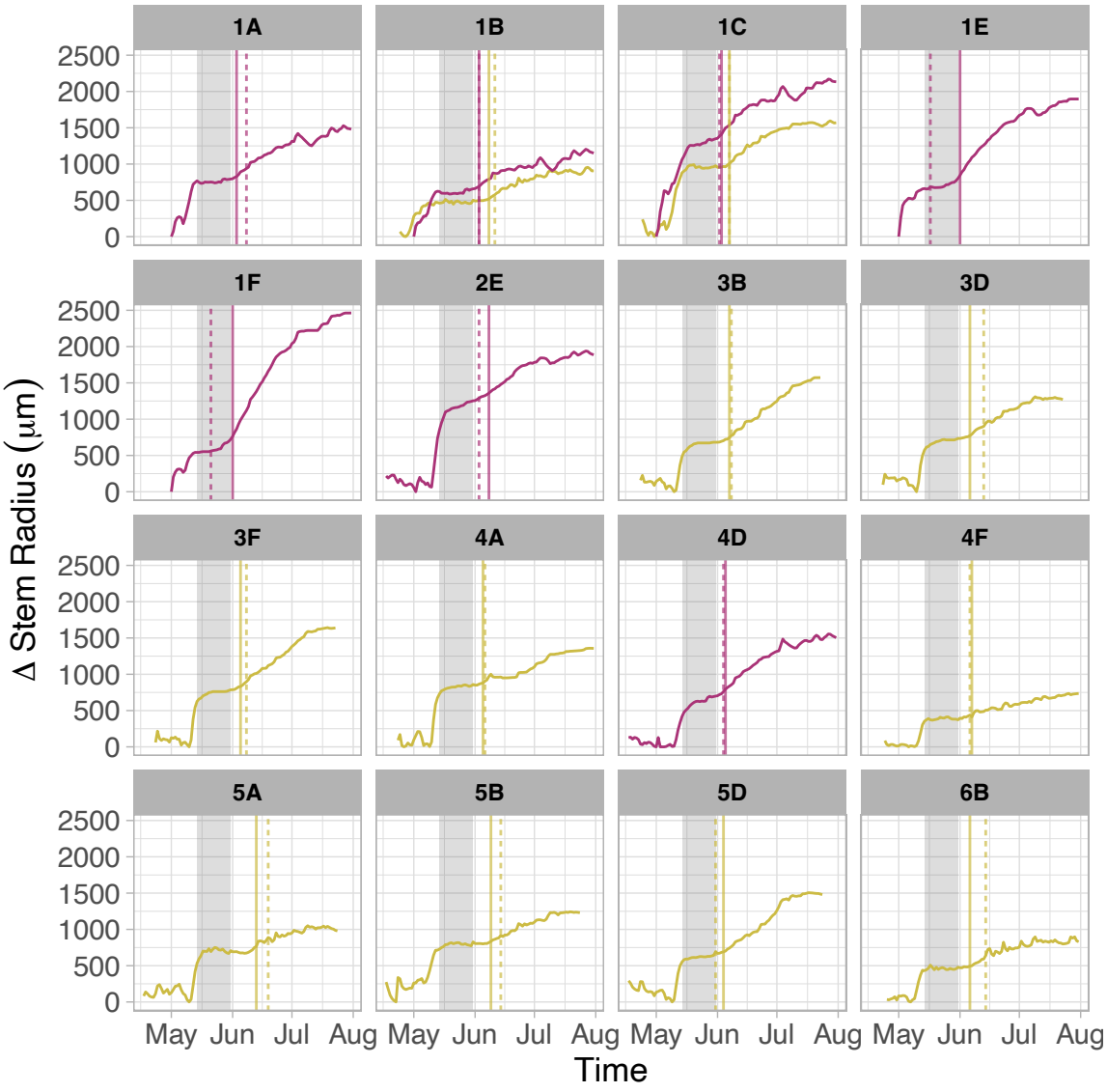

Supplementary Material Figure 3.1. Timeseries of changes in stem radius (μm) highlighting the similarity between detection methods of the onset of radial stem growth in 2018 (mustard yellow) and 2019 (purple). The light grey shaded region highlights the last two weeks of May during which the stem radius 'plateaus.' For each year, stem radius is normalized so that the minimum stem radius during the period shown is equal to zero. Each panel represents one of the 16 trees in which it was possible to detect the onset of radial stem growth using both methods. The vertical lines represent the onset of radial stem growth detected by the plateau method (solid lines) and the 95th percentile method (dashed lines). The difference in onset between the methods was not statistically different (Figure 1b, $p > 0.01$ Wilcoxon test, $n = 18$).

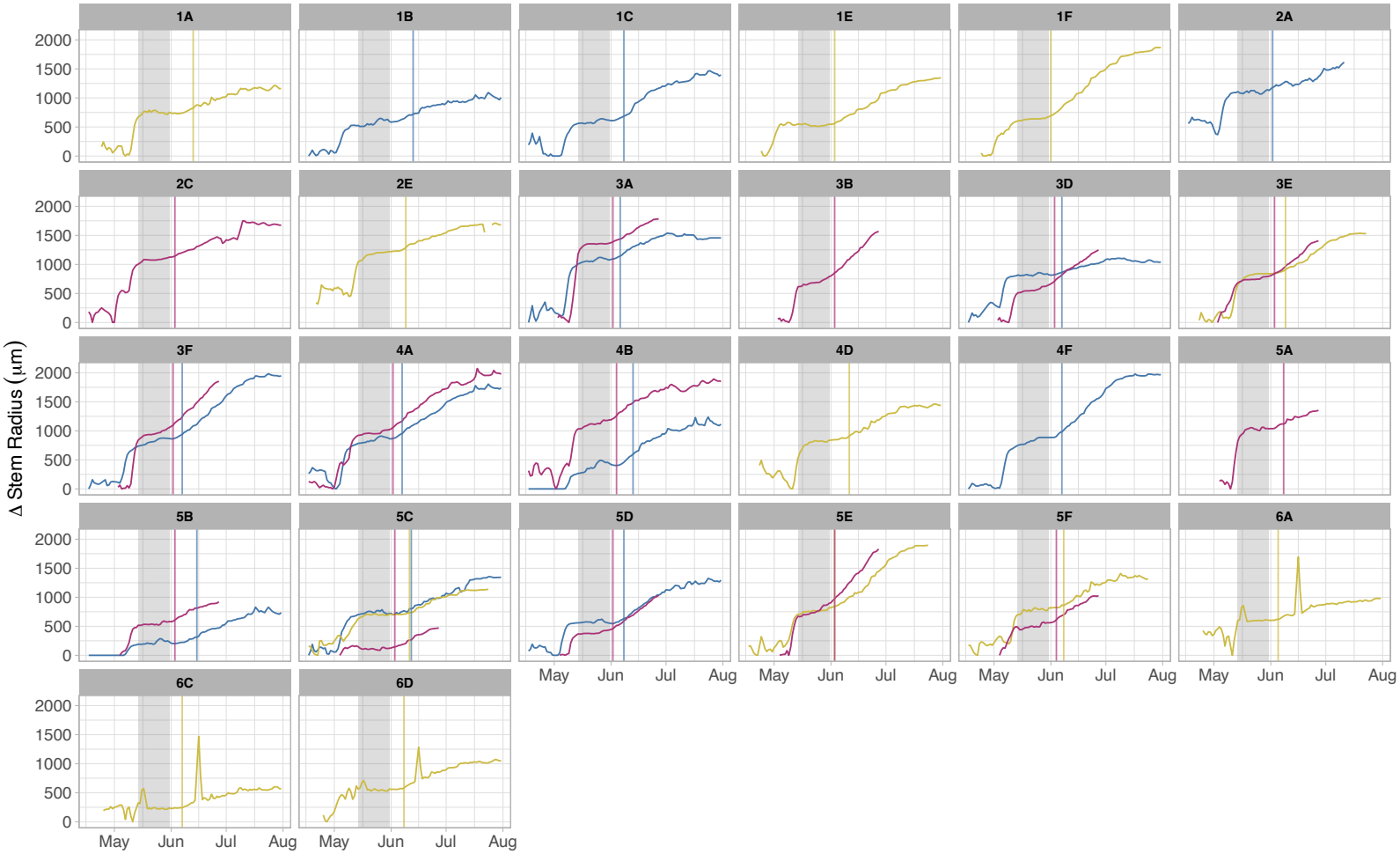

Supplementary Material Figure 3.2. Timeseries of the additional 38 tree-years used in the study with onset of radial stem growth detected by the plateau method. For various reasons (mainly missing data), detecting the onset of radial stem growth via the 95th percentile method was not possible in the trees presented here. Lines represent changes in stem radius in 2017 (dark blue), 2018 (mustard yellow), and 2019 (purple). The light grey shaded region highlights the last two weeks of May during which the stem radius 'plateaus.' For each year, stem radius is normalized so that the minimum stem radius during the period shown is equal to zero. The vertical lines represent the onset of radial stem growth detected by the plateau method.